Technical Report GL-99-7
July 1999

US Army Corps of Engineers
Waterways Experiment Station

Phenomenological Investigations of the Jefferson Proving Ground UXO Technology Demonstrations

by Dwain K. Butler, José L. Llopis, Janet E. Simms

WES

Prepared for U.S. Army Environmental Center
and Headquarters, U.S. Army Corps of Engineers

Technical Report GL-99-7
July 1999

Phenomenological Investigations of the Jefferson Proving Ground UXO Technology Demonstrations

by Dwain K. Butler, José L. Llopis, Janet E. Simms

U.S. Army Corps of Engineers
Waterways Experiment Station
3909 Halls Ferry Road
Vicksburg, MS 39180-6199

Final report

Prepared for U.S. Army Environmental Center
Aberdeen Proving Ground, Maryland 21010-5401

U.S. Army Corps of Engineers
Washington, DC 20314-1000

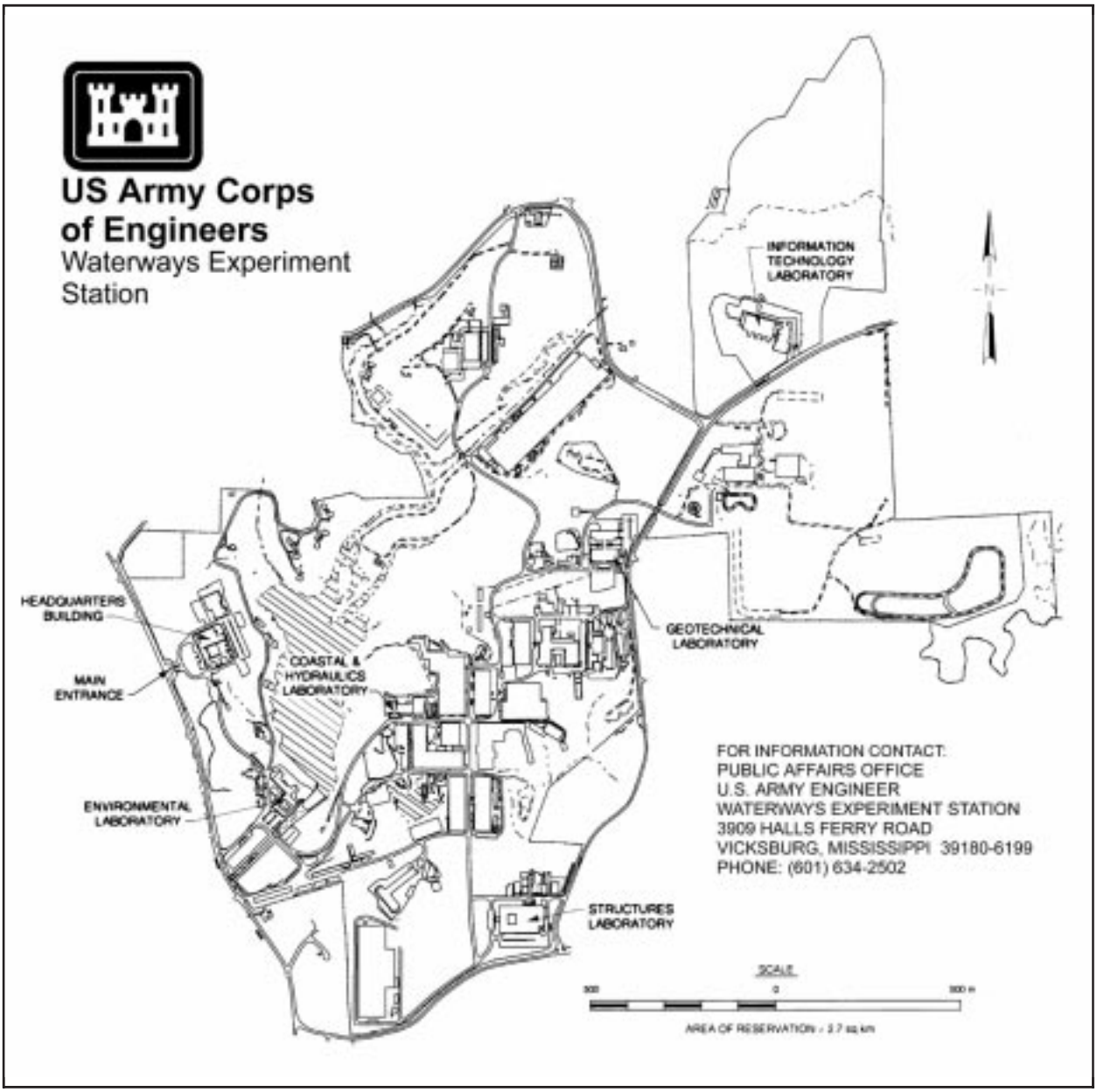

Waterways Experiment Station Cataloging-in-Publication Data

Butler, Dwain K.

Phenomenological investigations of the Jefferson Proving Ground UXO technology demonstrations / by Dwain K. Butler, Jos'e L. Llopis, Janet E. Simms ; prepared for U.S. Army Environmental Center ; U.S. Army Corps of Engineers.

96 p. : ill. ; 28 cm. — (Technical report ; GL-99-7)

Includes bibliographic references.

1. Ordnance —Detection. 2. Military weapons — Detection. 3. Explosives, Military — Detection. I. Llopis, Jos'e L. II. Simms, Janet E. III. United States. Army. Corps of Engineers. IV. U.S. Army Engineer Waterways Experiment Station. V. Geotechnical Laboratory (U.S. Army Engineer Waterways Experiment Station) VI. U.S. Army Environmental Center. VII. Title. VIII. Series: Technical report (U.S. Army Engineer Waterways Experiment Station) ; GL-99-7.

TA7 W34 no.GL-99-7

Contents

Preface

The work documented in this report was performed during the period August 1997 to December 1998 as part of a science and technology component to the Jefferson Proving Ground (JPG) Unexploded Ordnance (UXO) Technology Demonstration Program, Phase IV. The science and technology component was executed by personnel of the Geotechnical and Environmental Laboratories, U.S. Army Engineer Waterways Experiment Station (WES), Vicksburg, MS, a complex of five laboratories of the U.S. Army engineer research and Development Center (ERDC), for the U.S. Army Environmental Center (AEC). The work was jointly sponsored by the AEC under MIPR Number MIPR3767, 15 April 1997, and by the ERDC Environmental Quality Technology (EQT) Program, Work Unit "Innovative Geophysical Technologies for Enhanced Buried UXO Discrimination" (AF25, 6.2). Mr. George Robitaille was Program Manager, USAEC, for JPG Phase IV, and Dr. M. John Cullinane was Program Manager, USAERDC, for the EQT Program.

Co-Principal Investigators for the science and technology component of the JPG Phase IV work were Drs. Ernesto R. Cespedes, Environmental Laboratory (EL), and Dwain K. Butler, Geotechnical Laboratory (GL). The work reported herein was performed by the GL UXO Team of Drs. Butler and Janet E. Simms and Mr. José Llopis. Mr. Michael K. Sharp assisted with data processing. The assistance of Drs. Nagi Khadr, Thomas Bell, and Bruce Barrow, AETC Inc., Arlington, VA, and Drs. Herbert H. Nelson and James R. McDonald, Naval Research Laboratory, Washington, DC is gratefully acknowledged.

Dr. M. John Cullinane, EL, UXO programs coordinator for USAERDC, provided guidance during this work. General supervision was provided by Dr. William F. Marcuson III, Director, GL.

At the time of publication of this report, COL Robin R. Cababa, EN, was Commander and Acting Director, USAERDC.

Conversion Factors, Non-SI to SI Units of Measurement

Non-SI units of measurement used in this report can be converted to SI units as follows:

Multiply	By	To Obtain
acre	0.4047	hectare
acre	4,047	m^2
feet (ft)	0.3048	meters (m)
nanoTesla (nT)	1×10^{9}	Tesla

1 Introduction

Background

The requirement for UXO cleanup or remediation is divided into two mission areas: (1) UXO active range clearance and (2) UXO environmental cleanup. *UXO environmental cleanup* is currently the highest priority Department of Defense (DOD) environment quality "problem." Key features of the UXO problem are:

a. Millions of hectares of land *potentially* contaminated.

b. Hundreds of sites and locations.

c. Extremely diverse geologic and environmental conditions.

d. UXO at the surface and buried to depths as great as 10 m.

e. UXO sizes from 20-mm projectiles to 2,000-lb bombs.

UXO environmental cleanup is required in two primary settings: (1) sites or facilities scheduled to close as part of Base Realignment and Closure (BRAC), and (2) Formerly Used Defense Sites (FUDS). UXO environmental cleanup is covered under the DOD Range Rule, which defines and covers closed, transferred and transferring ranges containing UXO. While the motivation, urgency, and regulatory climate differ depending on the setting for UXO cleanup, the challenges and requirements are similar. Surface and subsurface UXO must be mapped or located over the areas of interest, and then the UXO must be remediated (by "blowing in place" or excavating, removing, and rendering safe).

The task of UXO location over large areas is challenging and problematic. Johnson et al. (1996) consider a four-stage systems process of "UXO sensing." Following the example of Johnson et al., Butler et al. (1998) propose a modified four-stage UXO location process: *screening, detection, discrimination, and identification/classification.* While surface UXO can be located visually and with remote (airborne) imaging techniques in some cases, the surface area to be surveyed is commonly very large and cluttered with metallic and other cultural debris. In addition, the vegetative cover of the UXO-contaminated lands varies greatly as do the surface soil and rock type and texture. Although the surface UXO problem is

large and complex, the fact that it can be addressed with remote imaging systems is a major advantage, since such systems can survey large areas rapidly with high resolution. Demonstrations of the WES Remote Minefields Detection System (REMIDS) airborne system have successfully located and mapped surface UXO (Bennett 1995). Since surface UXO and large concentrations of surface ordnance debris are indicators of the possible presence of buried UXO, airborne imaging survey systems such as REMIDS, possibly augmented with additional sensors, can make a major contribution to the *screening* stage for location of buried UXO.

The second stage in the sensing hierarchy involves the *detection* of buried UXO. General-purpose detection of buried UXO requires the application of ground surface geophysical surveys to detect anomalies caused by the buried UXO. Detection of buried UXO is identified as a major technology shortfall in numerous recent studies and field demonstrations (e.g., Johnson et al. 1996, U.S. Army Environmental Center (AEC) 1994, Office of the Secretary of Defense (OSD) 1997), and is a considerably more difficult problem than surface UXO mapping. *Discrimination* of anomalies likely caused by ordnance targets from "false alarm" anomalies caused by other buried objects (particularly metallic objects) and geologic features is even more difficult. UXO *identification (classification)* is the final step in UXO sensing (location), and consists of determining the specific type of ordnance that most likely produces a given ordnance-like anomaly.

The current capability to detect, discriminate, and identify buried UXO is summarized as follows: *(a) can detect UXO, within definable limits; (b) cannot effectively discriminate UXO anomalies from "false alarm" anomalies; (c) cannot identify UXO.* The definable limits for item (a) refer to combinations of ordnance size and burial depth that result in geophysical anomalies at the surface which can likely be detected relative to site-specific background noise (geologic background and cultural clutter). "False alarm" anomalies are caused by buried ordnance debris, other metallic objects, gravel and cobbles, soil heterogeneities, tree roots, and other natural and cultural features. Without significant discrimination capability, large numbers of false alarms that must be verified (dug up) are the dominant cost and time drivers for UXO site cleanup (remediation). This assessment is strongly supported by the results of a major Department of Defense investment in the Jefferson Proving Ground UXO Technology Demonstration Program.

Jefferson Proving Ground (JPG) UXO Technology Demonstration Program

History of the JPG UXO Program

In 1993, Congress mandated that the U.S. Army conduct a program at Jefferson Proving Ground, IN, to demonstrate and evaluate systems and technologies that can be used to detect, identify, and remediate buried UXO. The U.S. Army Environmental Center, Aberdeen, MD, was designated as the program manager. AEC tasked the Naval Explosive Ordnance Technology Division (NAVEOD-TECHDIV), Indian Head, MD, with the technical lead. Two controlled test sites (40- and 80-acres; approximately 16 and 32 hectares) were created by burying inert ordnance and clutter at documented but unpublished locations at the sites. The first phase of the program was completed in October 1994. This phase included demonstrations of 29 systems. The data collected from Phase I were compared to the known (baseline) target data, and technical reports were published (AEC 1994, 1995). From May through September 1995, Phase II of the program was conducted in a manner similar to Phase I, and 17 additional systems were demonstrated. Data collected from Phase II were again compared to the baseline targets, and a technical report was published (AEC 1996).

AEC conducted a Phase III program during September through November 1996. It was conducted in a similar manner as Phases I and II, but the overall program goals and objectives were expanded. In Phase III, the two test sites were subdivided to encompass realistic UXO scenarios. The main objective was focused to assess system performance in the various UXO scenarios. The site layouts for the 40- and 80-acre sites included the following scenarios:

a. *Scenario 1 - Aerial Gunnery Range.* An aerial gunnery range results from both helicopter and fixed wing aircraft aerial delivery of ordnance, ranging in size from 2.75-in. rockets to 2000-lb bombs, and found at depths ranging from near surface to 3 m.

b. *Scenario 2 - Artillery and Mortar Range.* A typical artillery and mortar range contains assorted types of conventional ground-fired ordnance; ordnance typically ranges in size from 60-mm mortars to 8-in. projectiles and is found at depths ranging from near surface to 1.2 m.

c. *Scenario 3 - Grenades and Submunitions Range.* The grenades and submunitions range represents a portion of a conventional impact area that has been set aside for sensitive-fuzed submunitions firing. These submunitions are delivered by aircraft and field artillery. The purpose of Phase III demonstrations was to detect only submunitions and grenades at depths shallower that 0.5 m.

d. *Scenario 4 - Interrogation and Burial Area.* The interrogation area represents a conventional impact area. At this area, demonstrators were given target location and required to classify and precisely position targets. The

target type, size, orientation, and depth of ordnance were not provided. The targets used in this area were aerial weapon systems ranging from 2.75-in. rockets to 2000-lb bombs as well as conventional ground weapons ranging from 60-mm mortars to 8-in. projectiles. Burn or burial sites may be present in this impact area as well as fragments from exploded munitions and other ordnance components, such as mortar fins and empty illumination rounds. Ordnance was buried at depths ranging from near surface to 2 m.

Results of the Phase III program were published in April 1997 (AEC 1997).

The JPG Demonstrations (AEC 1994, 1995, 1996, 1997; Altshuler et al. 1995), exhibit buried ordnance detection probabilities that exceed 90 percent by the end of Phase III (as indicated in Tables 1 and 2).

Table 1
A Synopsis of JPG UXO Technology Demonstration, Phase II Results

(160 UXO Targets Buried for Phase II)				
Demonstrator	Targets Reported	Ordnance Detection Rate (%)	"False Alarms" Per Hectare	No. False Alarms Per Ordnance Item Detection
Geophex	398	71	19.7	3.41
Geometrics	521	83	26.9	3.96
Parsons	602	85	32.5	4.68
Bristol	566	62	38.3	6.97
ADI (Combined)	598	65	34.5	9.35
Coleman	280	29	15.9	9.56
Scintrex	255	50	45.3	10.10
GeoPotentia	168	11	12.0	13.00
Geo-Centers	1,409	72	84.0	20.70
Vallon	1,903	57	225.9	68.00

However, even with ordnance detection improving to acceptable rates, the number of false alarms is unacceptably high, i.e., poor discrimination capability. For JPG Phase II, four demonstrators had ordnance detection rates > 70 percent; the number of false alarms for each ordnance item detected, however, ranged from 3.4 to 20.7 for these demonstrators (Table 1). Since JPG Phase III was easier for ordnance detection than Phase II, in that the ordnance items were consistently shallower (Figure 1; discussed in greater detail later in this report), the ordnance detection rates improved considerably. Four demonstrators for JPG Phase III *Scenario 2* (Table 2) had ordnance detection rates ≥ 90 percent, but the numbers of false alarms per ordnance item detected ranged from 1.4 to 20.2, still unacceptably high although showing improvement. The JPG and other field demonstrations exhibit limited capability for ordnance identification or classification (item c above). Even classification into broad ordnance categories, such as bombs, projectiles, and mortars, cannot be reliably accomplished with currently fielded systems. The capability to verify explosive content in *buried* ordnance does not exist.

Table 2
A Synopsis of JPG UXO Technology Demonstration, Phase III Results

Artillery and Mortar Range (Scenario 2) (117 Targets -- 67 Ordnance; 50 Nonordnance)				
Demonstrator	Targets Reported	Ordnance Detection Rate (%)	"False Alarms" Per Hectare	No. False Alarms Per Ordnance Item Detection
NAEVA	202	97	19.0	1.37
Gophex	174	67	21.1	2.20
Geometrics	282	90	38.4	3.00
Ensco	279	70	43.6	4.34
Geo-Centers	486	93	80.7	6.10
ADI	456	85	76.8	6.32
Rockwell	151	21	27.1	9.07
GeoPotential	23	3	4.3	10.00
GRI	1,319	90	258.2	20.15

It can be argued that much of the performance improvement during the first three UXO technology demonstrations at JPG, particularly between Phases I and II, do not specifically reflect advances in sensor technology. The basis of this position results from observations that improvements in successive phases came primarily from (a) demonstrators learning "the rules of the game," (b) repeat demonstrators having first-hand knowledge of site conditions, (c) site layout becoming easier and more focused, and (d) somewhat more relaxed demonstration controls. Regardless of the validity of this argument, however, there has been steady improvement in the performance and efficiency of UXO detection technologies, and much of this improvement can be attributed to the stimulation provided by the JPG UXO Technology Demonstration Program (e.g., Stanley, Clark, and Griffin 1997). Although some of the detection improvements can be attributed to new sensors and/or sensor performance enhancements, the primary improvements are in areas of philosophy and methodology:

a. Program managers and demonstrators learned that ground penetrating radar (GPR) is not a method of choice for efficient surveying of large areas for UXO detection, and airborne methods of any type generally cannot detect buried ordnance.

b. Better performers learned to rely on complementary methods for target declarations, e.g., electromagnetic (EM) induction and magnetometer systems.

c. Better procedures or algorithms were developed for integrating multi-method (multi-sensor) survey data.

d. Better navigation/positioning capability improved percentage of target declarations within critical radius of target.

Another factor that contributed to the improved performance was the increasing participation of demonstrators that specialize in conducting geophysical surveys for subsurface characterization.

JPG Phase IV

JPG Phase IV was initiated in 1997 and completed in December 1998. The Phase IV program consisted of three major components: (1) technology enhancement projects (each project concluding with a demonstration); (2) technology demonstrations; and (3) a complementary Science and Technology Program. The thrusts of the Phase IV projects and demonstrations were UXO discrimination and identification. All demonstrations were scheduled for the 40-acre site and a 1-hectare site developed as part of Phase IV, and all demonstrators were allowed access to the 80-acre site for self-tests prior to their demonstrations. A total of 160 targets were buried on the 40-acre site for the demonstrations. Samples of all the targets were available for inspection in a building close to the sites, and samples of all the targets were buried at the 80-acre site for the self-tests. Targets consisted of both inert ordnance and nonordnance (clutter). Positions of the targets were marked with flags, and the demonstration objective was to interrogate as many of the targets as possible within a 40-hr period. The demonstrators made ordnance or nonordnance declarations for all targets investigated within the allotted time. Additionally the demonstrators were to produce a rank ordering of the declarations in terms of confidence in the declaration, and provide as many additional parameters for the targets as possible. For the ordnance target declarations, additional parameters of interest include depth, orientation, size (length, diameter, mass, volume), and ordnance type (i.e., identification).

Motivation for the JPG Phase IV science and technology component

Due to the time constraints on execution of the Congressionally-mandated UXO Technology Demonstration Program, intensive contracting activities, major site preparation considerations, and intense program oversight and scrutiny, many activities which normally might be performed before and during the program were curtailed, omitted, or not considered. Among the frequently cited perceptions of program deficiencies for Phases I, II, and III are:

a. The sites were not thoroughly characterized (geological, geotechnical, and geophysical investigations) prior to any site disturbance.

b. There was limited phenomenological modeling done in advance to predict which of the baseline targets (1) should be easily detected, (2) could be marginally detectable, (3) would not be detectable, and (4) are close enough together to produce significantly superimposed anomalies.

c. There was no feedback loop for demonstrator self-evaluation; the baseline target data was not released after the phases were complete.

d. Demonstrators were not required to submit "raw" and/or processed sensor data.

e. Demonstrators were not required to describe their rationale for target detection and ordnance declarations.

f. The demonstrations were initially designed as "competitions" and not technology assessments.

g. The Program assessed demonstrator performance and not technology, since many demonstrators used the same sensor systems.

h. The demonstrators were not prepared for site conditions, particularly during Phase I.

i. The demonstrations were unrealistic in that geophysical surveys are not generally conducted without knowledge of site conditions or under arbitrarily established time constraints.

j. There was no obvious effort to respond to concerns of the scientific community.

The validity of some these perceptions and concerns is debatable, but the perceptions exist nonetheless.

In an effort to address selected aspects of the perceptions and concerns described above, a science and technology component was included as part of the JPG Phase IV UXO Technology Demonstration Program. The science and technology component and the tightly focused objectives of the Phase IV demonstrations are an effort to bring some closure to the Congressionally-mandated JPG UXO Technology Demonstrations and serve as a foundation for future efforts. The Phase IV demonstrations address *discrimination*, the next major and logical stage in "UXO sensing" capability development. The science and technology component supports the Phase IV demonstrations, documents the JPG sites for future use, reference, and comparison to other UXO test sites and cleanup sites, and addresses selected perceptions and concerns of the scientific community.

Scope of the JPG Phase IV Science and Technology Component

Supplemental site characterization of the 40- and 80-acre sites

To support detailed assessments of past and future UXO technology demonstrations at the 40- and 80-acre JPG sites and to allow comparisons of the JPG sites to UXO demonstration and live sites in other locations, supplemental site characterization investigations were performed at JPG. The objective is to

supplement the original site characterization data to the maximum extent possible consistent with time and funding constraints and the existing site disturbance (including the buried ordnance and clutter items). The following list is an outline of the major activities of the supplemental site characterization investigations:

a. Collect and synopsize the original site characterization efforts.

b. Conduct detailed topographic, vegetation, and site condition surveys.

c. Perform additional soil sampling at depths to 1 m.

d. Soils studies.

(1) Visual classification, water content, organic content, and specific gravity.

(2) Particle size gradation and engineering soils classification.

(3) Determination of engineering index parameters.

(4) X-ray diffraction studies of clay content and mineralogy.

(5) Laboratory measurements of EM properties as a function of frequency and water content.

e. Site geophysical surveys.

(1) Vertical electrical resistivity soundings at selected locations.

(2) EM induction (terrain conductivity) measurements over the sites.

(3) Ground penetrating radar (GPR) surveys along selected profile lines.

(4) In situ EM properties measurements (DICON probe) at selected locations and multiple depths.

The results of site characterization investigations and all data acquired are documented in Llopis et al. (1998).

Establishment and characterization of 1-hectare site

As part of the Defense Advanced Research Projects Agency (DARPA) UXO Backgrounds Program, four sites were selected, two each at Fort Carson, CO, and Fort A. P. Hill, VA. The selection of the four sites was guided by the considerations in Table 3 in terms of a simplified matrix of soil particle size and soil moisture regime. The four DARPA sites are shown as satisfying the criteria of three of the four classifications in the simplified matrix; while JPG is shown as completing the simplified soil particle size and moisture regime classification matrix. Since JPG

Table 3
Simplified soil particle size and moisture regime classification guiding the selection of the DARPA 1-hectare sites

Qualitative Particle Size Classification	Qualitative Moisture Regime Classification: *Moist*	*Dry*
Sand	Fort A. P. Hill, VA (Firing Points 20 and 22)	Fort Carson, CO (Turkey Creek Site)
Clay	Jefferson Proving Ground, IN *	Fort Carson, CO (Seabee Site)

* See page 16 for discussion of the JPG soils classifications.

complements the four previously established DARPA sites for characterization of UXO backgrounds, a 1-hectare site was selected, established, and characterized following the same procedures used for the DARPA sites. The details of site characterization investigations for the JPG 1-hectare site and the four DARPA 1-hectare sites are documented in Simms et al. (1998).

Independent assessment of prior JPG demonstration phases

The prior JPG demonstration phases were assessed with respect to (a) baseline ordnance and nonordnance items, (b) the site layouts and ordnance item spacing and depth of burial, and (c) an overall assessment of demonstrator performance changes and improvements from Phase I to Phase III. As a contribution to establishing the perceived missing feedback loop, four demonstrators performed self-assessments of their Phase III demonstrations. The self-assessments included (1) a detailed review of equipment and field procedures, data processing and interpretation procedures, error analyses, criteria for ordnance declaration decisions, and delivery of all demonstration data ("raw" and processed) and (2) a critical performance assessment relative to the target baseline (provided by the government). Details and results of the self-assessments will be documented in a separate report.

Participation in Phase IV technology enhancement efforts and technology demonstrations

Members of the science and technology team participated in all aspects of the Phase IV program, participating in contractor selection committees for the technology enhancement efforts and the technology demonstrations. Observers were present at each of the demonstrations at JPG Phase IV to assess the strengths and weaknesses of the geophysical methods and field procedures and assist in demonstration oversight. Environmental monitoring was conducted throughout the demonstrations. A weather station monitored precipitation, humidity, temperature, barometric pressure, etc. Soil samples were collected on the 40-acre site at three

locations and two depths each week during the demonstrations for determination of soil water contents. Additionally, five vertical electrical resistivity soundings, approximately in the center of the 40-acre site, were acquired during the course of the demonstrations.

Phenomenological studies

In UXO detection and discrimination surveys, the geophysical sensor responses are a superposition of the signatures of (a) the host medium (including any vegetation), (b) cultural sources, and (c) the buried ordnance. Signatures due to the host medium and cultural sources constitute the background. The host medium in most cases is a soil; however, occasionally the buried ordnance will be in rock. Part of the response to the host medium will be due to materials (soil and rock) below the depth of burial of the UXO as well as surface topography. The host medium will generally be heterogeneous both vertically and horizontally on multiple size-scales (e.g., Butler 1975, Isaaks and Srivastava 1989, Sahimi 1995). Sometimes the host medium may contain rocks (gravels or cobbles) or tree roots or animal burrows comparable in size to the buried ordnance. In some cases the geophysical methods used for detection and discrimination of buried UXO may be unaffected by the nature of the host medium, such as magnetic surveying for UXO buried in typical soils. However, there are conditions where the nature of the host medium makes buried UXO detection problematic (Khadr et al. 1997), such as:

a. High electrical conductivity soils that produce large EM induction responses and attenuate GPR signals after short distances of propagation.

b. Soils with high magnetic susceptibility or with rock inclusions having high magnetic susceptibility, e.g., the problems encountered with the Kaho'olawe Island Reserve, HI, UXO cleanup.

c. Soils with large rocks, tree roots, and/or animal burrows that produce GPR signatures similar to GPR signatures from UXO.

Cultural sources that contribute to sensor responses are of two types: (1) objects ("clutter") on or buried in the host medium, such as exploded ordnance debris and other metallic objects and (2) interference signals from power lines and EM transmitters of various types. The geophysical signatures of the buried ordnance depend on (a) size, shape, depth, orientation, composition, and physical properties of the ordnance, (b) physical properties of the host medium, and (c) inclination and declination of the local earth's magnetic field (for the magnetic signature). Whether or not the geophysical signatures of buried ordnance are detectable depends on the magnitudes, spatial wavelengths, and other features of the signatures relative to the signatures of all other sources, i.e., the background. Even though the signatures of buried ordnance are detectable for given sensors relative to the background, the signatures may not actually be detected due to the details of the data measurement/acquisition process, e.g., measurement spacing along survey tracks and the track spacing (inadequate sampling).

Scope of Report

This report documents the phenomenological studies conducted as part of the JPG Phase IV UXO Technology Demonstration Program science and technology component. In particular, this report documents the spatial and temporal variability of the backgrounds at JPG (partially documented in Llopis et al. 1998), evaluates the effects of geologic and environmental variability on geophysical sensor signatures, and presents the results of magnetic and EM induction modeling of the JPG Phase II and III baseline ordnance target set. A companion report by the U.S. Army Cold Regions Research and Engineering Laboratory presents the results of GPR modeling and associated phenomenological considerations (O'Neill and Arcone 1999).

2 Geologic, Geophysical, and Environmental Considerations

Environmental and Climatic Variability

Significant environmental and climatic factors

The climate of Jefferson Proving Ground, IN, is briefly described as moderately humid, and cold in the winter and hot in the summer (Nickell 1985, McWilliams 1985). The primary environmental and climatic factors that can affect geophysical sensor response are wind speed, vegetation, temperature, and rainfall. The time and spatial variability of these factors are important considerations when assessing or comparing performance of different sensor systems and demonstrators at different times. An example 24-hr record of environmental and climatic variables at the JPG 40-acre site is shown in Figure 2 for a date during the Phase IV demonstrations. These data were acquired continually during the Phase IV demonstrations from approximately mid-August to mid-November 1998. Rainfall is the major environmental and climatic variable affecting geophysical sensor response, through the dependence of soil moisture (water) content on rainfall. The effects of soil moisture and variations in soil moisture on the physical properties of the JPG soils and resulting variation in geophysical sensor response are discussed later in this chapter.

Wind speed

Wind speed and changes in speed and direction primarily affect gravity and seismic measurements (sensor responses), directly through flow against and around the sensor cases and indirectly through ground vibrations caused by wind coupling to the ground by vegetation and cultural surface features. Wind speed and direction at JPG are highly variable as with most locations, but generally will not pose an instrument vibration problem except during thunderstorms and other severe weather. The prevailing winds are from the south, and the *average* wind speed is *highest* in the spring, about 5 m/s (11 mph) (see Figure 2 for an example 24-hr

wind speed and direction record). To date, gravity and seismic methods have not been demonstrated at JPG.

Vegetation

Vegetation affects measurements with all of the geophysical methods in various ways. For example, larger trees and shrubs alter the uniformity of measurement grids and result in areas of no measurements. Variation in the height of grasses cause sensor elevation and orientation variations during surveys with hand-carried or vehicle mounted or towed sensor systems, resulting in increased "noise" levels. Trees and tree roots can sometimes produce EM induction and GPR sensor responses (anomalies) that may be misinterpreted as anomalies caused by buried UXO (false alarms). Also, soil moisture content is often greater in areas of higher vegetation density, which has implications for UXO detection with GPR and EM induction methods. The grass and wildflower cover for the 40-acre site was kept mowed to a height of 10-20 cm during the demonstrations, particularly for the Phase II to IV demonstrations. Other vegetation on the 40-acre site is scattered and generally isolated, ranging from shrubs and small trees, 1 to 1.5 m, to mature trees, 10 to 15 m. Generally the trees will interfere with measurements typically within a radius of 1 to 2 m. However there a few areas on the site where closely spaced trees or large trees with low growing limbs can interfere with measurements over an area with radius up to 5 m (Figure 3).

Temperature

Air and subsurface temperature and temperature changes affect sensor response in three primary ways: (1) instrumental noise and drift for some sensors is sensitive to ambient temperature and temperature changes, (2) changes in dimensions of components in a system can result in altered measurement geometry, and (3) some subsurface physical properties vary with temperature, e.g., resistivity or conductivity and density. Subsurface physical property variation with temperature is generally small for small temperature changes above the freezing point, e.g., a 10 degrees C temperature change will result in approximately a 20 percent change in electrical resistivity for electrolytic conduction in water *saturated* soil and rock. For relatively dry soil and rock, the change in electrical resistivity with temperature is quite small. For temperatures below the freezing point, the electrical resistivity is 1 to 2 orders of magnitude greater than at temperatures above the freezing point (Keller and Frischknecht 1970). The effects of temperature and temperature changes on instrument noise, drift, and altered measurement geometry is system dependent and requires assessment for each system.

At JPG the *average* daily temperature range in winter is approximately –4 to 7 degrees C (25 to 45 degrees F), and in summer is approximately 18 to 30 degrees C (65 to 87 degrees F). Thus there is an average 11 to 12 degrees C temperature change in any 24-hr period of the year (see Figure 2 for a 24-hr example record). It follows that the temperature effect on resistivity for saturated soil conditions at JPG will typically be 20 percent or less in any 24-hr period. The

effect of temperature change on resistivity between the extreme temperatures in summer and winter could be significant for saturated materials. However, the depth to "permanently saturated" materials, i.e., depth to the water table, in the area of the 40-acre site exceeds the subsurface depth extent of both the annual and diurnal temperature changes. Significant periods of temperatures below freezing are not common, and the depth of freezing in soil is limited to a few centimeters.

Topography, Site Conditions, and Soil Series Maps

The topography of the 40- and 80-acre sites is gently rolling, with minor drainage paths crossing the sites (Llopis et al. 1998, Nickell 1985, McWilliams 1985). Obvious cultural reshaping of the natural topography is minor, consisting of tire tracks, foot paths, small excavated soil mounds, and depressions resulting from ordnance burial activity associated with the UXO technology demonstrations. After heavy rainfall, the tire tracks and natural and manmade depressions are filled with water, due to low permeability near-surface soils, and thus readily apparent. For the Phase I demonstrations, the sites were tilled prior to the technology demonstrations to conceal the ordnance burial sites, leaving a highly irregular small scale surface topography; the sites were not tilled for the subsequent phases (Phases II, III, and IV).

The maximum topographic variation (lowest to highest elevation) across the 80-acre site is 10 m (33 ft), with surface runoff (drainage) occurring primarily to the east and south (Figure 4). For the 40-acre site, the maximum topographic variation is 8.8 m, with a well-developed drainage path from east to northwest across the northern part of the site and other surface runoff occurring primarily to the west. (Figures 3 and 5). Topography and site conditions affect geophysical surveys in three ways, which are not necessarily interrelated: (1) rugged topography inhibits effective coverage with vehicular mounted sensor systems, (2) small scale topography introduces noise and "false alarm" anomalies to survey measurements, and (3) topography is influenced by soil type, soil moisture conditions, and vegetation. There are only minor vehicular access problems due directly to rugged topography at the JPG sites. The depressions or "bathtubs" over emplaced ordnance, particularly in Phase IV, collect water during rainfall and cause some measurement access problems and increased measurement noise and EM attenuation (due to increased moisture content). Indirectly, however, topography restricts vehicular system access to some areas with greater than normal density vegetation, since vegetation correlates to some extent with topography (Figure 3). The site tilling done for Phase I caused considerable survey problems for vehicular-mounted demonstration systems and created a major source of false alarms for the GPR systems. The noise levels for all survey systems in Phase I, both hand-held and vehicular-mounted, were increased due to varying sensor height and orientation relative to the surface and the buried ordnance.

Soil unit definitions and descriptions include typical surface slopes, thus it is not surprising that there should be some correlation between soil types and topography (Nickell 1985, McWilliams 1985). An overlay of topography (Figure 5) and

the general soils map for the 40-acre site (Llopis et al. 1998) is given in Figure 6. The areas of greatest observed surface slope, correlating with the apparent drainage paths, are in areas of RoB2 (Rossmoyne silt loam, 2 to 6 percent slopes, eroded) and CcC3 (Cincinnati silt loam, 6 to 12 percent slopes, severely eroded) soils with the largest slope descriptors. The largest portion of the site has measured surface slopes of 0 to 2 percent, corresponding to areas of AvA (Avonburg silt loam, 0 to 2 percent slopes) and Cm (Cobbsfork silt loam, nearly level, ~ 0 percent slope) soils (Nickell 1985, McWilliams 1985). Other correlations between topography and/or soil types and geophysical properties are noted in the following sections.

Soil Water Content

For a given site, soil water content is generally the major time-dependent sub-surface variable that can affect geophysical sensor response. Above the water table, soil water content is time-variable due to rainfall, infiltration, and evapo-transpiration. Below the water table, soil and rock are completely saturated and hence have time-independent water content. The rate of infiltration is controlled by the vertical hydraulic conductivity of the soils, surface slope, vegetation, and other factors. JPG soils have very low hydraulic conductivity, typically 10^{-7} cm/s, leading to ponding conditions in depressions after rainfall, including tire tracks and settlement depressions over ordnance burial locations, followed by slow infiltration into and through the soil column to the water table (PRC Environmental Management, Inc. 1994; Nickell 1985; McWilliams 1985).

During prolonged dry periods, the ground surface becomes very hard and dry, and during prolonged wet periods (frequent, heavy rainfall), the ground surface becomes very soft and appears to be saturated. During prolonged wet periods, the near surface soil regime that is significantly influenced by infiltration ("nearly saturated" zone) will extend to depths of 0.5 m or more, whereas after moderate rainfalls the "nearly saturated" zone is confined to the upper few centimeters. A dramatic example of soil water content variation with depth is illustrated in Figure 7, for soil samples collected on 3 August 1997 (very dry conditions) and 29 April 1998 (very wet conditions) at grid location G7 approximately in the center of the 40-acre site. In Figure 5, the numbers in parentheses by the nine soil sampling locations (triangles) are weight-based water contents (in percent) from August 1997 (dry conditions) at 10, 50, and 100 cm sampling depths. The mean water content for 10-cm depth for the nine locations is 13 ± 1 percent (dry conditions). For samples acquired at five locations in April 1998 (wet conditions) at 10-cm depth, the mean water content is 33 ± 3 percent. The 10-cm depth water content spatial variation, for the major soil types, is seen to be small (± 1 to 3 percent) for both dry and wet conditions at JPG.

For JPG Phase IV, water contents were determined for 10-cm and 50-cm samples from three locations on the 40-acre site (K1, G7, C13; Figure 5) each week during the extent of the demonstrations. These water content data are shown in Figure 8 as a function of time. Comparing the August 1997 values to the other water content values confirms that the August 1997 conditions are comparable to

the driest conditions encountered during the Phase IV demonstrations (15 September 1998). The April 1998 water contents for location G7, however, are higher than values observed for any of the three locations monitored during the Phase IV demonstrations. Thus the August 1997 and April 1998 site conditions effectively represent the extremes in shallow soil moisture during the period of investigations. Thus the range of soil water content effects on geophysical properties of shallow subsurface materials is likely captured by the August 1997 and April 1998 conditions, although the results of electrical resistivity measurements at location G7 during the complete extent of the Phase IV demonstrations are presented.

Soils Classifications

Failure of surface and airborne GPR systems at JPG Phases I to III has been attributed to high soil electrical conductivity (leading to high GPR signal attenuation), scattering and subsequent false alarms associated with rocks in the soil, and rough surface conditions (particularly for Phase I) (Altshuler et al. 1995; AEC 1995, 1996, 1997). The high ground conductivity and signal attenuation are commonly and logically attributed to high clay content soils, exacerbated by high water contents at certain times (AEC 1996).

The fact that the water content of the shallow soils (samples from ≤ 1.0-m depth) varies considerably during the year is documented in the previous section. Also, shallow JPG soils classify as sandy clay, silty clay, and clay, based on particle size distribution, and as low to high plasticity clays, based on visual inspection (Llopis et al 1998; PRC Environmental Management, Inc. 1994). Engineering classification of the shallow JPG soils results in classification primarily as low plasticity clays. However, when plotted on a graph of engineering index parameters, the JPG soils generally plot very close to the A-line (which generally separates inorganic soils from organic soils; Means and Parcher 1963; Casagrande 1948), in a region of the plot space where soils can be either low plasticity clays or slightly plastic silts or very fine silty sands (Figure 9; Llopis et al. 1998). Also, x-ray diffraction analyses of the JPG soils reveals only trace amounts of clay minerals, with quartz being the predominant mineral (Llopis et al. 1998*). Thus the shallow JPG soils are very fine-grained, quartz silts and sands, and attenuation of GPR signals cannot be attributed to high clay content soils in the shallow subsurface.* Results of field and laboratory investigations to determine the cause of past failures of GPR at the JPG sites are documented in Llopis et al. (1998), in the following sections, and in O'Neill et al. (1999).

Variability of Geophysical Properties

Geophysical site characterization

The purposes of the field and laboratory investigations for the 40- and 80-acre sites and the 1-hectare sites, discussed in Chapter 1 and documented in Llopis et al. (1998), were to (a) characterize the shallow geology at the sites, (b) map the details of spatial and temporal variability of geophysical properties that affect the performance of geophysical sensors, and (3) determine the variability of key electromagnetic parameters as a function of frequency and water content. The site geophysical surveys were intuitively planned to investigate and map the horizontal and vertical variability of the geophysical parameters that were thought most likely to affect sensor performance. These key parameters are the electromagnetic properties as a function of frequency and water content. The electromagnetic properties were determined using electrical resistivity sounding, terrain electromagnetic conductivity, in situ complex dielectric permittivity at a GPR frequency, GPR site surveys, and laboratory sample testing to determine complex dielectric permittivity as a function of frequency and water content. From the in situ and laboratory complex dielectric permittivity measurements, the conductivity, loss tangent, attenuation factor, and phase velocity can be determined as functions of frequency and water content.

Initially, it was assumed that the magnetic susceptibility of the natural geologic materials would not vary significantly over the sites. Thus the original site characterization did not include investigations addressing the spatial or temporal variability of the magnetic susceptibility. However, subsequent feedback from Phase II and III demonstrators indicates some significant areas of magnetic anomalies that are apparently geologic in origin. These anomalies are large enough in magnitude and size to interfere with target magnetic anomaly detection. Field magnetic susceptibility measurements were made over two of the most significant geologic anomaly areas as part of the Phase IV supplemental site characterization.

Electrical resistivity: Spatial and temporal variability considerations

Conductivity Maps. Electrical conductivity (the reciprocal of the resistivity) maps for the 40-acre site for dry (August 1997) and wet (April 1998) site conditions are shown in Figure 10. The data for the conductivity maps were acquired with a Geonics EM-31 system and are frequently called terrain conductivity measurements. The maps indicate variability of soil and rock type and/or water content over the site. The EM system is a bistatic, frequency domain EM system that operates at 9.8 kHz and has a transmitter-receiver (Tx-Rx) spacing of approximately 3.7 m. The depth of investigation of the system, a volume average conductivity weighted by the system response, is nominally 4 to 5 m but is most strongly influenced by material in the upper 1 to 2 m. Each of the maps in Figure 10 illustrates the spatial variability of electrical conductivity for a given date, while comparing the two maps indicates the effects of different site moisture (soil

water content) on the conductivity distribution. As documented previously, the site conditions for the dates of the two maps in Figure 10 represent the minimum/driest (left map) and the maximum/wettest site conditions (right map) for the period August 1997 to November 1998 at the JPG 40-acre site. There is a general correlation between the conductivity distribution and soil types as illustrated in Figure 11, where the soils map is superimposed on the August 1997 conductivity map. The correlations between soil type and conductivity are complicated by the facts that (a) soil type correlates with topography and (b) generally the topography correlates with soil water content (i.e., higher elevation areas are typically dryer than lower elevation areas).

The general patterns of conductivity are similar in the two maps (Figure 10). Localized differences between the two maps relate to localized differences in soil water content or site disturbance, resulting from ponding of water in depressions and target burial activities occurring between the times of the two maps. Simple statistical analyses of the values in the two conductivity maps are shown in Table 4. The *average (mean) and the standard deviation of the conductivity* increases only slightly (approximately 1 mS/m) from the dry to wet conditions map. Even though the depth of significant soil water content increase following rainfall is small (see Figure 7) and the terrain conductivity values are volume averages of the upper 4 to 5 m, the small increase in average conductivity for the site is counter-intuitive. The *range of conductivity* (difference between maximum and minimum values) increases by a factor of 4 from the dry to wet conditions map. The significant increase in the maximum conductivity value for the wet site conditions compared to dry site conditions is caused by intervening site disturbances and associated localized soil water content increase.

Table 4
EM Terrain Conductivity Statistics-- 40-Acre Site, Jefferson Proving Ground, IN

Statistic	Dry (Aug 1997)	Wet (Apr 1998)
Minimum, mS/m	10.5	12.2
Maximum, mS/m	32.5	94.9
Average, mS/m	19.9	20.8
Standard Deviation, mS/m	3.6	4.8

Electrical resistivity monitoring. Vertical electrical resistivity soundings (VES) were conducted on the 40- and 80-acre sites and the 1-hectare sites to assess the vertical electrical resistivity variation. Detailed VES results and correlations with site geology, e.g., depth to rock and soil types, are discussed by Llopis et al (1998). Generally the VES results indicate a three- or four-layer geoelectrical structure beneath the sites. For the four-layer structure, the simplified correlations with geology are as follows: layer 1 – near surface, silty soils with high organic content and porosity; layer 2 – moist, silty materials; layer 3 – wet, higher clay-content materials; layer 4 – limestone. VES interpretations for grid location G7 for three dates are shown in Figure 12. The first two VES results (for August

1977 and October 1977) are for dry site conditions, while the third is for the April 1998 wet site conditions. The interpreted thickness for layers 1 and 2 at G7 remains approximately constant, and the interpreted resistivity for layer 2 remains approximately constant. The major change from dry to wet site conditions is the dramatic decrease in layer 1 resistivity, from approximately 830 to 780 to 310 ohm-m for August 1997, October 1997, and April 1998, respectively, corresponding to increasingly wet site conditions. The terrain conductivity values at location G7 in Figures 10 and 11 are approximately 18 mS/m. Considering the response functions for the EM system, the predicted conductivity values over the geoelectric section in Figure 12 are in the range 10-15 mS/m. Thus the electrical resistivity and EM conductivity measurements are in relatively good agreement and consistent with the different measurement procedures and volumes of influence of the techniques.

Grid location G7, approximately at the center of the 40-acre site served as a monitoring location for the Phase IV demonstrations. Results of seven VES interpretations for the period 18 August to 27 October 1998 are shown in Figure 13. The major changes in the geoelectrical structure are with the resistivities and thicknesses of layers 1 and 2. The parameters for the upper two layers are well defined (resolved) in the inversions, while the resistivity and thickness of layer 3 are not as well resolved (equivalence). The resistivity of layer 4 is constrained to be constant for the inversions in Figures 12 and for the inversions in Figure 13. A summary of the variation of the parameters of the geoelectrical sections in Figure 13 is indicated in Table 5.

Table 5
Ranges and Means of Geoelectrical Layer Parameters for the G7 VES Monitoring Location for the Period 18 August to 27 October 1998

Layer Parameter	Range	Mean
Layer 1 – Resistivity, ohm-m	450 - 880	655
Layer 1 – Thickness, m	0.3 - 0.6	0.5
Layer 2 – Resistivity, ohm-m	80 - 160	135
Layer 2 – Thickness, m	1.0 - 1.6	1.2
Layer 3 – Resistivity, ohm-m	25 - 38	30
Layer 3 – Thickness, m	2.6 - 3.5	3.1

Dielectric permittivity: Spatial and water content variability

The field and laboratory investigations of dielectric permittivity are thoroughly documented in Llopis et al. (1998). Laboratory dielectric permittivity results are illustrated in Figure 14 for 200 MHz (results for the frequency range 45 MHz to 4.045 GHz are given in Llopis et al. 1998). Data plots for other frequencies are similar qualitatively but will shift up or down. The plots in Figure 14, for all locations and all depths (surface to 1-m depth) on the 40- and 80-acre sites, are for the real and imaginary components of the relative complex dielectric permittivity (measured parameters; top plots) and for the EM attenuation (dB/m) and

conductivity (mho/m = 1000 mS/m) (derived from measured parameters; bottom plots) as a function of volumetric moisture content (percent). There is no obvious separation of values for samples from the 40- and 80-acre sites; although there is apparently more scatter in the 80-acre data than the 40-acre data. The increased scatter at the 80-acre site may reflect the greater occurrence of mineralogical clays near the surface at some locations. For the 40-acre site, the real and imaginary components of the relative dielectric permittivity vary approximately linearly between 10 and 40 percent volumetric moisture content, with a variation of less than ± 2 at any specific moisture content. This implies that the spatial variability of the complex dielectric permittivity at the 40-acre will be similar to the spatial variability of the soil moisture content.

In addition to the laboratory dielectric permittivity measurements, two other field tests give insight to the spatial, volume, and frequency variability of the dielectric permittivity. Results of GPR surveys can be interpreted to give the *real part* of the complex relative dielectric permittivity, by conducting wide-angle reflection-refraction surveys and by analyses of diffraction hyperbolic events. Llopis et al. (1998) present results of analyses of 70 hyperbolas in 300 MHz GPR profiles and 48 hyperbolas in 600 MHz GPR field profiles from the 40-acre site. Analyses of the results indicates no statistically significant difference in the mean and standard deviation of the real, relative dielectric permittivity values for the 300 and 600 MHz data (10.5 ± 4.2 versus 10.4 ± 3.5, respectively). Dielectric permittivity determined from GPR survey data are clearly representative of volume-average values over the propagation paths that define the hyperbolic events.

An in situ probe was also utilized to investigate spatial dielectric permittivity variability (Llopis et al. 1998). The DICON probe (Miller, Malone and Blount 1992) makes a point (small volume) measurement of the complex dielectric permittivity at 60 MHz. Measurements were made at 10- and 50-cm depths at 25 locations on the 40-acre site. The DICON probe measurement locations and the real component of the complex relative dielectric permittivity are shown in Figure 15. The permittivity values increase with depth everywhere. There is no general pattern to the values and no obvious correlation to soil type or topography, except to the extent that soil type and topography correlate to moisture content.

Table 6 is a summary of the measurements or determinations of real, relative dielectric permittivity for laboratory measurements, GPR interpretations, and DICON probe measurements. The laboratory measurements are for a moisture content of 25 percent, an appropriate moisture content for the time of the GPR surveys and DICON probe measurements. Considering the differences in data acquisition technique and volume of investigation factors, the values of relative dielectric permittivity agree remarkably well. There is a general trend toward decreasing relative dielectric permittivity as frequency increases.

Table 6
40-Acre Site Relative Dielectric Permittivities (Real Component) According to Test Type and Frequency for 25 percent Soil Moisture Content

Test Type	Frequency, MHz	Relative Permittivity
Laboratory	100	13
	200	11
	495	11
	1015	10
GPR	300	10.5
	600	10.4
DICON Probe	60	19.2

Magnetic susceptibility: Spatial variability

Magnetic susceptibility of near surface materials is not a parameter that is normally expected to vary significantly over short distances in non-igneous terrain. It is not uncommon, however, for soils to have higher magnetic susceptibilities than the parent rocks due to selective sorting of heavy minerals (Burger 1992). Soil magnetic susceptibility typically varies by factors of 2 to 3 over distances of tens of meters. Typical sedimentary rock susceptibilities average 5×10^{-4} (SI), while soils can be as high as 1 to 1.5×10^{-3} (SI). Commonly, the susceptibility variation of soils in an area (as portrayed in a histogram of values) will be unimodal with a rather narrow peak (Scollar et al. 1990). Anomalously high or complex spatial variability of magnetic susceptibility were not suspected for the JPG sites.

During preparation for and execution of the JPG Phase IV demonstrations, the presence of significant anomalies of the magnetic field, that are apparently not related to the baseline ordnance set, were revealed by some of the demonstrators, based on their Phase II and III demonstration experience. Figure 16 is a total field magnetic anomaly map from a Phase II demonstration (Blackhawk-Geometrics, Inc. 1998). In addition to magnetic anomalies due to buried targets (ordnance and non-ordnance targets), the magnetic map includes other anomalies caused by cultural and geologic sources. An obvious cultural feature anomaly is the linear anomaly pattern that trends nearly due north-south along the western side of the 40-acre site that is caused by a fence. Another linear anomaly occurs between east-west grid lines 10 and 11 and is likely caused by the buried remnants of a fence. The longer spatial wavelength anomalies, of which many are subtle in expression, are geologic in origin and likely from very shallow-origin sources. Two significant anomalous areas, that are not subtle, exist (1) in the northeast quadrant of the area and (2) in the northwest quadrant of the site. These apparently geologic anomalies follow the trends of drainage features across the 40-acre site.

Northwest quadrant magnetic anomaly. The large magnitude geologic anomaly feature in the northwest quadrant is approximately bounded by grid lines K and M and grid lines 4 and 6, nominally 50 m in east-west extent and variably 5 to 15 m in north-south extent. More subtle expressions of the anomaly extend outside

this area to the northeast and southwest, following the trends of drainage features. An enlarged view of the magnetic anomaly map of this feature is shown in Figure 17, from the Naval Research Laboratory MTADS survey of the site during JPG Phase III (McDonald and Nelson 1999). Although the overall anomalous feature is complex, the most obvious aspect of the anomaly is a dipolar pattern, with a large magnitude negative band (~ -130 nT) to the south and a large magnitude positive band (~ + 115 nT) to the north. The relative signs of the anomaly are opposite to that expected for a buried ferrous feature, pointing to a shallow geologic origin for the anomaly.

The obvious approaches to investigation of the causes of geologic-origin magnetic anomalies are (1) measure laboratory and in situ values of magnetic susceptibility and (2) conduct laboratory mineralogical analyses of soil and rock samples. The approach taken here was dictated by timing and funding constraints. Representative surface (< 10 cm depth) soil samples were acquired from background and anomalous areas for future detailed laboratory investigations, if funding is subsequently available. Two types of measurements were obtained in situ in the anomalous areas (in October 1998 during the Phase IV demonstrations). A frequency domain EM system (Geonics EM38) was used to acquire terrain conductivity and magnetic susceptibility measurements (McNeill 1986) over the area bounded by grid lines K, M, 4, and 6 (61- × 61-m or 200- × 200-ft area.). Measurements were acquired approximately on a 6- × 2-m grid for terrain conductivity and on a 6- × 6-m grid for magnetic susceptibility. Magnetic susceptibility measurements with the EM38 are estimated to be a volume-averaged value for the upper 0.5 m of the subsurface and are relative to the magnetic susceptibility of air. Magnetic susceptibility measurements were also acquired with a laboratory magnetic susceptibility system fitted with a field measurement search coil (Bartington MS2 Magnetic Susceptibility System; Bartington Instruments Ltd. 1994) on a 6-m grid within the same area as the EM38 measurements. In addition, MS2 measurements were acquired along grid lines K and L at approximately 30-m intervals (100 ft). MS2 magnetic susceptibility measurements are estimated to be volume-averaged values for the upper 15-to 20-cm of the subsurface and are relative to the magnetic susceptibility of air (Dearing 1994). For the MS2 measurements, surface vegetation was scraped away and the search coil placed in intimate contact with the soil. Both the EM38 and the MS2 magnetic susceptibility measurements should be considered relative (to air), real-component, volume magnetic susceptibilities in MKS or SI units.

Results of measurements to investigate the nature of the northwest quadrant geologic magnetic anomaly are presented in Figures 18 to 22. Figure 18 is the terrain conductivity map. The EM38 operates at 14.6 kHz and has a nominal depth of investigation of 1.5 m in the vertical dipole mode of operation (McNeill 1986; Butler 1986). Thus the terrain conductivity values in Figure 18 are effectively volume-averaged values for the upper 1.5 m of the subsurface. The conductivity values are low throughout the area (< 1 to ~ 17 mS/m), with the northern half of the area having an anomalously low average conductivity of ~ 2 to 3 mS/m. The same relative patterns of conductivity are evident in Figures 11 and 18. The conductivities in Figure 11, which are a volume-averaged value for a nominal 5-m depth of investigation, are higher than in Figure 18, likely due to the effects of saturated

materials within the 5-m depth but not the 1.5-m depth. There are no obvious correlations to soil type or depth to top of rock (Figure 11 and Llopis et al. 1998).

The EM38 magnetic susceptibility map is shown in Figure 19. Significant variations (an order of magnitude) in magnetic susceptibility occur over horizontal distances of 10 m or less. There are no obvious correlations to the terrain conductivity (Figures 11 and 18). However, the correlation to the Northwest quadrant total magnetic field anomaly (Figures 16 and 17) is obvious. Figures 20 to 22 present the MS2 magnetic susceptibility measurements along lines K, L, and M and compares them to the EM38 values where they overlap. The magnetic susceptibility along lines K and L both show a systematic decrease in values from approximately 6×10^{-4} (SI) in the north to approximately 1×10^{-4} (SI) in the south, with anomalous values in the area of the northwest quadrant magnetic anomaly. Both the EM38 and the MS2 values show the same trends in the anomalous area: proceeding from south to north, there is a high-low-high pattern. The EM38 values are generally higher in magnitude, indicating that magnetic susceptibility increases with depth in the anomalous area (at least in the upper 0.5 m of the subsurface). Line M is west of the major magnetic anomaly feature and, as indicated in Figure 22, the values are erratic and do not show the same pattern within the anomalous area. The close correlation between the magnetic susceptibility variations and the magnetic anomaly itself indicates that the magnetic anomaly is geologic in origin.

Northeast quadrant magnetic anomaly. Investigations of magnetic susceptibility variations in the northeast quadrant magnetic anomaly area were limited by close proximity to the Phase IV demonstration area. Measurements were obtained with the MS2 system at 16 locations on a 30-m (200-ft) grid, bounded by the E, K, 1, and 4 lines. These measurements are shown in Figure 23, where the trends of the major northeast quadrant drainage feature and a smaller drainage feature that crosses the southern part of the measurement grid and leads to the northwest quadrant magnetic anomaly area are also shown. Two additional measurements at the lowest elevation points of the major drainage feature are also shown, and are smaller by factors of 4 than the nearest grid measurement value. Measurements that were not recorded confirmed the fact that within the lowest elevation area of the drainage feature, susceptibility values are smaller by factors of 4 to 5 than values on the side slopes and higher elevations, with a short transition distance (~ 1 m).

Observations and Implications

The dominant environmental/climatic variable affecting geophysical parameters and subsurface detection capability is rainfall. Rainfall directly affects the soil water (moisture) content, which in turn plays a major role in determining the electrical resistivity (conductivity) and dielectric permittivity of subsurface materials. Due to the low hydraulic conductivity (permeability) of near surface soils at JPG, rainfall tends to pond on the surface and infiltrate very slowly. Thus after small rainfall amounts, evapotranspiration will dominate infiltration, particularly during the summer, and increased soil water contents will be limited to very shallow depths for short periods. Following large rainfall amounts, soil water contents are

elevated to greater depths (> 0.5 m) and persist for longer periods (short and long periods are used as purely qualitative terms, since the present work did not quantify the effects). The average surface (~ 10 cm) natural soil water content during very dry site conditions is 13 percent (approximate range 11 to 15 percent), while the average surface water content during very wet site conditions is 33 percent (approximate range 28 to 38 percent). At a given location during dry site conditions, the water content will increase with depth (at least to 1-m depth); while during wet site conditions, the water content will decrease with depth (Figure 7). The water content measurements presented in Figure 8 for three locations and two depths for the duration of the Phase IV demonstrations indicates large fluctuations in surface (~ 10 cm) water contents (as large as 20 percent), while the deeper (~ 50 cm) water content fluctuations are much smaller (5 to 7 percent).

The daily precipitation record during the JPG Phase IV demonstrations is shown again in Figure 24, along with air and soil temperatures and the variation in resistivities and layer thicknesses for the location G7 VES results (Figure 13 and Table 5). There are no obvious correlations between the interpreted VES parameters and temperature. There was a significant rainfall event (1.2 in. or 3 cm) on 20 September 1998, following a month with only trace amounts of rainfall. Following the rainfall event, the layer 1 thickness increased by approximately 0.4 m (with a corresponding decrease in layer 2 thickness) and the resistivity decreased from 620 ohm-m to 500 ohm-m. Overall, the resistivity of layer 1 increases from 450 to 750 ohm-m, with some fluctuation due to rainfall, over the course of the Phase IV demonstrations as a result of increasingly dry conditions and colder temperatures. Layers 2 and 3 resistivities remained practically constant during the demonstrations.

Comparisons of the electromagnetic terrain conductivity maps for wet and dry site conditions for the 40-acre are shown in Figure 10. Due to the depth of investigation (nominally 4 to 5 m) of the terrain conductivity system, the effect of the shallow soil water content changes on conductivity are small (Figure 10 and Table 4). Overall, the terrain conductivity values themselves are small, ranging from approximately 8 to 32 mS/m. The major factor affecting the terrain conductivity is likely the clay layer present nearly everywhere beneath the 40- and 80-acre sites. Beneath the 40-acre site the clay layer varies from approximately 1.5- to 5-m thick and the depth to top of the clay layer varies from approximately 0.3 m to 2 m (Llopis et al. 1998). For example, the shallow depth to top of clay (determined from the VES results) is apparently the cause of the high conductivity features approximately centered about locations D3 and K7, while depth to clay is apparently not the cause of the high conductivity area that extends from approximately I13 to A7 (Figures 10 and 11 and Llopis et al. 1998).

The conductivity and dielectric permittivity variations for small samples indicate significant changes as a function of water content. The laboratory EM properties at 200 MHz shown in Figure 14 show significant changes as a function of water content; this is illustrated in Table 7 for the measured water content extremes for dry- and wet-site conditions. The parameter ranges in Table 7 reflect the scatter in measurement data over the site (Figure 14) at or near the indicated water contents.

Table 7
EM Parameters at 200 MHz for the Average Dry Site and Wet Site Conditions on the 40-Acre Site

Average Water Content, percent	Real Component of Relative Dielectric Permittivity	Attenuation, dB/m	Conductivity, mS/m
Dry Site Conditions – 13	4 – 6	4 – 8	6 – 10
Wet Site Conditions – 33	17 – 19	15 – 25	40 – 60

The negative implications of the spatial and temporal variations of geophysical parameters over the 40-acre site for buried object detection are primarily for the magnetic methods and GPR. While the variations in electrical conductivity (resistivity) do have some implications for the EM induction methods, the impact on detectability considerations is minor for the methods normally employed for UXO detection. For the time domain EM (TDEM) methods that are typically used, the measurement time gate is set such that the transient response from near-surface geologic materials will decay to very small values, and the transient response from shallow-buried (< 2 to 3 m) metallic objects will dominate the superimposed measurement result (Butler et al. 1998). However, spatial variability in the conductivity will result in a small background noise component that will increase as the conductivity and its variability increase. Since the conductivity of metallic ordnance is of the order 10^7 S/m (perfectly conducting, for all practical purposes), only when the object is small and/or buried at depths > 2 to 3 m will the background geologic noise become a serious impediment to ordnance detection by TDEM (Barrow, Khadr, and Nelson 1996). The conductivity contrast of metallic ordnance to surrounding material is typically 10^9 at JPG.

The magnetic susceptibility magnitude and variations over the 40-acre site pose a similar, though potentially greater, implication for UXO detection with TDEM methods than does conductivity. For all other factors fixed, the TDEM response of a ferrous ordnance object is larger by a factor of 4 to 5 than a non-ferrous ordnance object (Das et al. 1990). For model calculations and laboratory measurements of TDEM response for ferrous metallic objects, the results are insensitive to the value of relative magnetic susceptibility, once it is large enough (Das et al. 1990). For conditions at JPG, the *contrast* in relative magnetic susceptibility of ferrous metallic ordnance to surrounding material s as small as 10^5.

Even though the magnetic susceptibility contrast between ordnance and geologic materials at JPG is large, since the total magnetic field anomaly is volume dependent, detection of ordnance objects can become problematic when "large volume" geologic magnetic susceptibility contrasts exist. The spatial distribution of magnetic susceptibility exhibited in Figures 19 to 22 is quite complex, and since the vertical distribution is not known in great detail, it is not possible to model the background total magnetic field anomaly in detail. It is possible, however, to qualitatively examine the magnetic field anomaly along a profile, such as line K. A two-dimensional total field magnetic anomaly calculation is performed for the magnetic susceptibility profile distribution shown in Figure 20. For the calculation, rectangular cross-section cylinders are used with appropriate widths and magnetic

susceptibility values from Figure 20, an assumed thickness of 1 m, and infinite length perpendicular to the profile. Results of the calculation, using a program based on the familiar line integral method (Talwani and Heirtzler 1964; Thorarinsson 1985), are shown in Figure 25; the magnetic susceptibility cross-section model is shown in the lower part of the figure. The maximum positive and negative magnetic field strength values (upper plot) from the calculation are consistent with the measured values discussed previously. The abrupt changes in susceptibility in the model are responsible for the spiked appearance of the calculated anomaly; including many more cylinders in the susceptibility model to simulate the transitional changes in susceptibility, would tend to smooth the calculated anomaly. The complexity of the calculated anomaly and the horizontal gradients are generally consistent with the measured magnetic anomaly (Figures 16 and 17). Detection of buried ordnance with comparable or smaller magnetic magnitudes and comparable spatial wavelengths is problematic in this setting.

Perhaps the most significant implications of geophysical parameters and their spatial and time variability, with respect to buried ordnance detection at JPG, are for GPR. The terrain conductivity maps in Figures 10, 11, and 18, which are frequently good predictors of GPR "performance," suggest variable GPR performance over the 40-acre site at a given time. A widely quoted criteria for qualitative prediction of GPR performance is based on conductivity: < 10 mS/m - excellent GPR performance; 10 to 30 mS/m - marginal to good GPR performance; > 30 mS/m poor or problematic GPR performance. For example, the dry site conditions map indicates conductivities ranging from 10 mS/m to > 30 mS/m, which are volume-weighted averages of the upper 4 to 5 m. Also, the data in Figure 14 and Table 7 suggest variable GPR performance as a function of environmental site conditions. For *dry site conditions*, GPR performance in terms of depth of investigation should be fair to good for buried UXO detection nearly everywhere on the 40-acre site.

Two rule-of-thumb guides for estimating depth of investigation d_{max} for GPR (i.e., maximum depth at which a high contrast buried feature can be detected) are (Annan and Cosway 1992, Annan and Chua 1992):

$$d_{max} < 30/\alpha \; ; \; d_{max} < 35/\sigma \; ;$$

where α is the EM attenuation in dB/m, σ is the conductivity in mS/m, and d_{max} is in m. These rules-of-thumb are based on experience with GPR in a variety of geologic settings and transmitter frequencies and the fact that most commercial GPR's "can typically afford to have a maximum of 60 dB attenuation associated with conduction losses (Annan 1997)." For the maximum in the attenuation and conductivity ranges for dry site conditions in Table 7 (200 MHz; samples from ≤ 1 m), d_{max} is 3.5 m for both rules-of- thumb. Rule-of -thumb depth of investigation predictions using the dry site conditions conductivities from Figures 10 and 11 range from approximately 1 to 3.5 m. Based on previous discussions about the subsurface geology, specifically that the variations in terrain conductivity are primarily controlled by the depth to the clay-layer (layer 3; see Figure 12 and Table 5), buried UXO detection with GPR for *dry site conditions* at JPG should be possible to depths of approximately 3 m in many areas.

For the extreme wet site conditions (using properties in Table 7), the rule-of-thumb guides give estimates of depth of investigation ranging from 0.5 to 2 m, with $d_{max} < 1$ m, most likely. Since the Table 7 properties are for depths < 1 m, it follows that GPR detection of UXO buried greater than 1 m depth will be problematic and likely extremely difficult for wet site conditions.

The GPR considerations thus far do not specifically address the issue of frequency dependence of depth of investigation. GPR surveys conducted at JPG as part of the JPG Phase IV supplemental site characterization work (Arcone et al. 1998, Llopis et al. 1998) used a number of different center frequency antennae. The references document the first reliably reported detection of UXO at JPG by GPR. Table 8 lists practical depths of penetration at JPG as a function of frequency for intermediate or moist site conditions (i.e., not the extreme dry or wet conditions of Table 7).

Table 8
Practical GPR Depths of Investigation at JPG for Selected Antenna Frequencies at Intermediate (Moist) Site Conditions

GPR Antenna Center Frequency, MHz	Depth, m	Type Target	Comments
50	> 3.5 m	Geologic Interface	Depth of investigation for localized high-contrast feature greater than interface depth
100	> 2 m	Geologic Interface	See Above
200	> 1 m	Interface; Localized Feature	See Above
300	1 m 2 – 3 m	UXO Noise/Attenuation Limit	Well-defined UXO signatures; Arcone et al. (1998)
600	< 0.5 m < 1 m	UXO Noise/Attenuation Limit	High Attenuation at this Frequency

The discussion on GPR thus far has considered limits on UXO detection capability caused by site conditions and signal attenuation. Another factor that is equally important in terms of detection implications is the antenna beamwidth in the subsurface, which depends on the dielectric permittivity. For example, the mean value of the real part of the relative dielectric permittivity, determined from an analysis of 118 diffraction signatures in the 300 and 600 MHz GPR records acquired at JPG, is 10.4. For this dielectric permittivity value and commercial dipole antennas, the beamwidth perpendicular to the profile or transect direction (in the plane of antenna polarization) is 22 degrees (Llopis et al. 1998; Arcone et al. 1998). This implies that a UXO would need to lie in or very close to the plane of the profile to insure detection, since out of plane reflections/diffractions will be highly attenuated. For the considerably higher dielectric permittivity values for some areas of the site and particularly for wet site conditions (Table 7 and Figure 14), the beamwidth becomes even smaller.

3 Geophysical Signature Considerations for JPG UXO Baseline Targets

Background

The planning and execution of the UXO technology demonstration program at JPG evolved and improved for each phase. In general, the phases became easier for the demonstrators for a number of reasons that were explored in Chapter 1. The JPG phases became progressively more realistic and focused in terms of the scenarios, while at the same time becoming easier for detection due to shallower ordnance burial depths and less closely spaced items. In this chapter, only the 40-acre (16 hectare) site is considered. Phase I is not considered in this report due to the uncertainties in the baseline target database and lack of sufficient data to perform geophysical signature calculations. For example ordnance items are classified as small, medium and large in size and as bomb, projectile, mortar, and cluster in type in the Phase I database, while nonordnance items are just identified as "others" and also assigned small, medium, and large size classification. The small, medium and large size classifications refer to ranges of ordnance diameter (e.g., medium refers to the range 100 to 199 mm diameter). For Phase I, the following information summarizes the baseline targets:

144 -- Ordnance targets, including bombs, projectiles, mortars, and clusters
9 – Clusters, included above, made up of closely spaced aircraft cannon rounds (e.g., 20 and 30 mm), classified solely as small, medium and large
22 – Mines (TS-50 and VS-50 anti-personnel mines)
75 – Others

Burial depths and orientations for Phase I ordnance targets were selected to correlate to depth ranges and orientations typically observed for each class of ordnance (AEC 1994). For the three major classes of ordnance, the *maximum* depths are: bombs – 4.1 m; projectiles – 2.2 m; mortars – 1.4 m.

The Phase II baseline database is more complete, in that emplaced ordnance items are more carefully documented in terms of orientation, length, diameter and specific type classification (e.g., 81-mm mortar, 500-lb bomb, etc.). Clusters are also better documented (e.g., 81 mm x 8). Also the nonordnance items are identified in greater detail (e.g., 5 lb 16d nails, 55 gal drums x 2), although there are some errors (e.g., "PVC pipe" identified as a ferrous material) and incomplete information (e.g., construction material, banding, wire, etc.). Most of the nonordnance targets are not documented in sufficient detail to enable any type of predictive geophysical signature response modeling. A synopsis of the Phase II baseline is as follows:

160 - Ordnance targets
9 - Clusters (included above)
69 - Other

The range of burial depths for each ordnance type classification is shown in Figure 1. Average (mean) burial depth for all ordnance baseline targets is 0.9 m. The median separation distance of ordnance baseline targets is 5 m, while 38 percent of all targets are closer than 2 m to another ordnance target.

For Phase III, the baseline ordnance targets were segregated into the four scenarios described in Chapter 1. The Phase III baseline target data were released to the demonstrators and the public in February 1998. Ordnance descriptions and burial depth and orientation descriptions are complete and adequate for predictive modeling. Nonordnance baseline targets are still not described in sufficient detail for even qualitative modeling. Clusters of ordnance items were eliminated for this phase. The median separation distance between ordnance targets increased to 7 m, and only 2 percent of all targets are spaced closed than 2 m to each other. The average burial depth for all ordnance targets is 0.4 m, and the range of burial depths by ordnance type classification is shown in Figure 1. A synopsis of the Phase III baseline is as follows:

Scenario 1 – Aerial Gunnery Range:

43 - Ordnance Targets
78 - Nonordnance Targets
5.04 m - Smallest distance between two ordnance targets

Scenario 2 – Artillery and Mortar Range:

67 - Ordnance Targets
50 - Nonordnance Targets
4.88 m - Smallest distance between two ordnance targets

Scenario 3 – Grenade and Submunitions Range:

98 - Ordnance Targets
39 - Nonordnance Targets
2.73 m - Smallest distance between two ordnance targets

Scenario 4 – Interrogation and Burial Area:

53 - Ordnance Targets
72 - Nonordnance Targets
3.36 m - Smallest distance between two ordnance targets

The Phase III baseline target site layout is illustrated in Figures 26 and 27, where the Scenarios 1 to 4 are the southeast, northwest, southwest, and northeast quadrants of the 40-acre (16-hectare) site, respectively. All baseline target locations are shown in Figure 26, while only the baseline ordnance targets are shown in Figure 27 and distinguished by ordnance class.

The Phase IV baseline database was released in February 1999. The baseline consists of 160 targets, with the location of each target indicated by pin flags during the demonstrations. The distribution of the baseline targets was concentrated in four areas of the 40-acre site, as shown in Figure 28. The ratio of ordnance to nonordnance is approximately the same in each area, with no differentiation in terms of ordnance type, class, or burial depth according to area. The baseline consists of 50 ordnance and 110 nonordnance items. The maximum burial depth of any item is 1.8 m, and the distribution of burial depths as a function of ordnance type is shown in Figure 28.

Geophysical Signature Modeling

Total magnetic field signatures

Background. The total magnetic field anomaly signatures of the baseline ordnance targets for Phases II and III were simulated with a multipole expansion magnetic modeling program that uses a prolate spheroid model for the ordnance items (Butler et al. 1998, McFee and Das 1990). Validation of the magnetic modeling program is documented in Butler et al. 1998. The program considers only the anomaly field induced by the Earth's field, i.e., does not include a remanent magnetization component. For JPG, the nominal Earth's magnetic field is approximately described by (Campbell 1997, Bloxham 1995):

Declination: 3 degrees West (assumed to be 0 for the calculations)
Inclination: 70 degrees (below horizontal)
Total Field Strength: 57,000 nT

For small magnetic surveys such as at JPG, the Earth's field does not vary spatially; thus the targets at JPG are considered to be in a uniform magnetic field. The induced magnetic anomalies from ferrous targets are superimposed on this uniform inducing field. For each ordnance item in the Phase II and III baseline, the input to the modeling program consists of the depth to the approximate geometric center, length, diameter, and spatial orientation of the ordnance and the parameters of the Earth's field. The spatial orientation consists of two angles (in the terminology of the baseline target database): the *declination* in degrees (or dip or inclination) of

the long axis below horizontal; the *azimuth* between the projection of the long axis on the horizontal and north, with positive defined as clockwise from magnetic north. Although the relative magnetic permeability (μ_r) of the ferrous target is an input to the modeling program, the permeability is held constant (μ_r = 1,000) for all the JPG signature modeling, since the signature magnitude is insensitive to permeability for μ_r > 150 to 200 (e.g., McFee and Das 1990).

Examples and phenomenological observations. Unlike simple magnetic dipole models of ordnance, which generally assume an equivalent mass or an equivalent radius (equal volume) uniformly magnetized sphere for the ordnance, the magnetic modeling program used here captures the demagnetization effects caused by the elongated shape of ordnance. The simple dipole model or uniformly magnetized sphere has no orientation dependence. The response calculation for the prolate spheroid model, however, depends on the orientation of the model in space relative to the earth's magnetic field. The orientation dependence effect is illustrated in Figure 29 for four orientations of a 105-mm artillery projectile model. *The model results in Figures 29a, c, and d correspond to actual Phase III baseline ordnance cases,* while the result in Figure 29b is included for completeness of the calculation set. The two left-side plots for each case are 3-D and 2-D (top and bottom, respectively) representations of the total field anomaly. The top right plot contains three north-south profiles of the total field anomaly; one profile crosses the geometric center of the model, and the other profiles cross 1-m east (y = -1.0 m) and 1-m west (y = 1.0 m) of the center profile. The inset legend gives the maximum and minimum total field values and the distance between the maximum and minimum for each profile. The distance between maximum and minimum is an important parameter, because it is one measure of the "spatial wavelength" of the anomaly and is related to the depth of the model (defined as the modeled burial depth plus the measurement plane height). Finally the lower right plot for each case is a 3-D portrayal of the prolate spheroid UXO model.

Cases a and b in Figure 29 are models oriented north-south and dipping at 0 and 45 deg, respectively. The total field anomalies (as well as the model predictions) for both cases are symmetric about a vertical, north-south plane and exhibit the familiar dipolar anomaly response to the earth's inducing field. Two features of the two cases are notable: (1) the spatial wavelength measures for the principal profiles are approximately equal; (2) the much larger magnitude for the 45 deg dip case. For the first feature, the depth is $\sim 0.8\ \lambda$, where the spatial wavelength measure λ is the distance between the maximum and minimum values. Although the same approximate relationship holds for the uniformly magnetized sphere, the equivalence will not hold for general orientations of the ordnance model. Figures 30-32 are plots of the spatial wavelength measure λ versus depth (burial depth plus measurement plane elevation) for the 60-mm mortars, 105-mm projectiles, and 250-lb bombs, respectively, from the Phase III baseline target set (*all orientations*). The straight lines in each plot are for the relations depth = λ (solid line) and depth = 0.8 λ (dashed line). Depth errors of 20 to 30 percent can result from depth estimates based on the uniformly magnetized sphere model.

The much larger magnitude for the 45-deg dip case results from two contributing factors: (1) the primary factor is that the induced field increases as the ori-

entation of the model approaches the orientation of the earth's field; (2) a secondary factor is that, as the model is inclined from horizontal, part of the model is located closer to the surface even though the depth to the center remains fixed. The case of maximum induced field would be for a case when I = 70 deg and A = 90 deg, where the long axis of the model is aligned with the earth's field direction. Maximum positive total field anomalies for all 105-mm projectiles (*all orientations*) in the Phase III baseline target set versus depth are shown in Figure 33, where the solid line represents a $1/depth^3$ decrease in anomaly magnitude with depth. The six outlier cases (circled points in Figure 33) are for baseline targets with I = 45 deg.

For cases c and d in Figure 29 with I = 45 deg, the long axis of the model is oriented outside the vertical plane containing the earth's field vector. The total field anomaly is no longer symmetrical about a north-south vertical plane, and the anomaly pattern is rotated in the direction of the azimuth of the long axis of the model. For the A = 45 deg case, the anomaly pattern rotation is approximately 30 deg; and for the A = 90 deg (east-west) case, the anomaly pattern is rotated approximately 45 deg (also see Altshuler 1996). When I = 0 deg and A = 90 deg (horizontal and east-west orientation; not shown), the model as well as the induced anomaly are symmetrical about the vertical north-south plane; the anomaly for this case is the minimum for any orientation of this model at the given depth.

Phase II and III baseline ordnance target set total magnetic field anomaly calculations. The ordnance targets and mean burial depths and burial depth ranges for Phases II and III are indicated in Figure 1. For each ordnance item, all orientations are included and the burial depths are to the shallowest point of the ordnance item (i.e., the depth convention used for the baseline target database). Figure 34 is a representation of the maximum positive total magnetic field anomaly as a function of ordnance type corresponding to Figure 1. For the magnetic anomaly calculations, the burial depths in Figure 1 are converted to model centered depths and a measurement elevation of 0.25 m is assumed. The magnetic anomaly calculation results in Figure 34 indicate the mean and range of total magnetic field anomaly values for each ordnance type for all orientations. The lines connecting the mean anomalies for each ordnance type dramatically emphasize that the magnetic anomalies are larger for Phase III, although there is considerable overlap in many cases. For the 81-mm mortar, the Phase III mean anomaly is approximately 30 nT larger than the Phase II mean anomaly, although the range of anomalies for Phase II is much larger than Phase III. The mean anomaly for the 175-mm projectile is approximately 800 nT larger for Phase III than Phase II. For the 60-mm mortar, the situation is reversed and the mean anomaly is larger in Phase II.

The smallest calculated peak positive total magnetic field anomaly for any of the Phase III baseline ordnance targets is approximately 18 nT. For the Phase II baseline ordnance targets, however, various 81-mm mortar, 90-mm projectile, and 152-mm projectile targets have anomalies < 10 nT. Examination of detailed total magnetic field survey maps of the 40-acre site indicate that magnetic background varies considerably over the site. Examples were discussed in Chapter 2, where well-defined "localized background" variations > ± 100 nT exist due to localized magnetic susceptibility variations. However, in general an area is characterized by a noise level that is "random" and caused by random variations in soil magnetic

susceptibility, sensor motion, induced sensor noise, and ferrous clutter. Qualitatively this random magnetic background varies from areas that are relatively quiet ($\leq \pm$ 5 nT) to areas that are "noisy" ($\leq \pm$ 20 nT). A commonly used rule-of-thumb is that an anomaly should be two times the background noise level to be reliably detected. Thus even for the magnetically quiet areas of the 40-acre site, detection of some Phase II baseline ordnance targets could be problematic. For the magnetically noisy areas, detection of some Phase III baseline ordnance targets could be problematic as well as a significant number of Phase II targets.

Sampling considerations (measurement spacing). As shown in Figure 29 in the example output plots from the magnetic modeling program, a measure of the spatial wavelength, λ, defined as the distance between maximum and minimum values along a profile line, is determined for north-south and/or east-west profiles. Also, Figures 30-32 plot the spatial wavelength measure versus depth (burial depth plus measurement height). The required measurement spacing to properly characterize the total magnetic field anomaly of a compact ferrous object is related to the spatial wavelength (or wavenumber = 2π/wavelength) spectral content of the anomaly (Nyquist sampling interval considerations; e.g., Blakely 1995). Of more practical utility for analyses of results or survey planning are the rules-of-thumb listed below, which in many cases will be equivalent:

a. Since the spatial wavelength measure λ is related to depth (Figures 30-32), choose measurement spacing (grid spacing) < 1/2 depth of shallowest ordnance object of interest; if detection of objects from the surface and deeper is required, then choose measurement spacing < 1/2 measurement height.

b. Choose measurement spacing to give at least 5 data points across the total extent of the total field anomaly.

c. Choose measurement spacing < $\lambda/2$; for a monopolar type anomaly, choose measurement spacing < 1/2 times the distance across the anomaly peak at the half-maximum value.

d. For detection of large ordnance objects at depths less than half their length, where the spatial wavelength measure is related to both object length and burial depth, choose measurement spacing ~ 1/5 the length of the ordnance item.

Clearly the manner in which these rules-of-thumb are used will depend on the situation. For planning purposes, magnetic measurements should be acquired at the minimum spacing predicted/expected for the type ordnance and burial depths at a site of interest. For assessment of magnetic survey data at a test site, the rules-of-thumb can be used to determine the adequacy of the field data acquisition measurement spacing for the baseline target set. For a live site survey assessment, the measurement spacing used for the survey can be used to predict the UXO, ordnance types and burial depths, that might have a significant probability of not being detected by the survey. A typical measurement height during JPG Phases II, III and IV is 0.25 m, and many of the ordnance items are at depths of a few

centimeters. Thus using rule-of-thumb 1 above indicates a desired measurement spacing of 0.15 to 0.20 m (15 to 20 cm); this spacing was achieved by many of the demonstrators at JPG along survey tracks, but not between tracks. From Figure 30, for Phase III 60-mm ordnance targets, rule-of-thumb 2 indicates a desired measurement spacing of ~ 0.2 m (~ 1/2 of the smallest spatial wavelength).

Time domain electromagnetic (TDEM) induction signature considerations

Background. Due to the complexity of general solutions of TDEM responses for realistic UXO geometry, the considerations in this section will be brief and more qualitative than the preceding section on baseline ordnance target magnetic signatures. Rigorous TDEM analytical solutions to date are for simple geometric models, e.g., layered earth, spheres, plates, and circular cylinders (McNeill and Bosnar 1996, Barrow et al. 1996, Ward and Hohmann 1987). Das et al. (1990) extend *consideration* to a prolate spheroid but point out that rigorous analytical solutions do not exist for the general case of a conducting, permeable spheroid. Analytical solutions often require numerical evaluation or approximation, but do not require problem discretization, as in finite difference, finite element, boundary integral, or hybrid computational techniques. Numerical modeling, involving space, time and/or frequency discretization, complex/realistic geometry, and the full range of physical properties and processes, is notoriously computationally intensive (Hohmann 1987, Laveley 1996); currently this type numerical modeling is reserved for phenomenological studies, but is not practical for the repetitive, iterative calculations generally required for geophysical inversion or large target sets. Thus numerical modeling and even analytical solutions resort to approximations of various types: asymptotic approximations; quasi-static solutions; low frequency or high frequency limit solutions for FDEM; early time or late time solutions for TDEM. Many of these approximations in time or frequency domains are equivalent for different combinations of physical properties (Wait 1982, Butler and Fitterman 1986, Butler 1986, Ward and Hohmann 1987).

Electromagnetic induction methods, particularly TDEM methods, are used extensively for UXO detection and mapping surveys. An extensively used TDEM system at JPG, the Geonics EM61 (standard system) consists of a 1-m × 1-m transmitter (Tx) coil and two 1-m × 1-m receiver (Rx) coils, with one Rx concentric to the Tx and the second Rx offset 0.4 m vertically. The EM61, like many TDEM systems, operates by rapidly turning off a current in the Tx and detecting transient (decaying) magnetic fields at the Rx's from induced current transients in the subsurface. The physics of the transient induction process and descriptions of general purpose TDEM systems are reviewed by Butler and Fitterman (1986), and the induction process in compact, conductive, permeable metallic objects is outlined descriptively by McNeill and Bosnar (1996). General purpose TDEM systems sample the transient signal with many time gates or channels, typically 20-30. The standard EM61 measures the vertical component of the secondary field and integrates the transient over one time gate extending from 0.47 to 0.87 ms; the time gate is selected to enhance sensitivity to metallic objects (for the Naval Research Laboratory's MTADS system, the time gate is moved closer to the transmit pulse

termination for even higher sensitivity; Nelson et al. 1997). The two Rx measurements for the standard EM61 give two integrated magnitude measurements and their difference (or vertical gradient) as a function of position as the system is pulled along the ground surface. Typically the EM61 data are displayed in map form, and signatures of shallow metallic objects are apparent, allowing accurate location of the positions of the objects. Depths can be estimated from the difference in top and bottom Rx-coil responses. Also, depth and size estimates are commonly estimated from the spatial wavelengths of the signatures and assumptions of a spherical model. Current efforts attempt to apply empirical adjustments based on measured signatures to spherical model predictions to account for ordnance shape and orientation effects (Barrow et al. 1997; Barrow, Khadr, and Nelson 1996) with increasing success.

McNeill and Bosnar (1996) discuss the response of compact, simple geometry objects to static and transient EM fields. Specifically, they reference spheres, plates (discs), rods (or cylindrical shells), and actual UXO and consider the contributions of finite electrical conductivity and finite magnetic permeability to the overall TDEM response. They present measured time decays of the induced fields in ferrous and non-ferrous spheres, plates and cylindrical shells and actual ordnance items; the responses for inducing fields parallel to and perpendicular to the long axis are given for the ordnance items. McNeill[1] (J.D. McNeill, Private Communication, July 1997) proposes an initial approach for time domain response of UXO that utilizes orthogonal dipoles, along and perpendicular to the long axis, to represent the total TDEM spatial response. The procedure then modifies the relative contribution of each dipole according to the measured decay characteristics of specific ordnance items, determined with the ordnance item parallel to and perpendicular to the primary inducing field of an EM61 Tx. The capability of this approach to replicate general observations of TDEM spatial signatures is shown by Butler et al. (1998)

TDEM response calculations for selected Phase III baseline ordnance items. Considerations in this section use the quasi-empirical approach of Barrow et al. (1997) to estimate the TDEM signatures for the standard EM61 configuration. Consistent with model studies (Butler et al. 1998) and field measurements, the following key features are apparent:

a. The anomaly response pattern is elongated in the direction of the long axis of the ordnance item.

b. The maximum of the response pattern is shifted in the "updip" direction of an inclined ordnance item.

c. The anomaly response pattern rotates unchanged as the ordnance item azimuth changes, for $I \neq 90$ deg.

d. The model signatures exhibit an intuitive transition from bi-orthogonally symmetric (symmetric about both the azimuth direction and perpendicular

[1] Personal communication, July 1997, James D. McNeill, Geonics Limited, Mississauga, Ontario Canada.

to the azimuth) for an inclination of 0 deg, proceeding to axially symmetric about the 45-deg azimuth for an inclination of 45 deg, and finally to completely radially symmetric for an inclination of 90 deg.

e. For a given ordnance type, the maximum anomaly response decreases as depth increases; the rate of decrease of peak anomaly response varies from $1/depth^3$, for very shallow depths of burial, to $1/depth^6$, for depth > 1.6 m (Bosnar 1999[2]).

These features are illustrated by the examples in Figures 35 to 37 from the JPG Phase III baseline ordnance set.[3] The case in Figure 35 is for a 155-mm projectile at an inclination of 90 deg, and has the required radial symmetry. Figure 36 is also for a 155-mm projectile, but the ordnance has an inclination of 45 deg and an azimuth of 45 deg. The anomaly response in Figure 36 exhibits symmetry about the azimuth of the ordnance item (coincident with the azimuth of the long axis of the projectile), elongation along the azimuth of the ordnance, and illustrates the "updip migration" of the maximum of the response pattern. Finally, Figure 37 presents the results for a 105-mm projectile oriented north-south and inclined horizontally (i.e., I = 0, A = 0). The anomaly response in Figure 37 is biaxially symmetric and elongated along the long axis of the ordnance item.

In order to illustrate the ranges of EM61 TDEM response for ordnance items, a selected number of targets were modeled[3] using the quasi-empirical approach of Barrow et al. (1997) from the JPG Phase III ordnance target baseline. The selected targets include the minimum and maximum depth cases for each ordnance type and a representative number of different orientations. Results of these model predictions are shown as range bars in Figure 38. The peak TDEM response anomalies vary by approximately 3 orders of magnitude, somewhat larger than the peak positive total magnetic field anomaly variation for Phase II and III (Figure 34). At sites with very low background geologic noise, buried objects producing anomaly magnitudes > 1 – 2 mV are detectable, since typical instrument noise levels are < 1 mV (Barrow, Khadr, and Nelson 1996). At the JPG sites, considerable areas exist where the background noise on TDEM maps is ≤ ± 2 mV, although some areas have geologic background noise ~ ± 5 – 10 mV. From Figure 38, only a small number of ordnance items are expected to produce peak anomalies < 2 mV, while a substantial number produce anomalies < 10 mV. Due to the peak response falloff with depth discussed previously and considering the higher ordnance depth ranges for JPG Phase II, a substantial number of baseline ordnance targets in Phase II are expected to produce anomalies < 1 – 2 mV. Thus while only a small number of ordnance targets at JPG Phase III are problematically detectable with an EM61 type TDEM system, a larger number of Phase II ordnance targets are potentially problematic, depending on the background noise magnitude and spatial wavelength characteristics of the area around the burial locations.

---

[2] Personal communication, February 1999, Miro Bosnar, President Geonics, Limited, Mississauga, Ontario Canada.

[3] Personal communication, April 1998, Nagi Khadr, AETC Inc., Arlington, VA.

Sampling considerations. In addition to depth and ordnance length considerations, the spatial wavelengths of TDEM anomaly responses are dependent on the dimension of the Tx coil (for the EM61 system the Tx is a 1-m square). For total depths (burial depth plus lower sensor height) less than the Tx dimension, the Tx dimension is the controlling factor on anomaly spatial wavelength; while for burial depths > 1 m, the depth is the controlling factor on spatial wavelength, for all except the larger ordnance items (e. g., 155-mm projectiles and larger). Since TDEM anomalies for ordnance are generally monopolar, though not necessarily symmetric about a vertical axis, the full-width at half-maximum is a convenient measure of spatial wavelength. Requiring a minimum of three measurements across the smallest full-width at half-maximum measure will be adequate for most cases covered by the prior considerations. *Thus for the EM61 system, a measurement spacing < 0.5 m is required to adequately delineate ordnance TDEM response anomalies.* Most demonstrators using EM61-like systems at JPG Phases II and III easily met the measurement spacing requirement along measurement tracks, although the track spacing for some demonstrators was only marginally adequate or not adequate in some cases.

4 Summary and Conclusions

Summary

This report considers environmental conditions and geophysical properties and their spatial and temporal variability for the JPG UXO test sites. Specifically the variability of the conditions and parameters for the 40-acre (16 hectare) site and implications for ordnance detectability are examined. The baseline target sets for Phases II, III, and IV are discussed and the ordnance burial depths are compared. Finally, geophysical anomaly signatures are calculated for Phase II and III baseline ordnance items. The peak magnitudes are compared to general noise and site specific noise backgrounds for detectability considerations. Anomaly spatial wavelengths are examined and compared to Phase II and III demonstrator data acquisition densities with regard to anomaly detection.

Conclusions

Rainfall and its resulting affect on soil water content is the dominant environmental parameter. While temperature does not have a significant direct affect on geophysical properties and their spatial and temporal variability, it indirectly affects soil moisture evaporation. Due to the small vertical, hydraulic conductivity of the JPG soils, soil water tends to remain very near the surface after rainfall, infiltrating to greater depths very slowly. Since electrical conductivity is strongly dependent on soil water content, the near surface soil electrical conductivity varies significantly between wet site conditions (for several days following rainfall events) and dry site conditions. Implications of wet versus dry site conditions for GPR detection of buried ordnance are significant; ordnance buried below the near-surface high water content zone during wet site conditions may *not* be detectable, while the same ordnance may be detectable during dry site conditions. Likewise for the TDEM method, the high water content near surface zone will have increased soil conductivity, resulting in a decreased conductivity contrast and a decreased signal to noise ratio. While the actual ordnance detection implications for TDEM are minor, cases where ordnance detection are predicted to be marginal under dry conditions may be *undetectable* under wet site conditions (generally cases where the ordnance is very small and/or deeply buried). Shallow soil water contents as well as electrical conductivity are observed to correlate to soil type and topography. Soil water content and electrical conductivity are not expected to impact ordnance detection by magnetic surveys at any time or location on the site.

A significant geological feature affecting spatial variability of electrical conductivity as a function of depth is the presence of a clay layer predicted to be present under a majority of the site. The clay layer is as shallow as 0.3 m and is 1.5- to 5-m thick. At locations where the clay layer is shallow and ordnance items are buried within the layer, detection by GPR becomes very problematic for any site condition (wet or dry). Also, the electrical conductivity contrast is reduced for ordnance items buried in the clay layer decreasing the signal to noise ratio for TDEM surveys. Above the clay layer, the material is predominantly very fine-grained quartz, with only small amounts of clay minerals (refuting prior claims that high-clay content soils limited the depth of investigation of GPR at the JPG sites). High dielectric permittivity values at the site results in small GPR antennae beamwidth perpendicular to the survey line direction; this results in small reflected and diffracted GPR signals from objects not directly under the survey line. The small GPR antennae beamwidth decreases the detectability of shallow, localized buried objects such as ordnance.

An unexpected result of the investigations is the discovery of significant spatial variation in near-surface magnetic susceptibility. The magnetic susceptibility of materials in the upper 0.5 m of the site can vary by an order of magnitude over horizontal distances of 2 to 3 m. The magnetic susceptibility variations produce "geologic" magnetic anomalies that significantly interfere with detection of the magnetic anomalies of buried ordnance and also can reduce the magnetic susceptibility contrast, decreasing the signal to noise ratio for magnetic surveys. The most significant geologic magnetic anomalies with associated higher background noise levels occurs in the northwest and northeast quadrants of the site and generally correlate spatially with the major drainage features of the site. The magnetic susceptibility anomalies could also contribute to poor GPR and TDEM performance in areas with high susceptibility and susceptibility variations.

Consideration of mean depth of burial of baseline ordnance leads to the following conclusions regarding general ease of detection and/or discrimination for Phases II, III, and IV: (a) Phase II was more difficult than both Phase III and IV; (b) Phase III was more difficult than Phase IV for small ordnance items (e.g., 60 mm, 81 mm, and 76 mm); (c) Phase IV was more difficult than Phase III for larger ordnance items (e.g., > 90 mm in size). These conclusions are illustrated by comparison of the maximum positive values of the total magnetic field signatures.

Examination of high-resolution, high-accuracy total magnetic field anomaly maps of the 40-acre site, reveals that the magnetic background (noise levels) of the 40-acre site vary from "quiet" ($< \pm 5$ nT) to noisy ($\sim \pm 20$ nT). The predicted total magnetic field anomalies for the Phase II and III baseline ordnance items indicate the minimum peak positive anomaly magnitude for Phase III is 18 nT, while some Phase II baseline ordnance targets have anomaly values < 10 nT. For the magnetically quiet areas of the site, only some of the Phase II baseline ordnance targets are problematically detectable. For magnetically noisy areas of the site, however, a small number of Phase III ordnance targets and a significant number of Phase II targets become problematically detectable.

Similarly, EM61 TDEM maps indicate considerable areas exist where background noise levels are < ± 2 mV, although some areas have noise levels ~ ± 5 - 10 mV. While only a small number of Phase III ordnance targets are problematically detectable with an EN61-type TDEM system, a significantly larger number of Phase II targets could be problematically detectable, depending on the burial location at the site.

General Extrapolation

The results documented in this report indicate the need to evaluate the results of UXO detection surveys based on site-specific criteria. That is, the probability of detection and false alarm rates can vary considerably (1) from site to site and (2) for areas at a given site based on site- or area-specific geologic conditions. Selection of appropriate geophysical survey methods should be guided by a priori assessment of environmental parameter variations, topography, accessibility, geology and soil type variations, and geophysical parameter variations. For live site survey planning, geophysical signature modeling for expected ordnance types and depths should be conducted to evaluate UXO detectability, using site-specific signal to noise considerations.

References

Altshuler, Thomas W. (1996). "Shape and orientation effects on magnetic signature prediction for unexploded ordnance," *Proceedings of the UXO Forum 1996*, Williamsburg, VA, 282-291.

Altshuler, Thomas W., Andrews, Anne M., Dugan, Regina E., George, Vivian, Mulqueen, Michael P., and Sparrow, David A. (1995). "Demonstrator performance at the unexploded ordnance advanced technology demonstration at Jefferson Proving Ground (Phase I) and implications for UXO clearance," IDA Paper F-3114, Institute for Defense Analyses, Alexandria, VA.

American Geophysical Union. (1995). *Global earth physics: A handbook of physical constants.* Thomas J. Ahrens, ed., American Geophysical Union, Washington, DC.

Annan, A. P. (1997). *Ground penetrating radar workshop notes.* Sensors and Software, Inc., Mississauga, Ontario, Canada.

Annan, A. P. and Cosway, S. W. (1992). "Ground penetrating radar survey design," *Proceedings of the Symposium on Application of Geophysics to Engineering and Environmental Problems, SAGEEP 92*, Oakbrook, IL, 329-351.

Annan, A. P. and Chua, L. T. (1992). "Ground penetrating radar performance predictions," Paper 90-4, The Geological Survey of Canada, 5-13.

Arcone, Steven A., Delaney, Allan J., Sellmann, Paul V., and O'Neill, Kevin. (1998). "UXO detection at Jefferson Proving Ground using ground-penetrating radar," *Proceedings of the UXO Forum 1998 (24 pgs, CD ROM).*

Barrow, Bruce, Khadr, Nagi, and Nelson, Herbert H. (1996). "Performance of electromagnetic induction sensors for detecting and characterizing UXO," *Proceedings of the UXO Forum 1996*, Williamsburg, VA, 308-314.

Barrow, Bruce, DiMarco, Robert, Khadr, Nagi, and Nelson, Herbert. (1997). "Processing and analysis of UXO signatures measured with MTADS," *Proceedings of the UXO Forum '97.* Nashville, TN, 8-18.

Bartington Instruments LTD. (1994). *Operation manual for MS2 Magnetic Susceptibility System.* OM0408 Issue 1, Bartington Instruments LTD, Oxford, UK.

Bennett, Hollis H. (1995). "Remote sensing of surface unexploded ordnance at Black Hills Army Depot, Edgemont, South Dakota," Technical Report EL-95-28, U.S. Army Engineer Waterways Experiment Station, Vicksburg, MS.

Blackhawk-Geometrics, Inc. (1998). Private communication. Blackhawk-Geometrics, Inc., Golden, CO.

Blakely, Richard J. (1995). *Potential theory in gravity and magnetic applications.* Cambridge University Press, New York, NY.

Bloxham, Jeremy. (1995). "Global Magnetic Field," in *Global Earth Physics: A handbook of Physical Constants*, Thomas J. Ahrens ed., American Geophysical Union, Washington, DC.

Burger, H. Robert. (1992). *Exploration geophysics of the shallow subsurface.* Prentice Hall, Englewood Cliffs, NJ.

Butler, Dwain K. (1975). "An analytical study of projectile penetration into rock," Technical Report S-75-7, U.S. Army Engineer Waterways Experiment Station, Vicksburg, MS.

Butler, Dwain K. (1986). "Military Hydrology, Report 10: Assessment and field examples of continuous wave electromagnetic surveying for ground water," Miscellaneous Paper EL-79-6, U.S. Army Engineer Waterways Experiment Station, Vicksburg, MS.

Butler, Dwain K. and Fitterman, David V. (1986). "Transient electromagnetic methods for ground-water assessment," Miscellaneous paper GL-86-27, U.S. Army Engineer Waterways Experiment Station, Vicksburg, MS.

Butler, Dwain K., Cespedes, Ernesto R., Cox, Cary B., and Wolfe, Paul J. (1998). "Multisensor methods for buried unexploded ordnance detection, discrimination, and identification," Technical Report GL-98-10, U.S. Army Engineer Waterways Experiment Station, Vicksburg, MS.

Campbell, Wallace H. 1997. *Introduction to geomagnetic fields.* Cambridge University Press, New York, NY.

Casagrande, A. (1948). "Classification and identification of soils." *Transactions of the American Society of Civil Engineers*, 113.

Das, Yogadhish, McFee, John E., Toews, Jack, Stuart, Gregory C. (1990). "Analysis of an electromagnetic induction detector for real-time location of

buried objects," *IEEE Transactions on Geoscience and Remote Sensing*, 28 (3), 278-288.

Dearing, John. (1994). *Environmental magnetic susceptibility using the Bartington MS2 System.* Chi Publishing, Kenilworth, UK.

Hohmann, Gerald W. (1987). "Numerical modeling for electromagnetic methods of geophysics," *Electromagnetic Methods in Applied Geophysics*, Misac N. Nabighian ed., Society of Exploration Geophysicists, Tulsa, OK.

Isaaks, Edward H., and Srivastava, R. Mohan. (1989). *An introduction to applied geostatistics.* Oxford University Press, New York.

Johnson, B., Moore, T. G., Blejer, B. J., Lee, C. F., Opar, T. P., Ayasli, S., and Primmerman, C. A. (1996). "A Research and development strategy for unexploded ordnance sensing," Project Report EMP-1, Lincoln Laboratory, Massachusetts Institute of Technology, Lexington, MA.

Keller, George V., and Frischknecht, Frank C. (1970). *Electrical methods in geophysical prospecting.* Pergamon Press, New York.

Khadr, Nagi, Bell, Thomas, Williams, Scott, Bacon, William B. (1997). "UXO detection in highly magnetic soils," *Proceedings of the UXO Forum 97*, Anaheim, CA, 222-228.

Laveley, Eugene M. (1996). "Model based approach to UXO imaging using the time domain electromagnetic method," *Proceedings of the UXO Forum '96*, Williamsburg, VA, 315-324.

Llopis, Jose L., Simms, Janet E., Butler, Dwain K., Curtis, John O., West, Harold W., Arcone, Steven A., and Yankielun, Norbert E. (1998). "Site characterization investigations in support of UXO technology demonstrations, Jefferson Proving Ground, Indiana," Technical Report GL-98-20, U.S. Army Engineer Waterways Experiment Station, Vicksburg, MS.

McDonald, James R. and Nelson, Herbert H. (1999). "Results of the MTADS technology demonstration #3," NRL/PU/6110-99-375, Naval Research Laboratory, Washington, DC.

McFee, John E., and Das, Yogadhish. (1990). "A multipole expansion model for compact ferrous object detection," *Proceedings of the ANTEM Symposium on Antenna Technology and Applied Electromagnetics*. Manitoba, Canada, 633-638.

McNeill, J. D. (1986). "Geonics EM38 ground conductivity meter, operating instructions and survey interpretation techniques," Technical Note TN-21, Geonics Limited, Mississauga, Ontario, Canada.

McNeill, J. D., and Bosnar, Miro. (1996). "Application of time domain electromagnetic techniques to UXO detection," *Proceedings of the UXO Forum 1996.* Williamsburg, VA, 34-42.

McWilliams, Kendall M. (1985). *Soil survey of Ripley County and part of Jennings County, Indiana.* Soil Conservation Service, U.S. Department of Agriculture, Washington, DC.

Means, R. E. and Parcher, J. V. (1963). *Physical properties of soils.* Charles E. Merrill Publishing Co., Columbus, OH.

Miller, C. A., Malone, C. R., and Blount, C. B. (1992). "Guide for the conduct of predeployment site characterization surveys for the AN/GSS-34 (V) Ported Coaxial Cable Sensor (PCCS)," Instruction Report EL-92-1, U.S. Army Engineer Waterways Experiment Station, Vicksburg, MS.

Nelson, H. H., McDonald, J. R., and Robertson, R. (1997). "Multisensor ordnance signatures for algorithm development and model training," *Proceedings of the Symposium on the Application of Geophysics to Engineering and Environmental Problems.* Reno, NV, 863-869.

Nickell, Allan K. (1985). *Soil survey of Jefferson County, Indiana.* Soil Conservation Service, United States Department of Agriculture, Washington, DC.

Office of the Scretary of Defense. (1997). "Unexploded ordnance clearance: annual report to congress," UXO Clearance Steering Group, Washington, DC.

O'Neill, Kevin and Arcone, Steven. (1999). "Ground penetrating radar surveying and modeling for buried UXO sensing: some applications to JPG," Technical Report CR670, U.S. Army Cold Regions Research and Engineering Laboratory, Hanover, NH.

PRC Environmental management, Inc. (1994). "Geotechnical investigation report," Task 3: Preparation of demonstration site, Jefferson Proving Ground, Indiana, U.S. Naval Explosive Ordnance Disposal Technology Division, Indianhead, MD.

Sahimi, Muhammad. (1995). *Flow and transport in porous media and fractured rock.* VCH Verlagsgesellschaft mbH, Weinheim, FRG.

Scollar, I., Tabbagh, A., Hesse, A., Herzog, I. (1990). *Archaeological prospecting and remote sensing.* Cambridge University Press, New York.

Simms, Janet E., Llopis, Jose L., Butler, Dwain K., and Smith, Lawson M. (1998). "Geophysical site characterization for UXO backgrounds study at Fort Carson, Colorado, Fort A. P. Hill, Virginia, and Jefferson Proving Ground, Indiana," Technical Report GL-98-16, U.S. Army Engineer Waterways Experiment Station, Vicksburg, MS.

Stanley, John M., Clark, Peter J., and Griffin, Stephen M. (1997). "UXO detection in mineralised and volcanic environments," *Proceedings of the UXO Forum '97*, Anaheim, CA, 322-328.

Talwani, M., and Heirtzler, J. R. (1964). "Computation of magnetic anomalies caused by two-dimensional structures of arbitrary shape," Computers in the Mineral Industry, Part 1, Stanford University Publications, 464-480.

Thorarinsson, Freyr. (1985). "Two-dimensional graphically interactive modeling of gravitational and magnetic anomalies," Digitus International, Golden, CO.

U.S. Army Environmental Center (AEC). (1994). "Unexploded ordnance advanced technology demonstration program at Jefferson Proving Ground (Phase I)," Report No. SFIM-AEC-ET-CR-94120, U.S. Army Environmental Center, Aberdeen Proving Ground, MD.

AEC. (1995). "Evaluation of individual demonstrator performance at the unexploded ordnance advanced technology demonstration program at Jefferson Proving Ground (Phase I)," Report No. SFIM-AEC-ET-CR-95033, U.S. Army Environmental Center, Aberdeen Proving Ground, MD.

AEC. (1996). "Unexploded ordnance advanced technology demonstration program at Jefferson Proving Ground (Phase II)," Report No. SFIM-AEC-ET-CR-96170, U.S. Army Environmental Center, Aberdeen Proving Ground, MD.

AEC. (1997). "UXO Technology Demonstration Program at Jefferson Proving Ground, Phase III," Report No. SFIM-AEC-ET-CR-97011, U.S. Army Environmental Center, Aberdeen Proving Ground, MD.

Wait, James R. (1982). *Geo-Electromagnetism*, Academic Press, New York, NY.

Ward, Stanley H. and Hohmann, Gerald W. (1987). "Electromagnetic theory for geophysical applications," *Electromagnetic Methods in Applied Geophysics*, Misac N. Nabighian ed., Society of Exploration Geophysicists, Tulsa, OK.

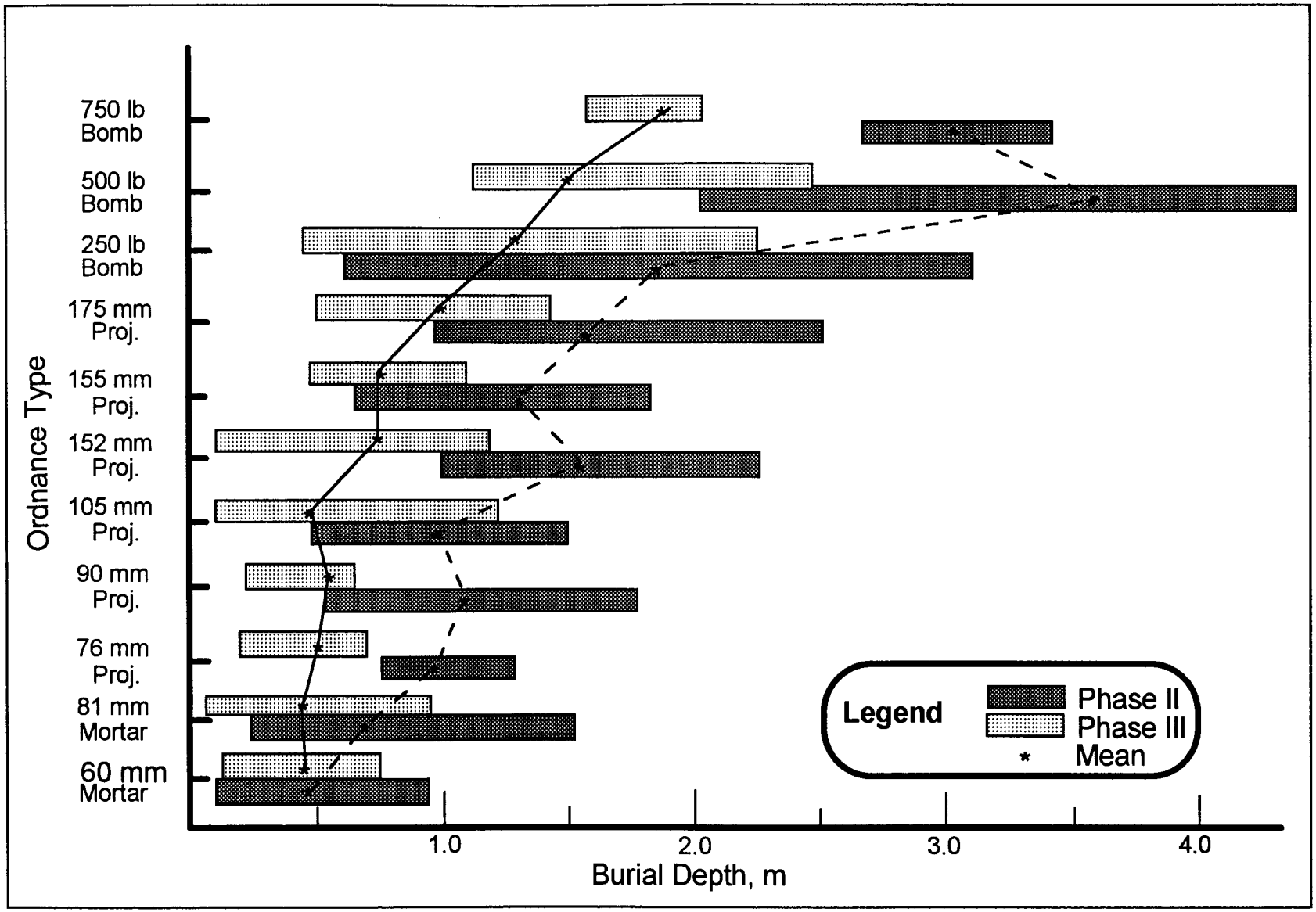

Figure 1. Comparison of ordnance target burial depths for JPG Phases II and III, 40-acre site

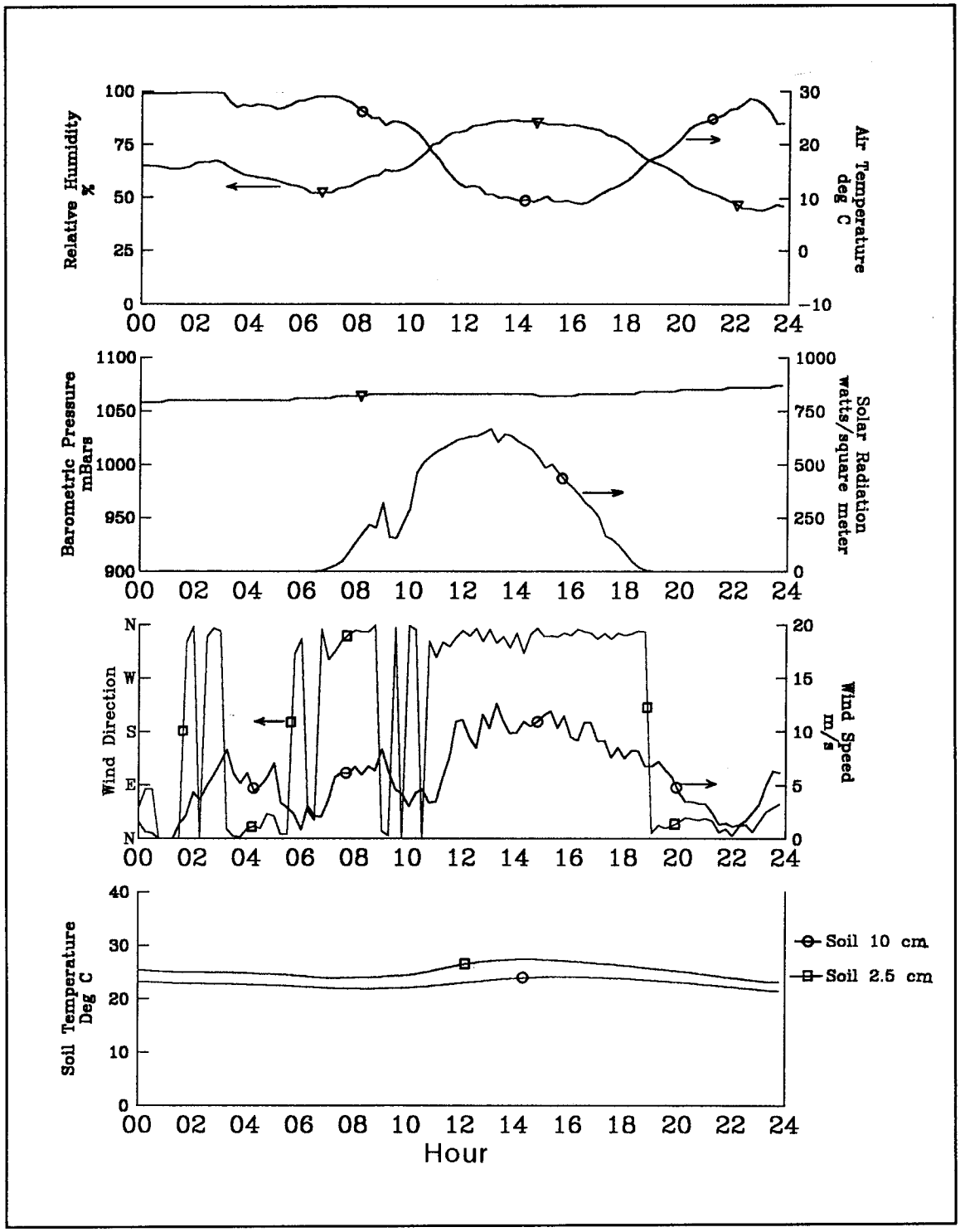

Figure 2. Example of types of environmental parameters recorded during the JPG Phase IV demonstrations: Tuesday, 22 September 1998

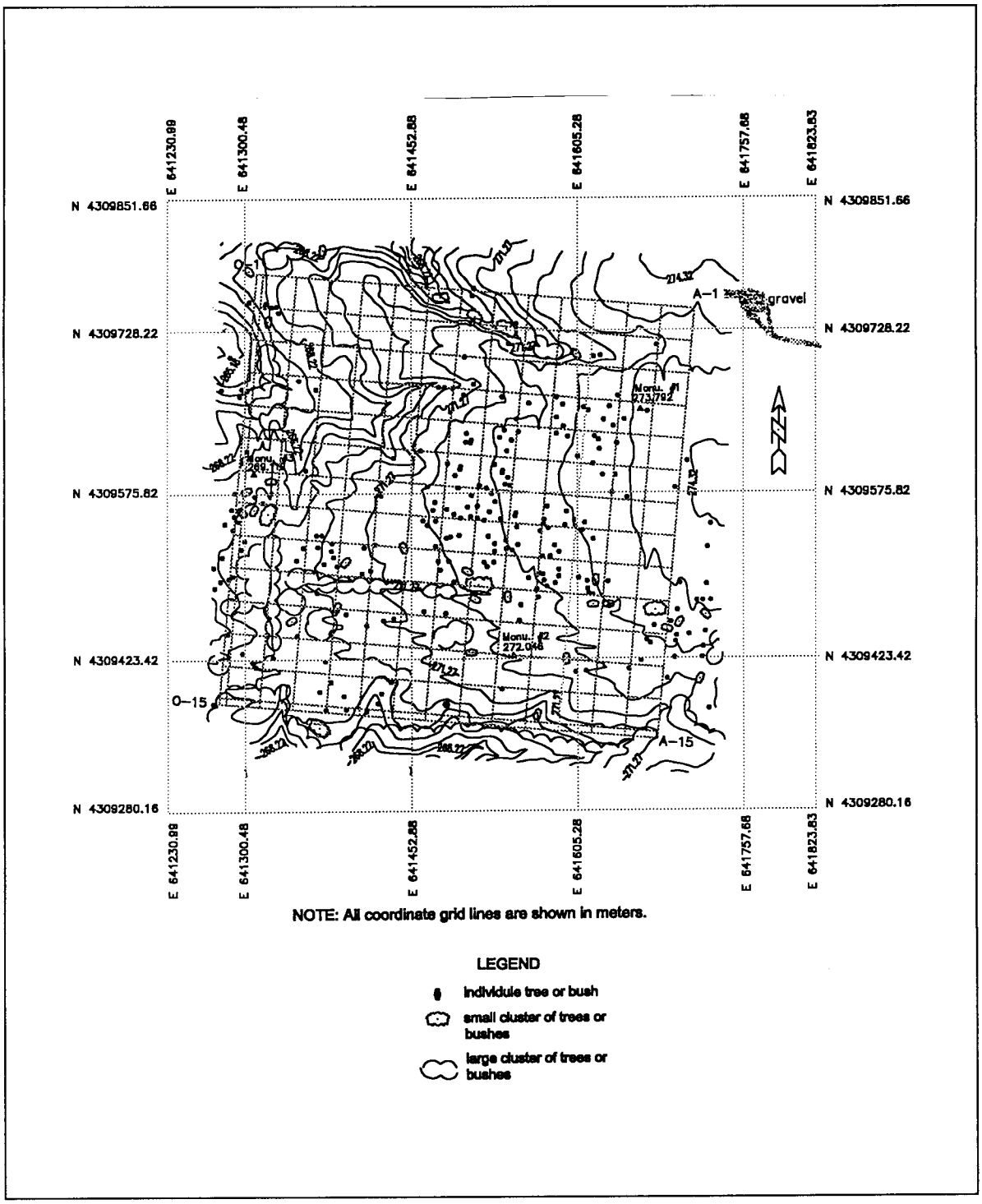

Figure 3. JPG 40-acre site map, showing topography (elevation in m, with 0.61 m or 2 ft contour interval, vegatation, site reference grid (e.g., A-1), and northing-easting coordinates in m

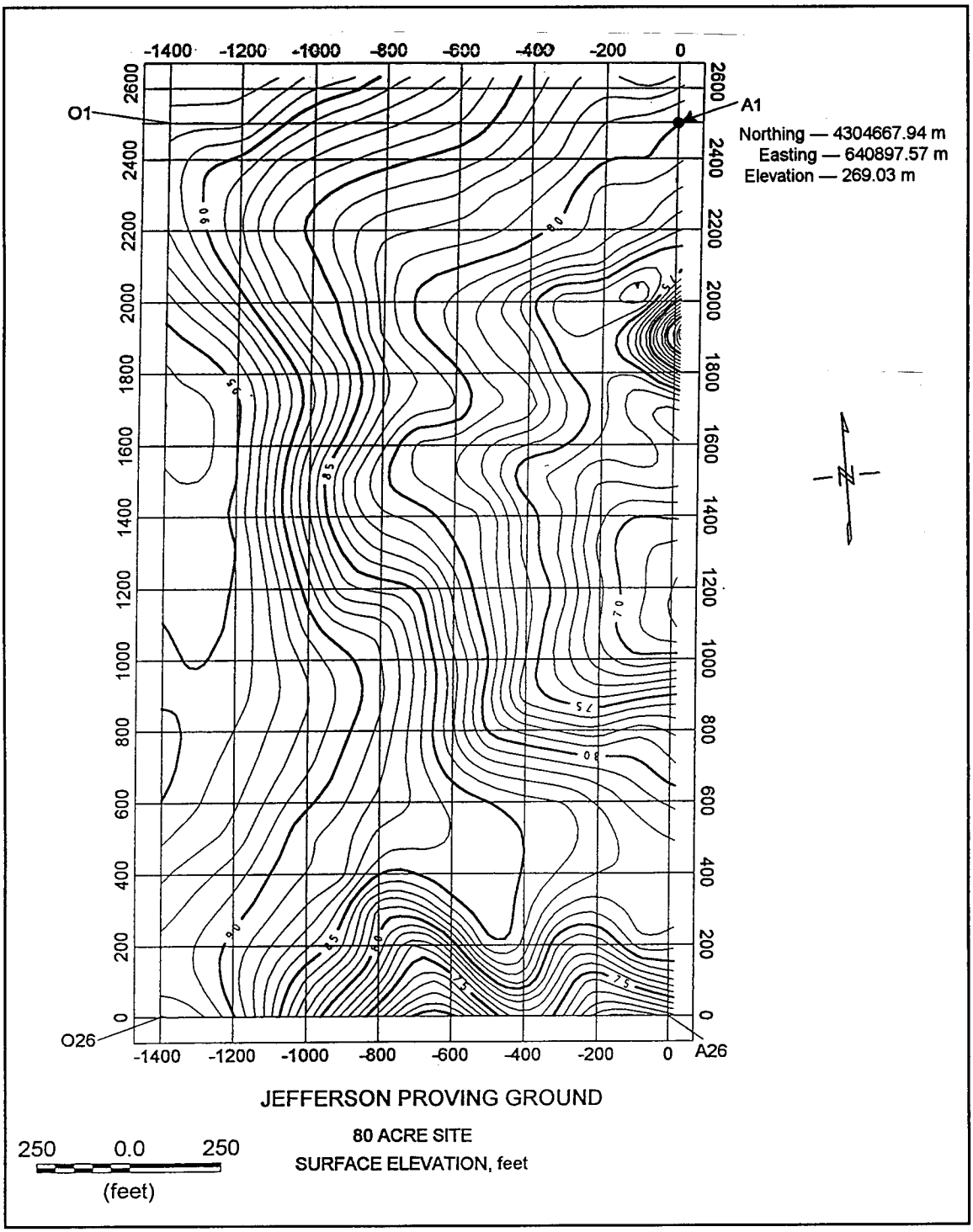

Figure 4. JPG 80-acre site map, showing topography (elevation in ft relative to local datum, 0.305-m or 1-ft contour interval) and site reference grid (e.g., A1); northing, easting and absolute elevation, all in m, shown for location A1

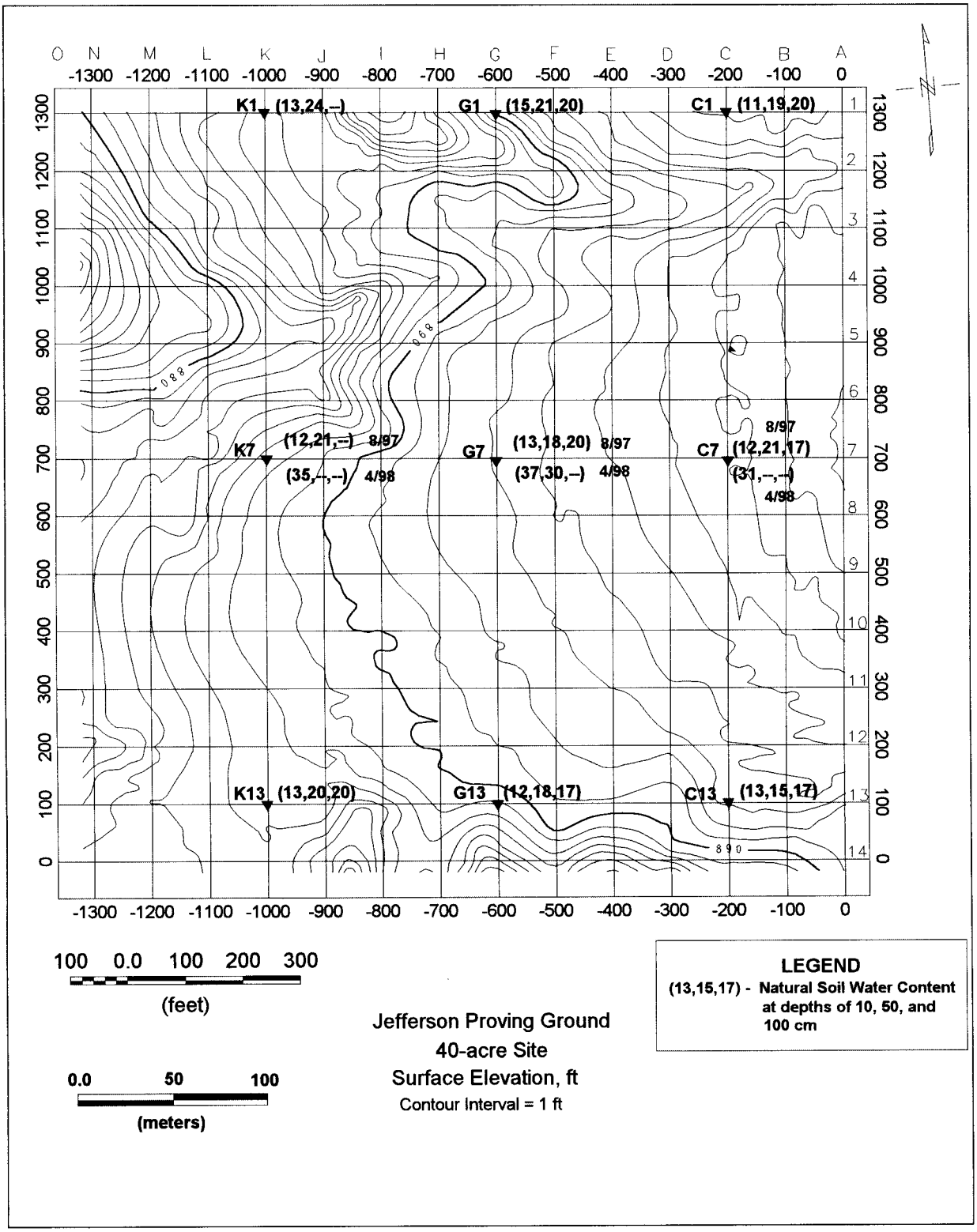

Figure 5. JPG 40-acre site map, showing nine locations where water contents were determined for 10-, 50-, and 100-cm depths for dry site conditions (8/97) and three sites where water contents were determined for wet site conditions (4/98)

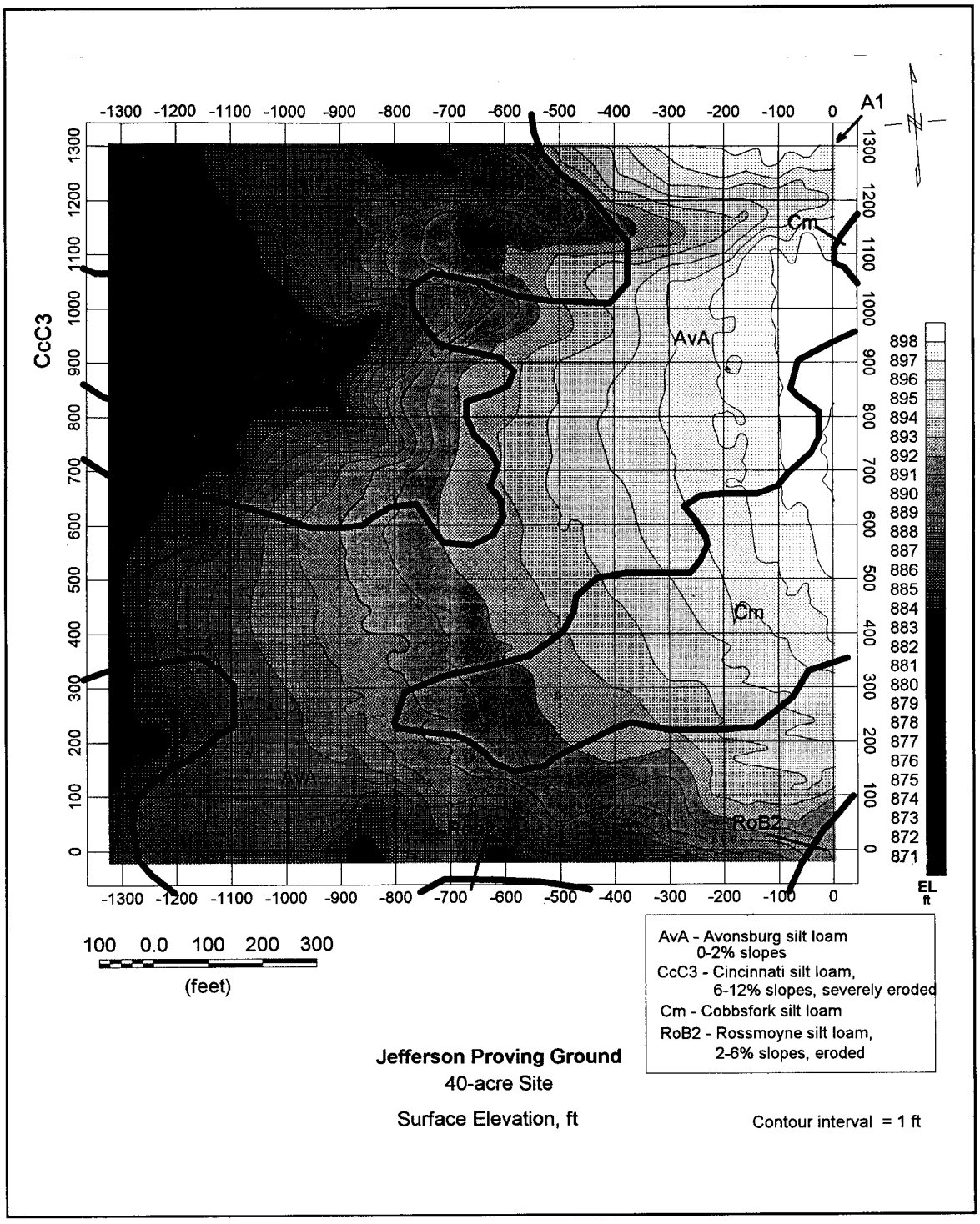

Figure 6. JPG 40-acre site: soils map superimposed on topograpy

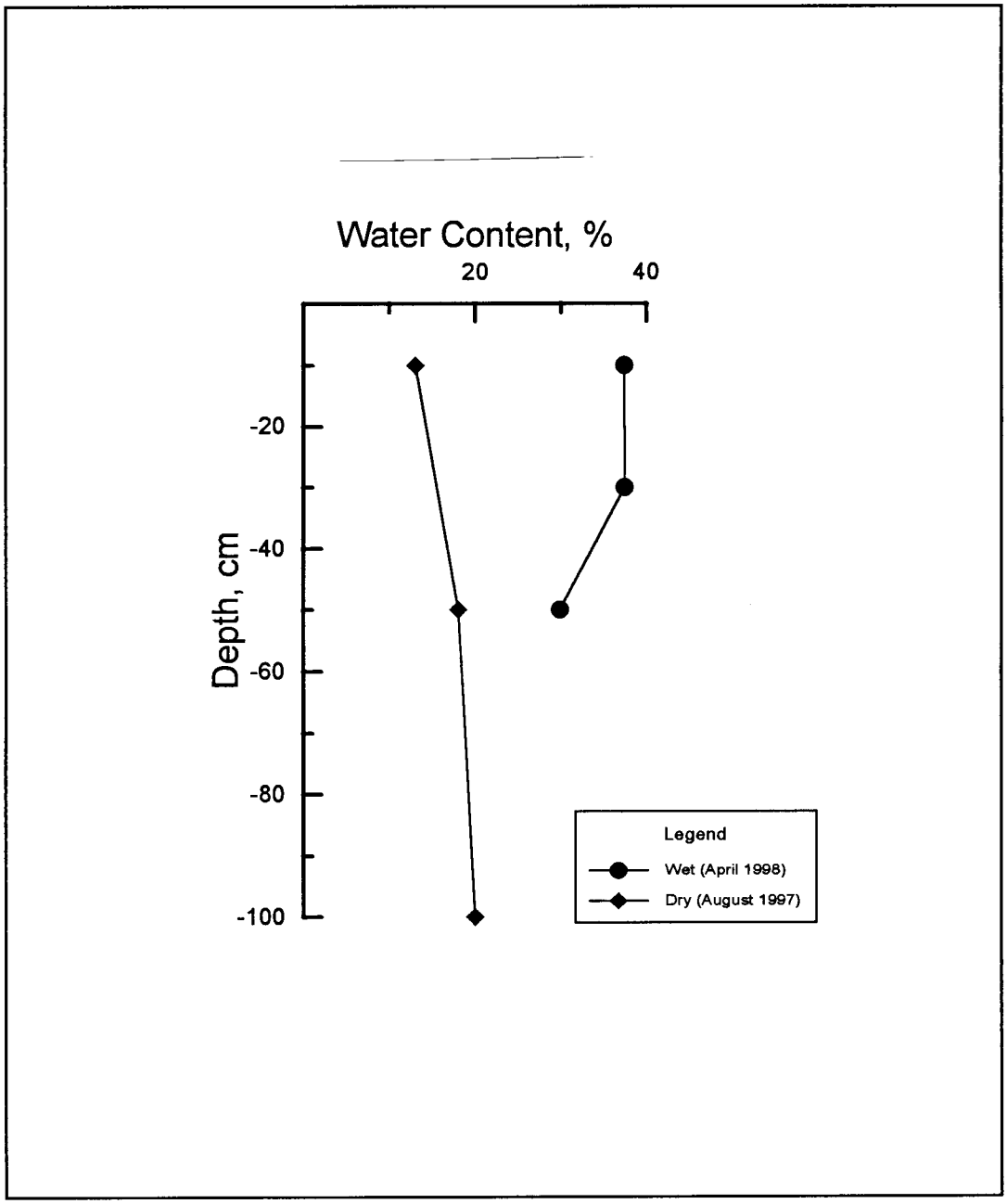

Figure 7. Variation of soil water content with depth for wet and dry site conditions at location G7, 40-acre site

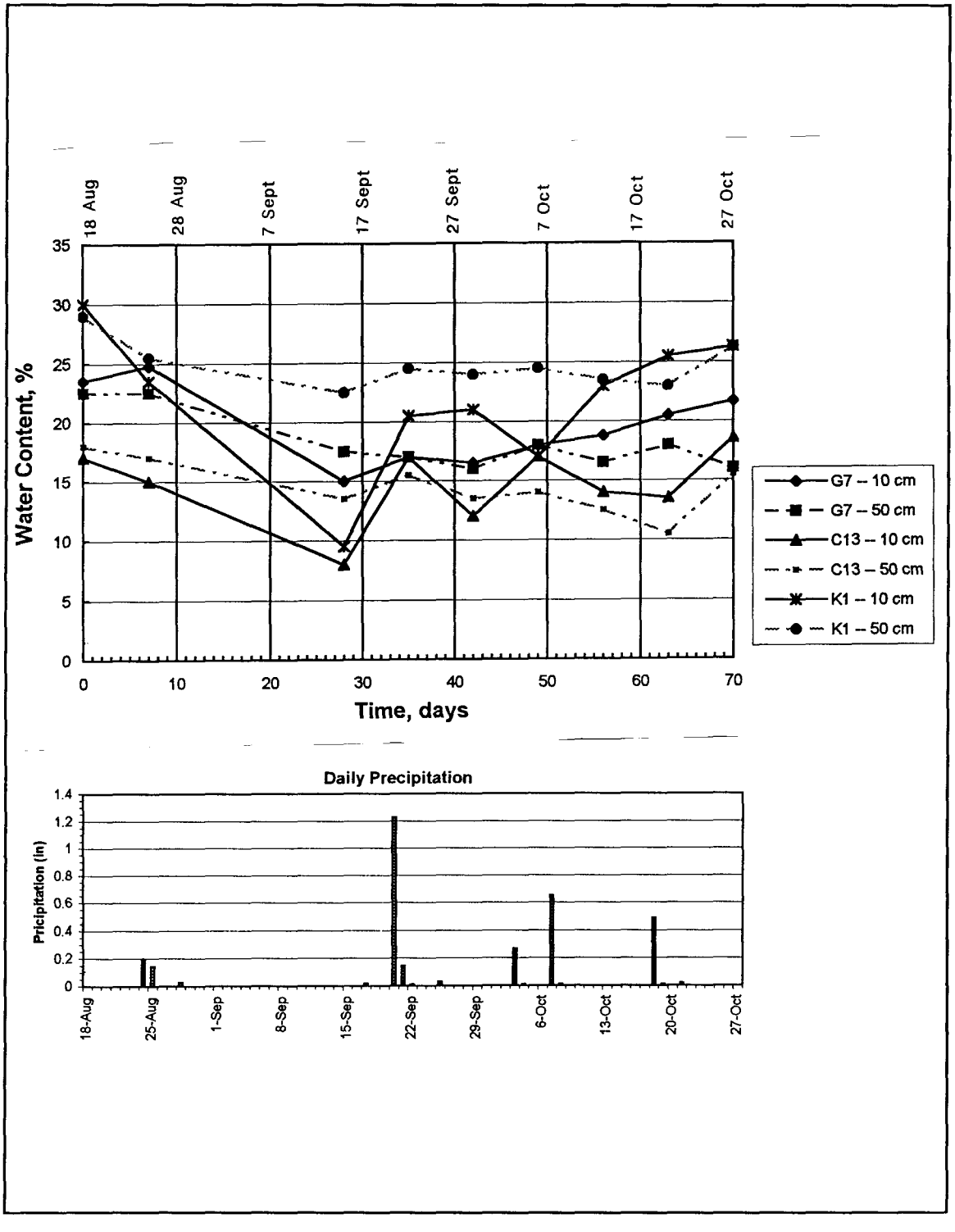

Figure 8. Natural water contents, for two depths and three locations, and precipitation during JPG Phase IV demonstrations (1998)

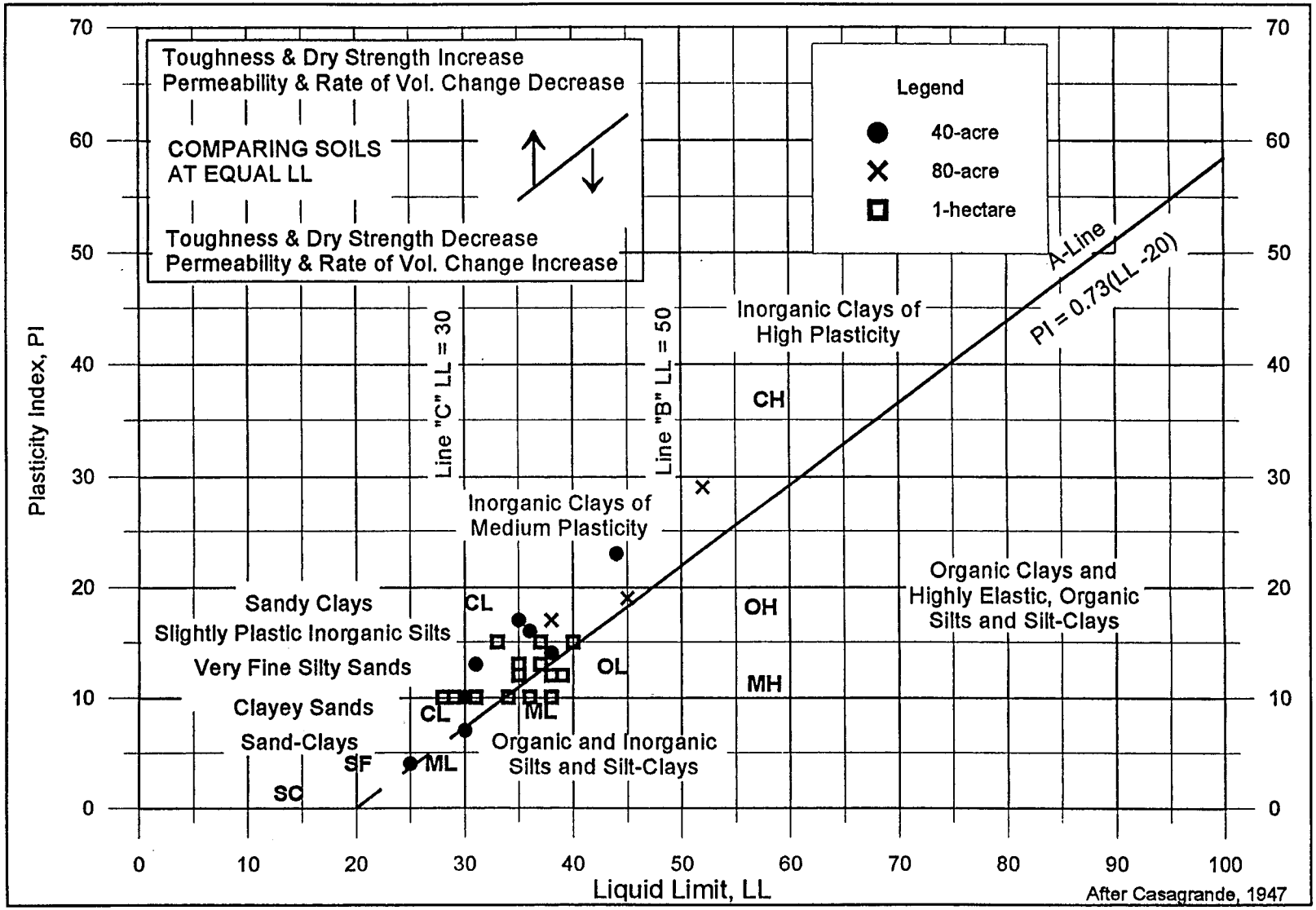

Figure 9. Soil index parameter classification chart (e.g., see Means and Parcher 1963) and JPG soils analysis results

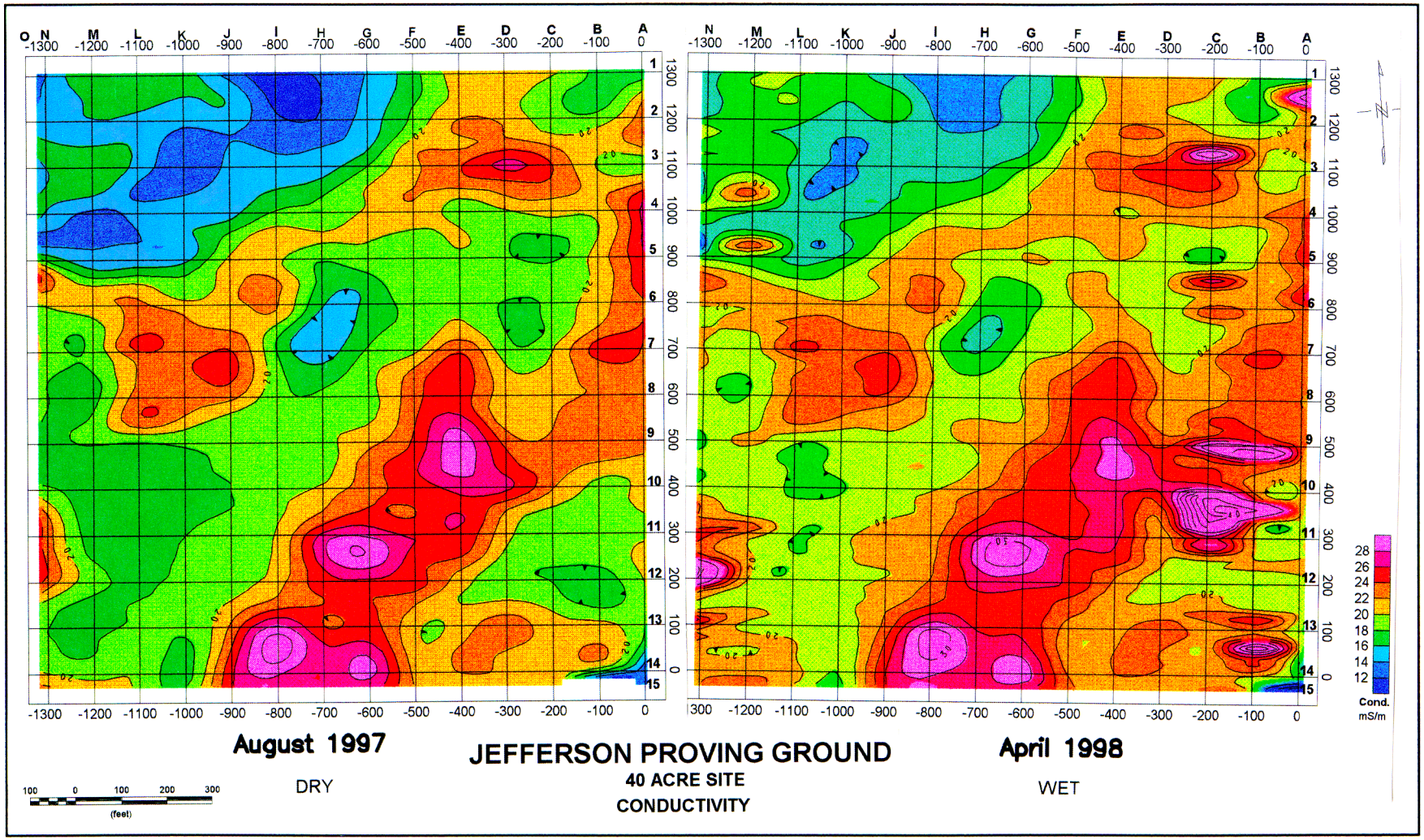

Figure 10. Electromagnetic terrain conductivity map for 40-acre site during dry (left) and wet (right) site conditions; determined with Geonics EM-31 (frequency domain EM induction system, 9.8 kHz)

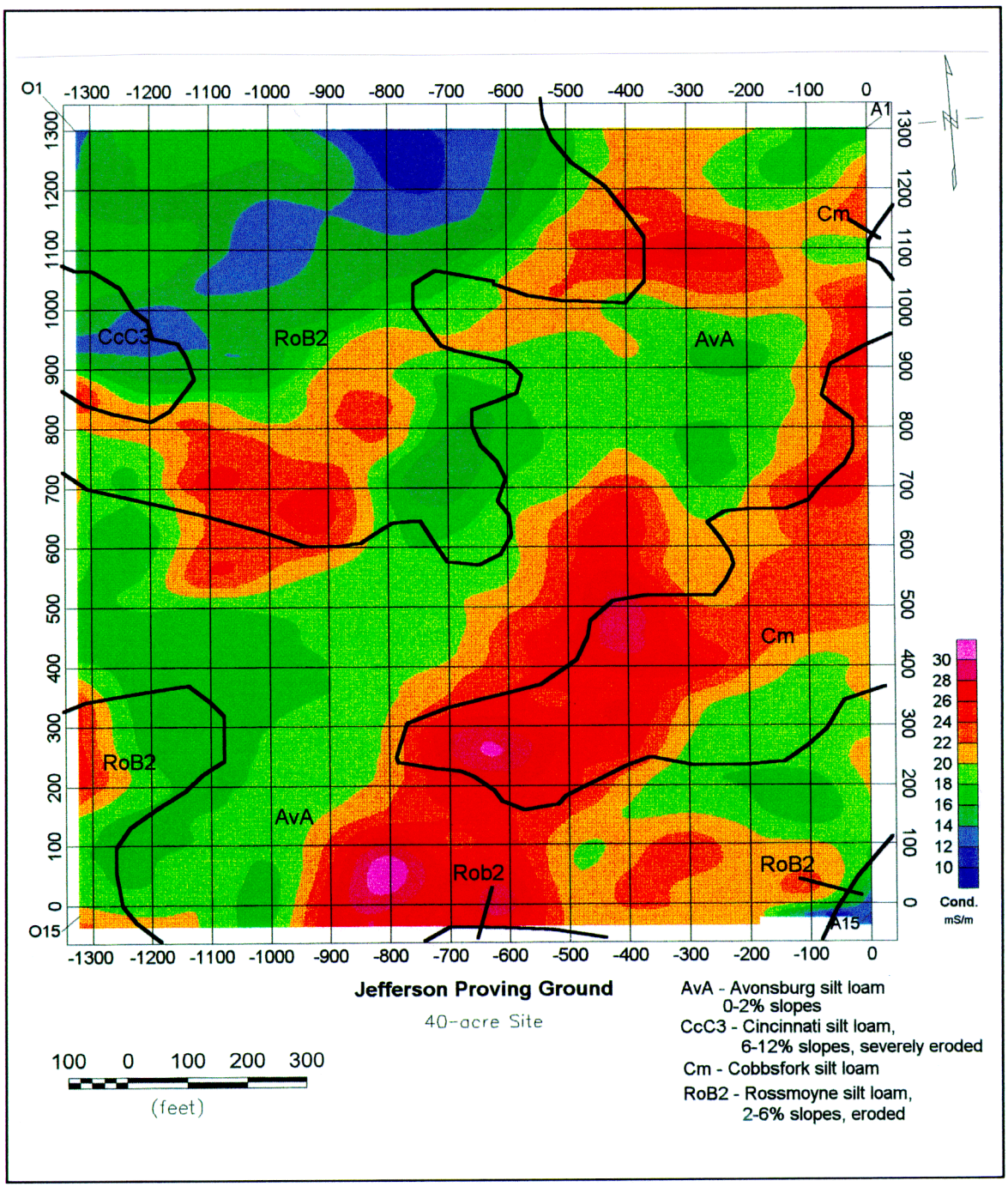

Figure 11. JPG 40-acre site: soils map superimposed on terrain conductivity map

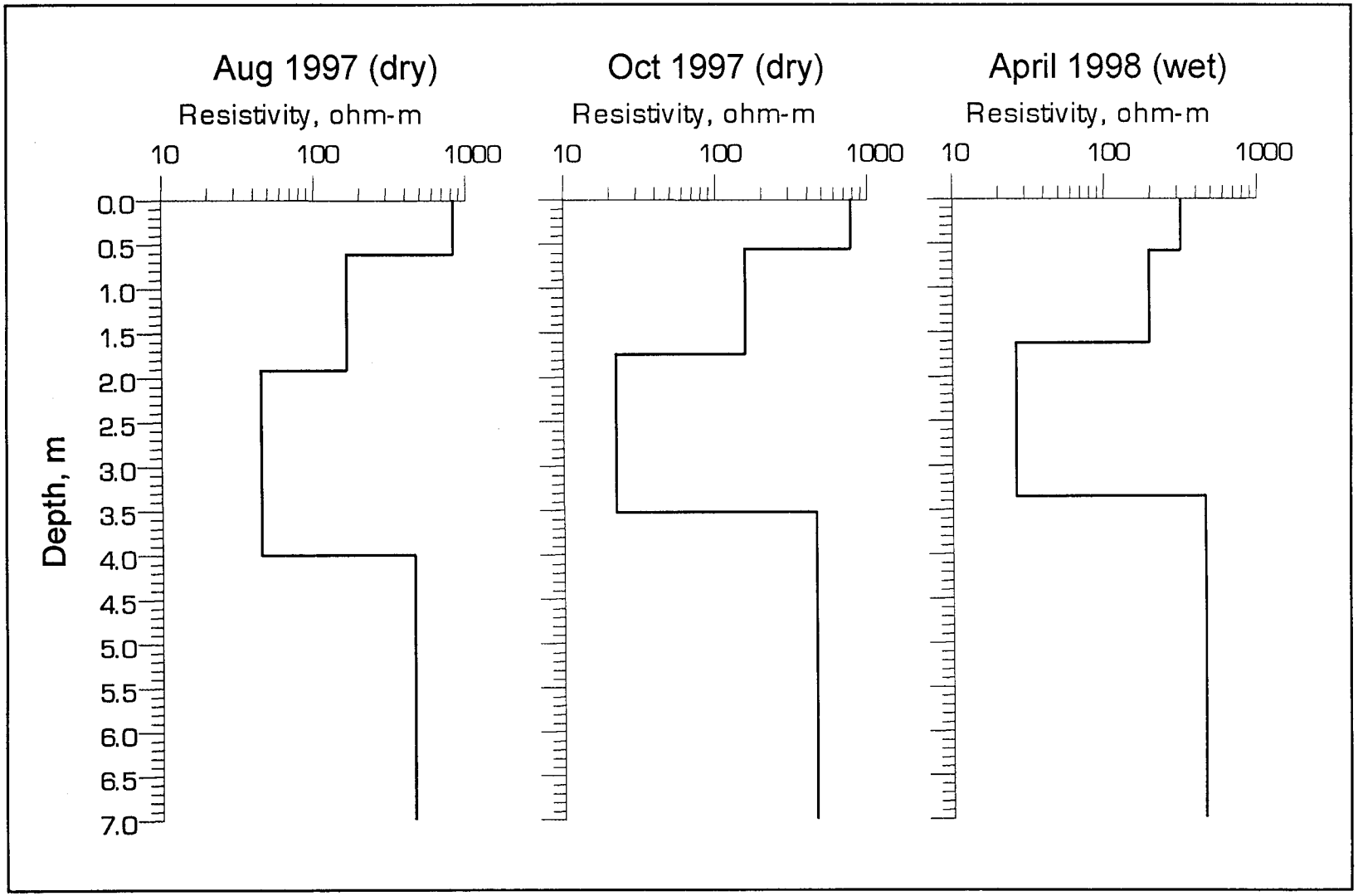

Figure 12. Electrical resistivity sounding interpretations for three dates at Location G7, 40-Acre Site

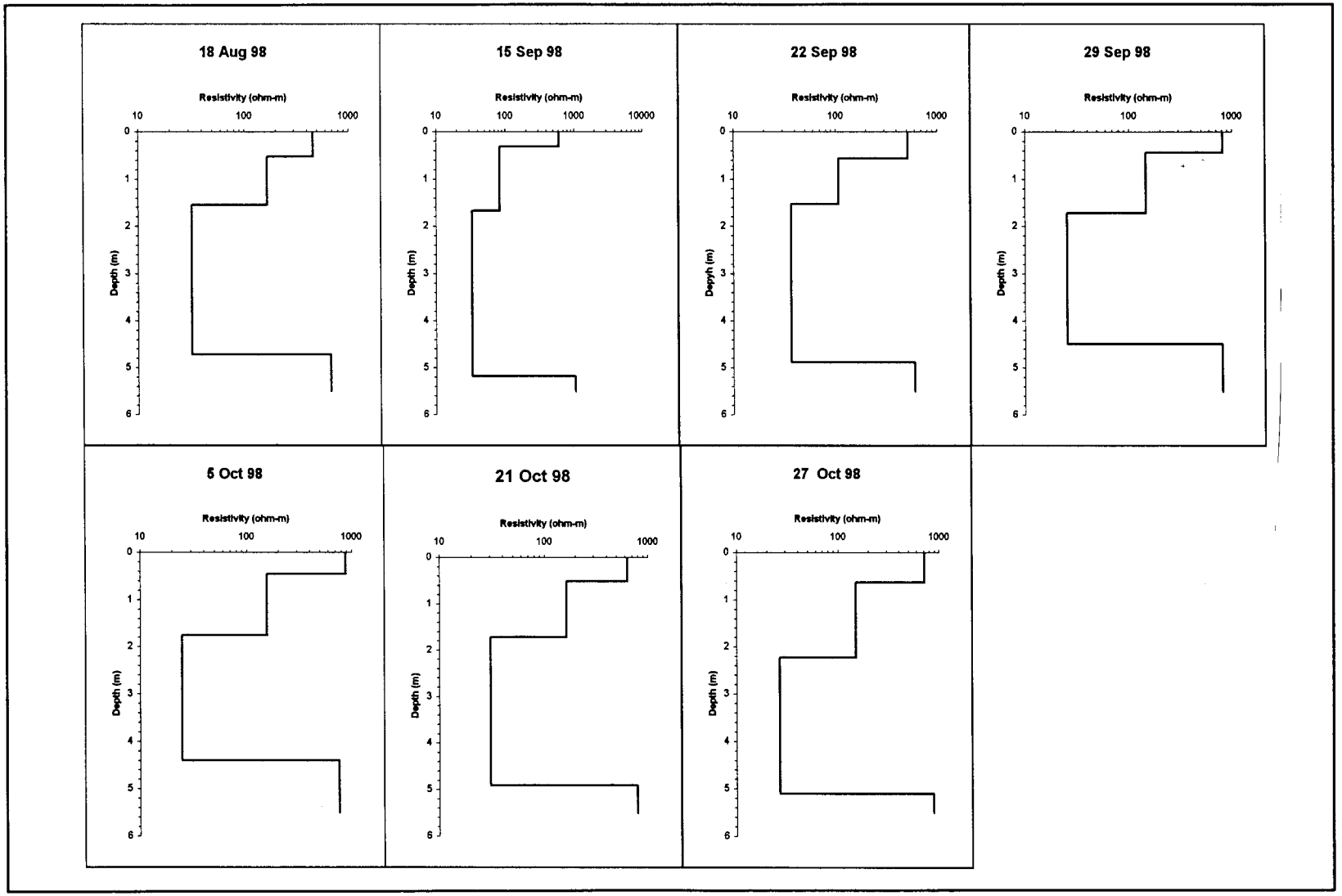

Figure 13. Electrical resistivity sounding interpretations for seven dates during the Phase IV demonstrations; Location G7, 40-Acre Site

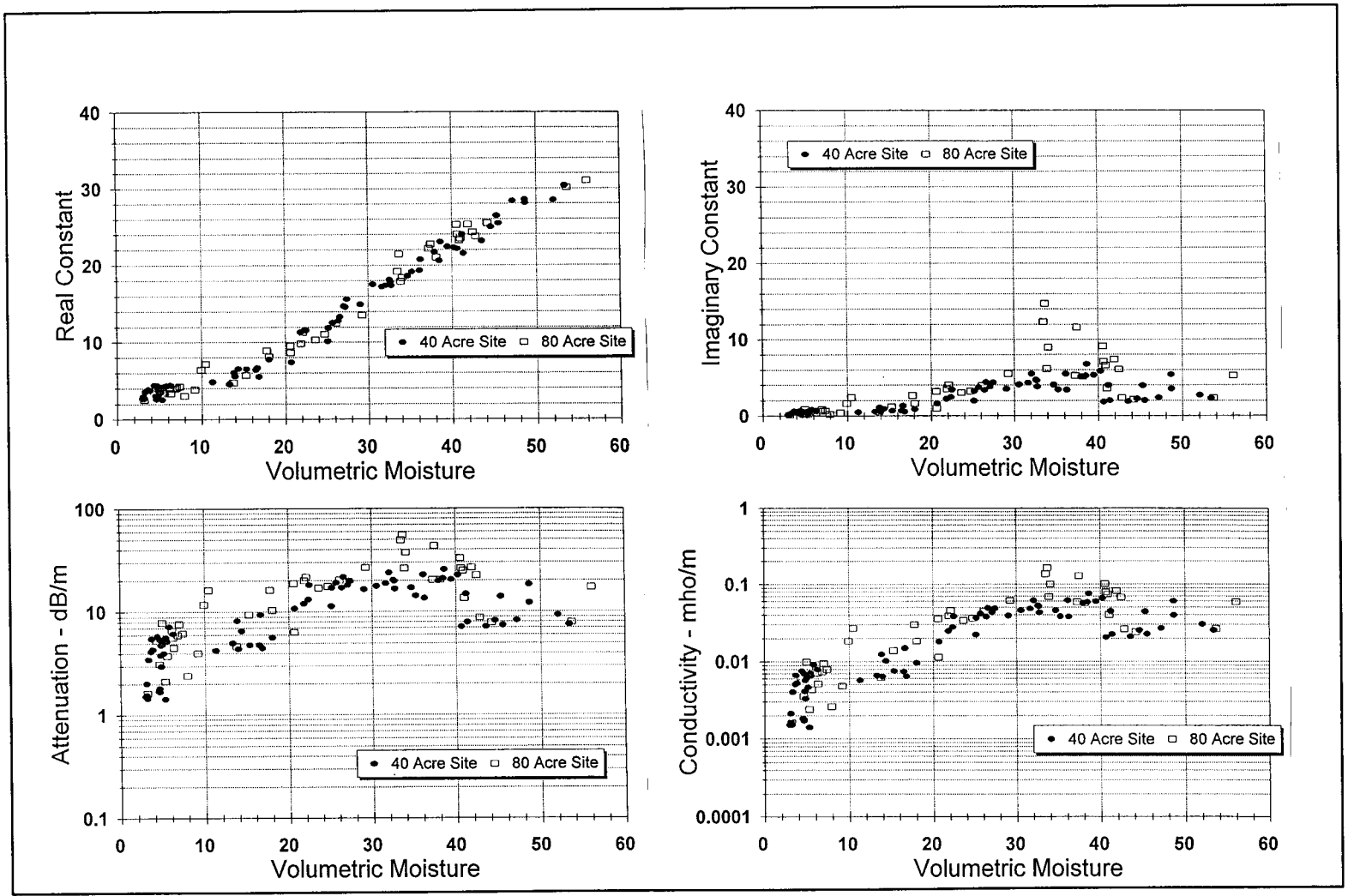

Figure 14. Example of laboratory electromagnetic properties measurements for shallow JPG soils at 200 MHz as a function of volumetric moisture content (see Llopis et al.1998)

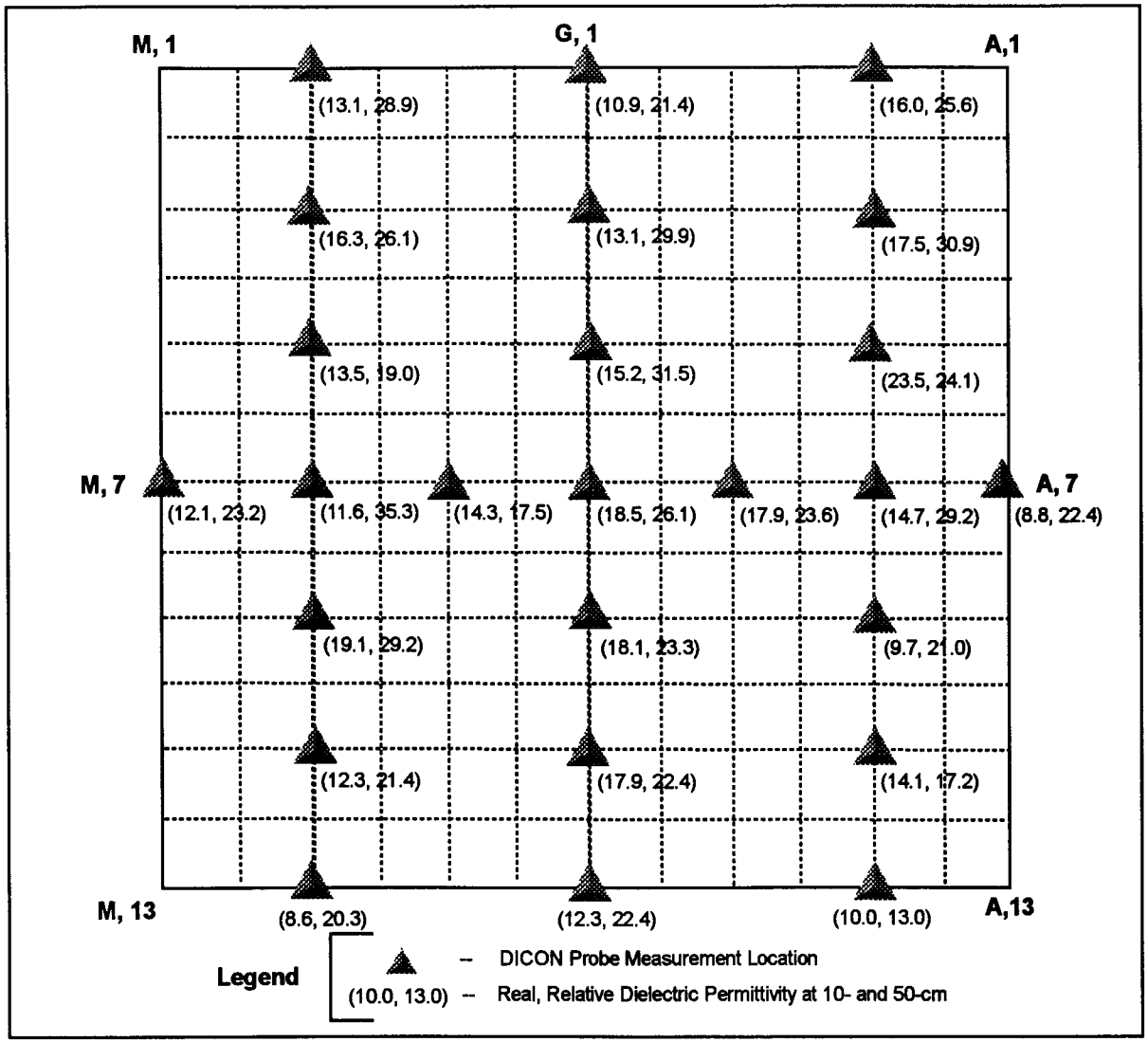

Figure 15. DICON probe measurements of the real component of the complex dielectric permittivity at 10- and 50-cm depths at the 40-acre site.

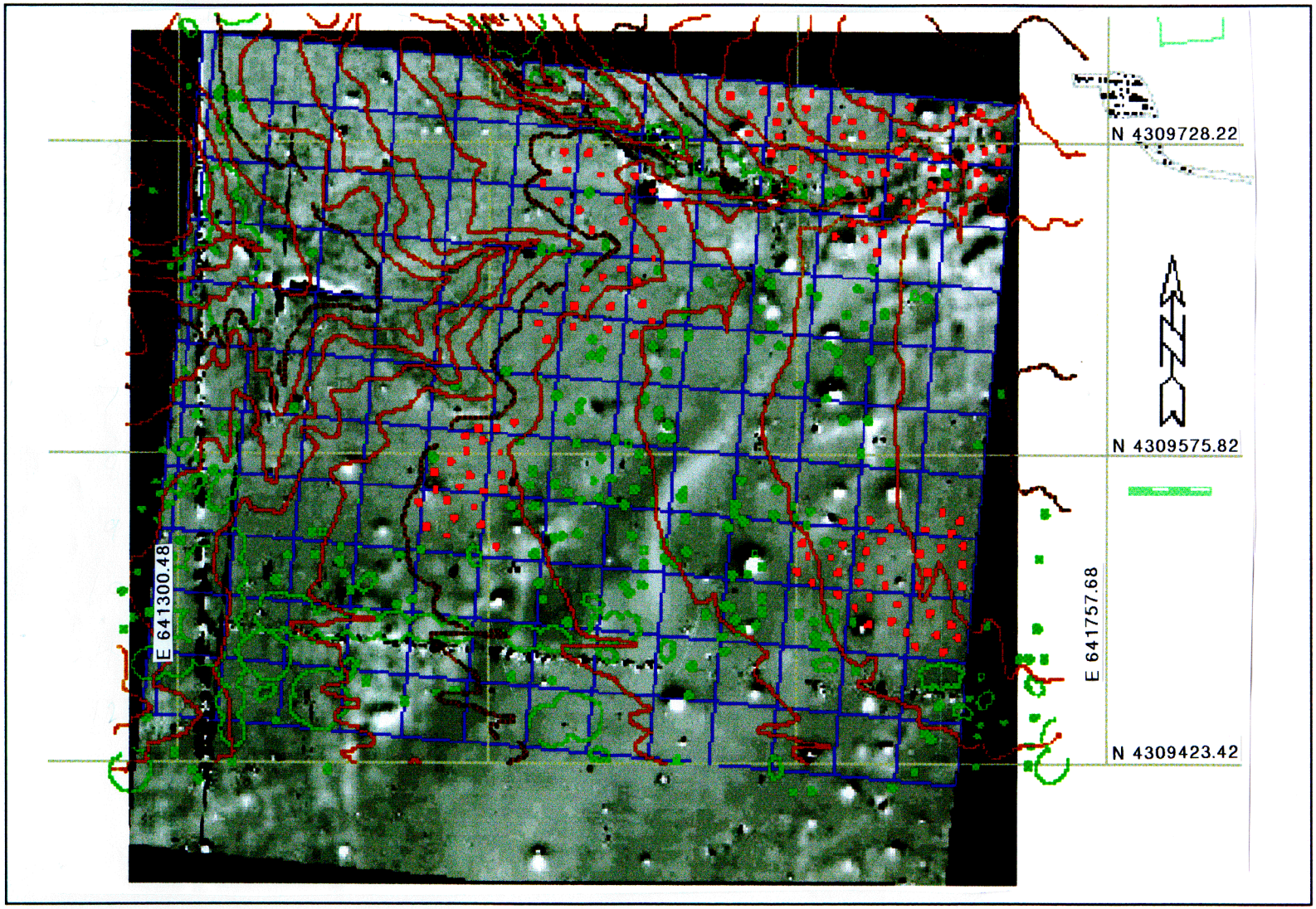

Figure 16. Overlay of Phase II total magnetic field anomaly map, topography, vegetation, and site grid map for 40-Acre Site

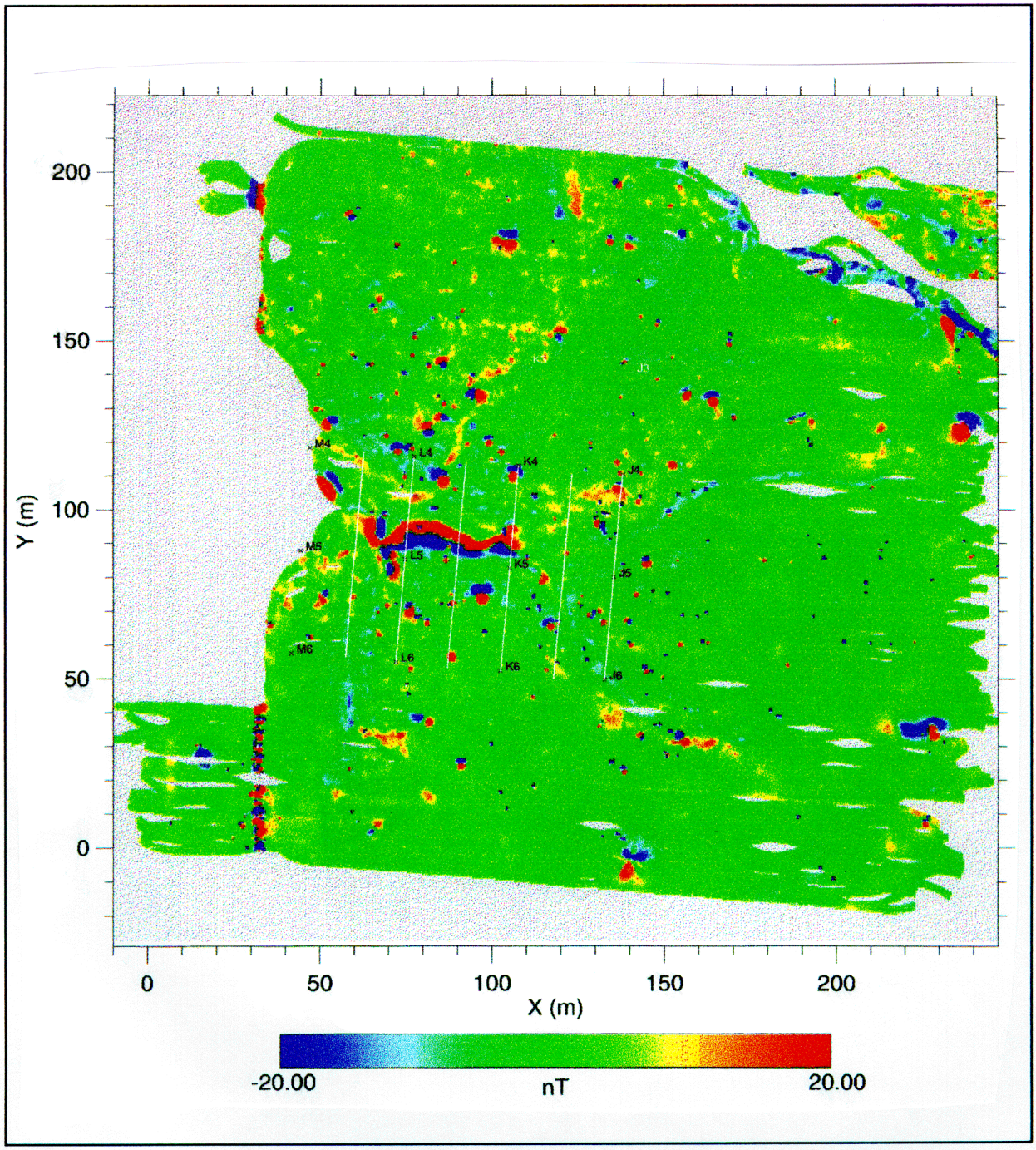

Figure 17. Phase III Naval Research Laboratory MTADS total magnetic field map of northwest quadrant of 40-Acre Site

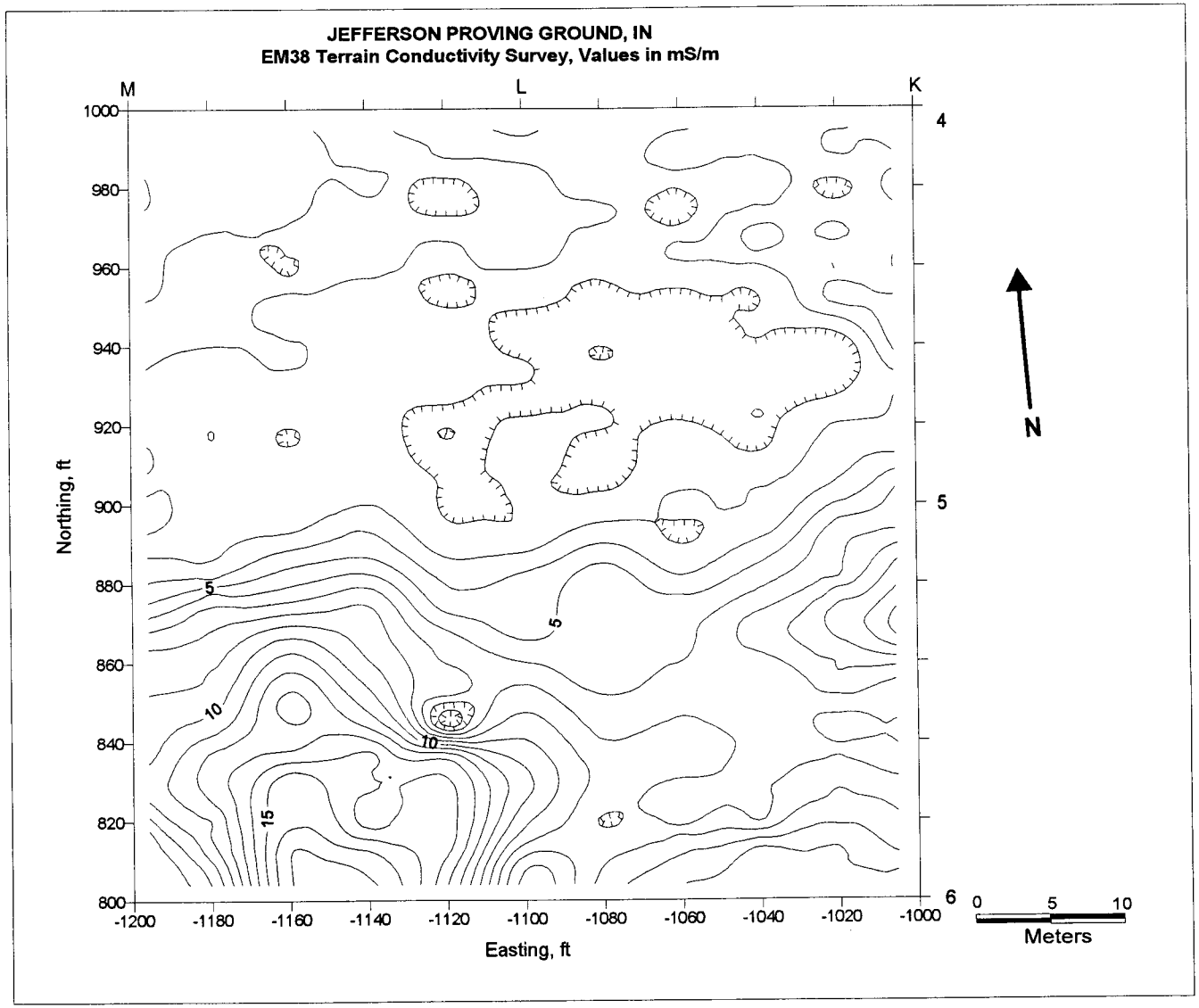

Figure 18. Terrain conductivity map determined with Geonics EM-38 (frequency domain EM induction system, 14.6 kHz) of a portion of the northwest quadrant of the 40-Acre Site, approximately centered on the anomalous magnetic feature shown in Figure 17

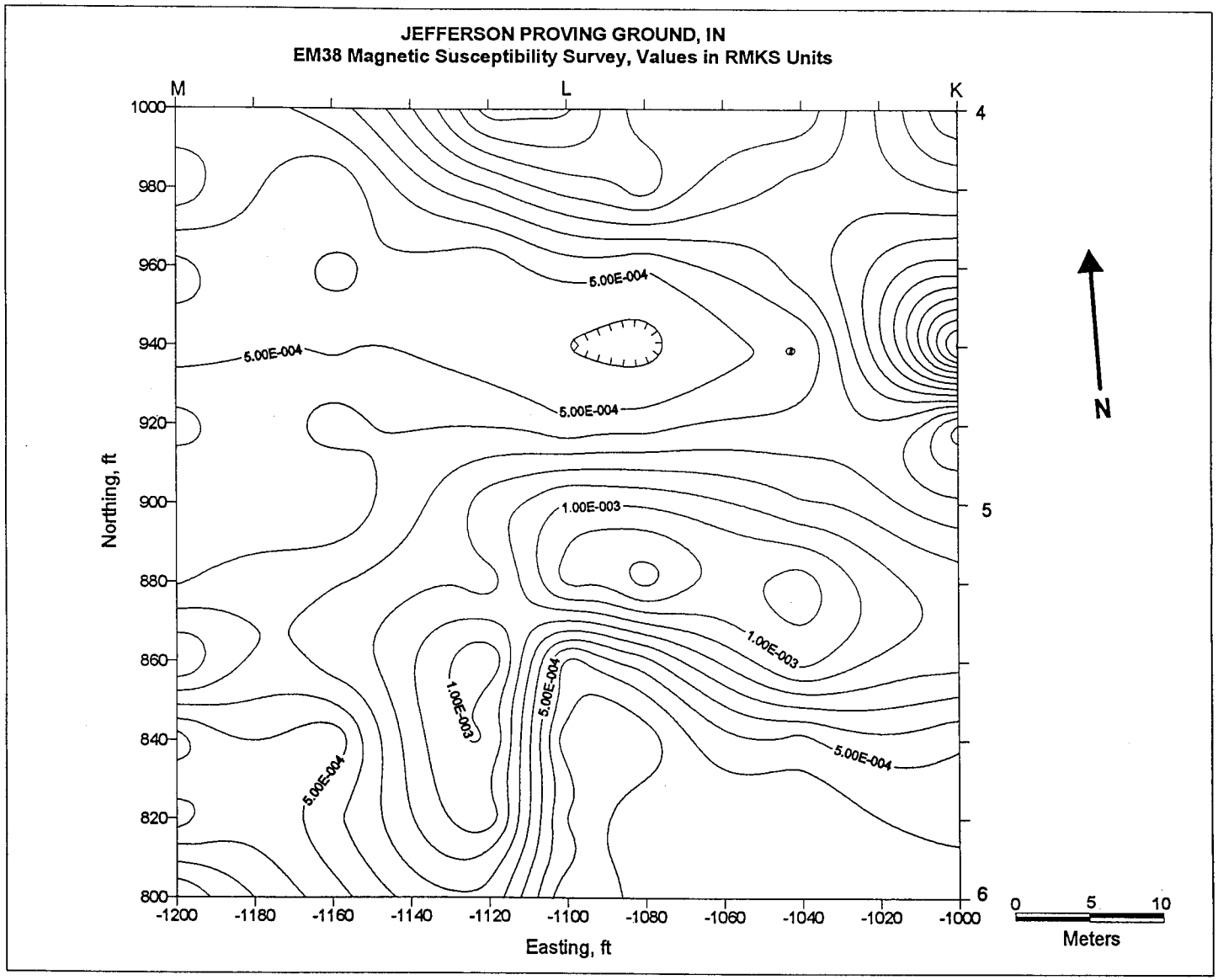

Figure 19. Magnetic susceptibility map (SI units) of a portion of the northwest quadrant of the 40-Acre Site, corresponding to the area shown in Figure 18 and approximately centered on the anomalous magnetic feature shown in Figure 17

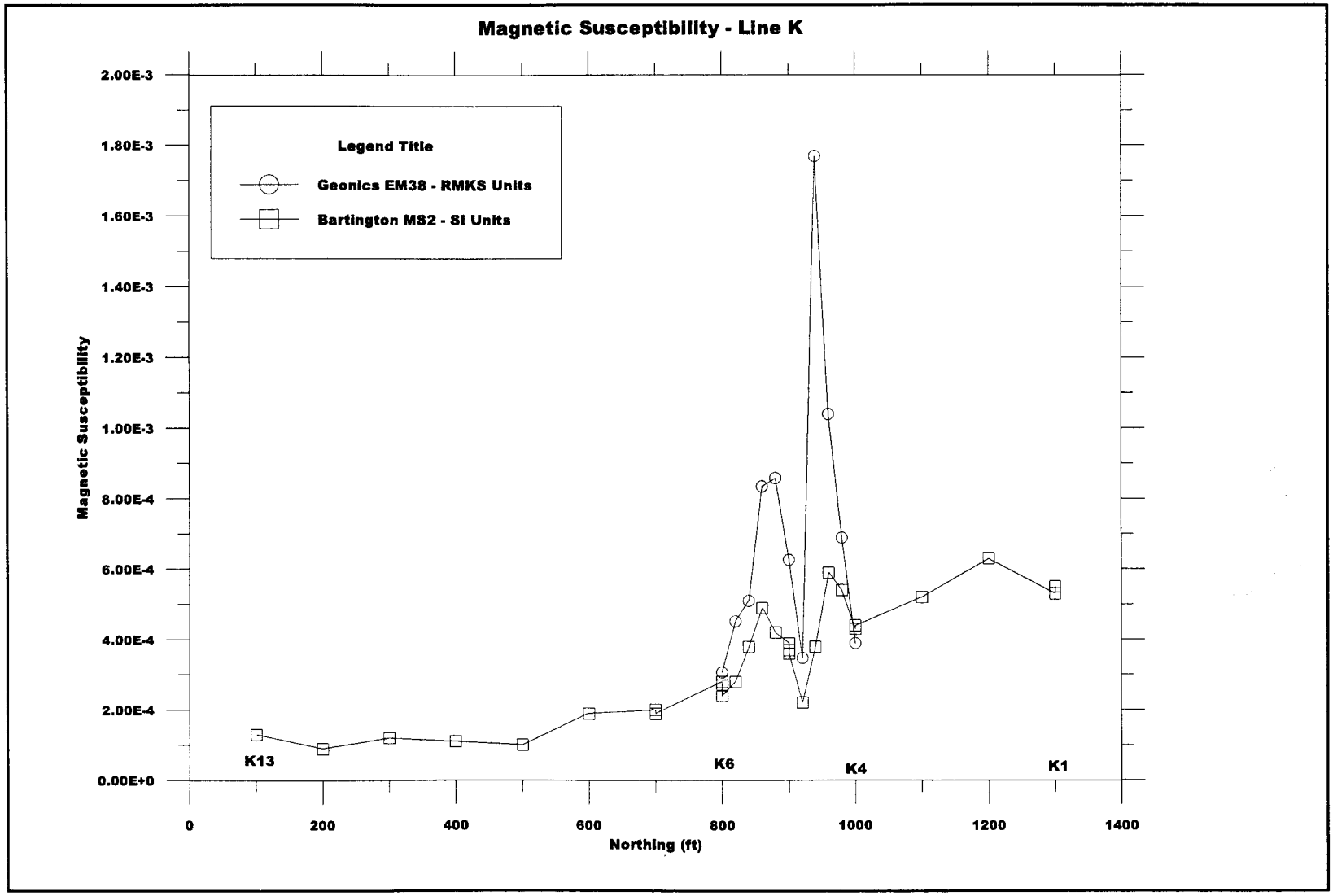

Figure 20. Magnetic susceptibility profiles along grid line K, from K13 to K1

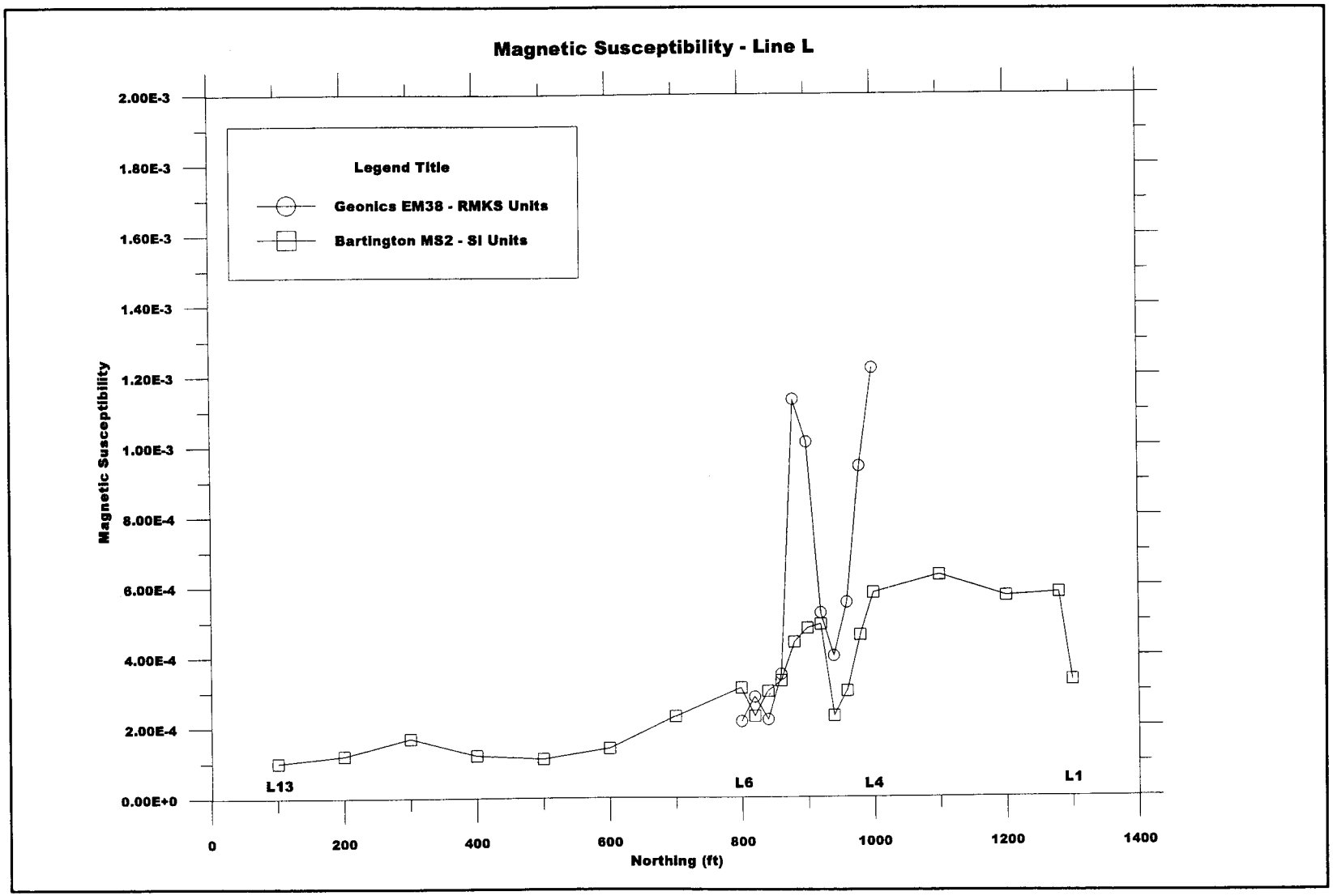

Figure 21. Magnetic susceptibility profiles along grid line L, from L13 to L1

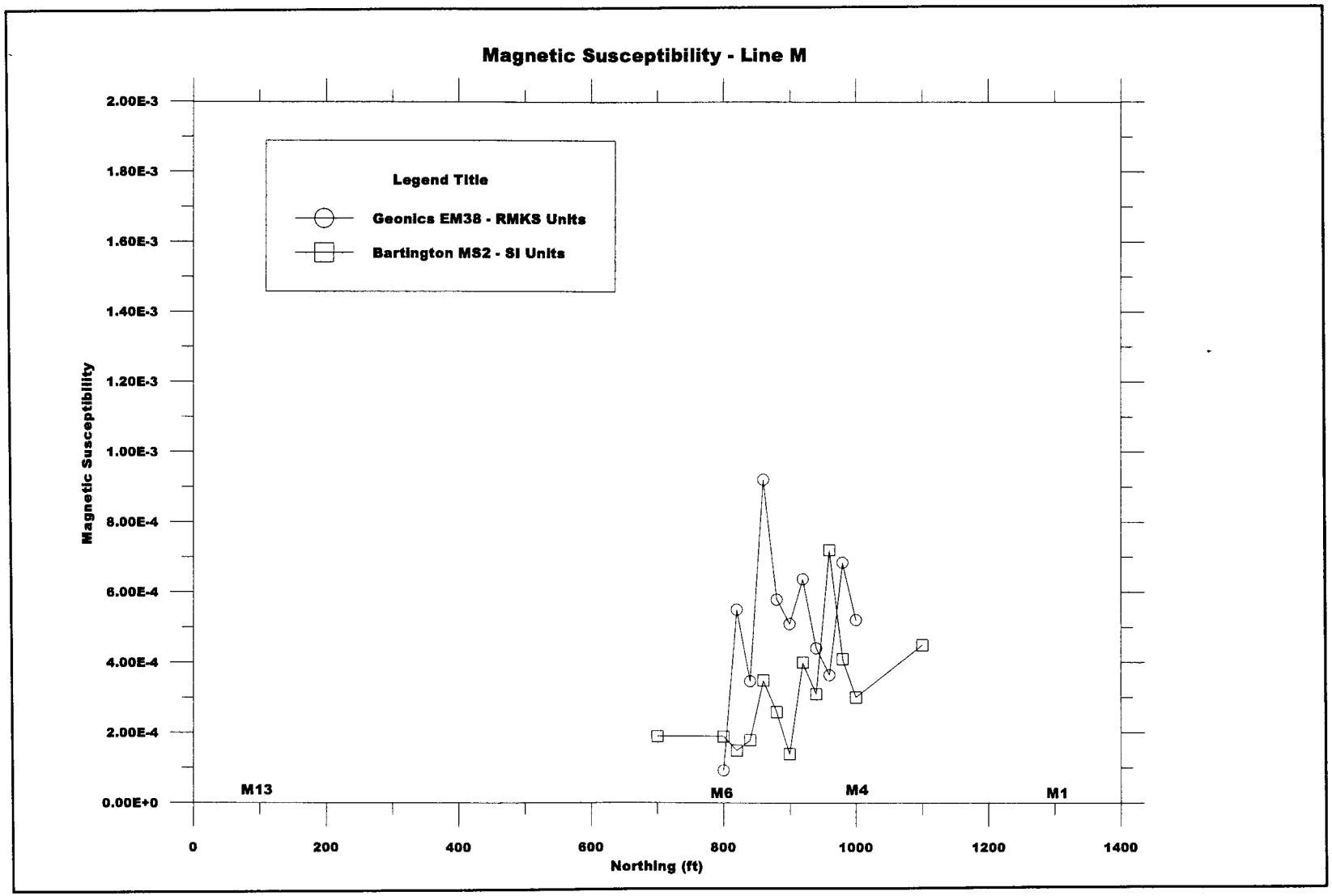

Figure 22. Magnetic susceptibility profiles along grid line M, from M7 to M3

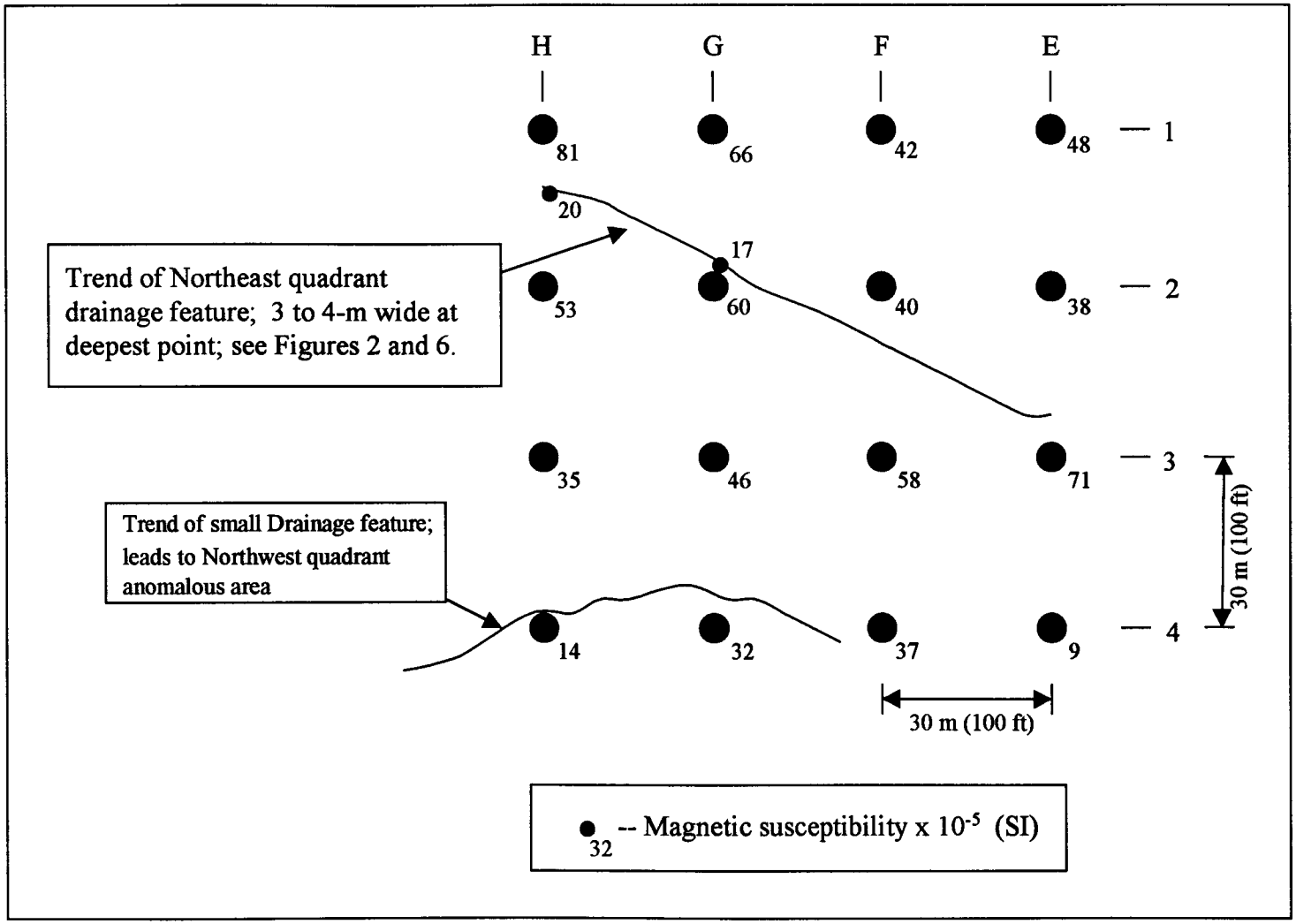

Figure 23. Magnetic susceptibility values over a portion of the Northeast quadrant magnetic anomalous area

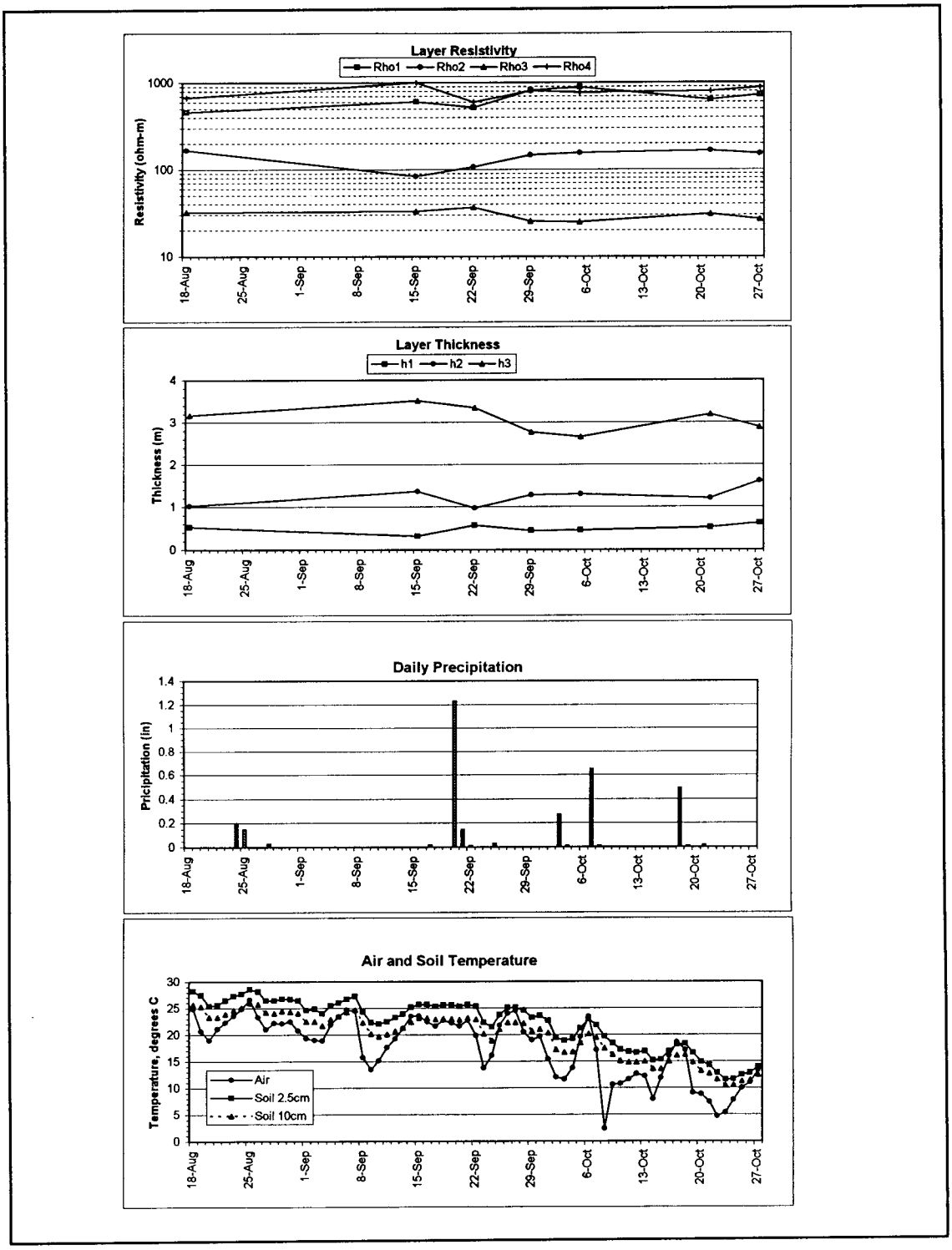

Figure 24. Electrical resistivity model parameters, precipitation, and air and soil temperatures as a function of date during the Phase IV demonstrations

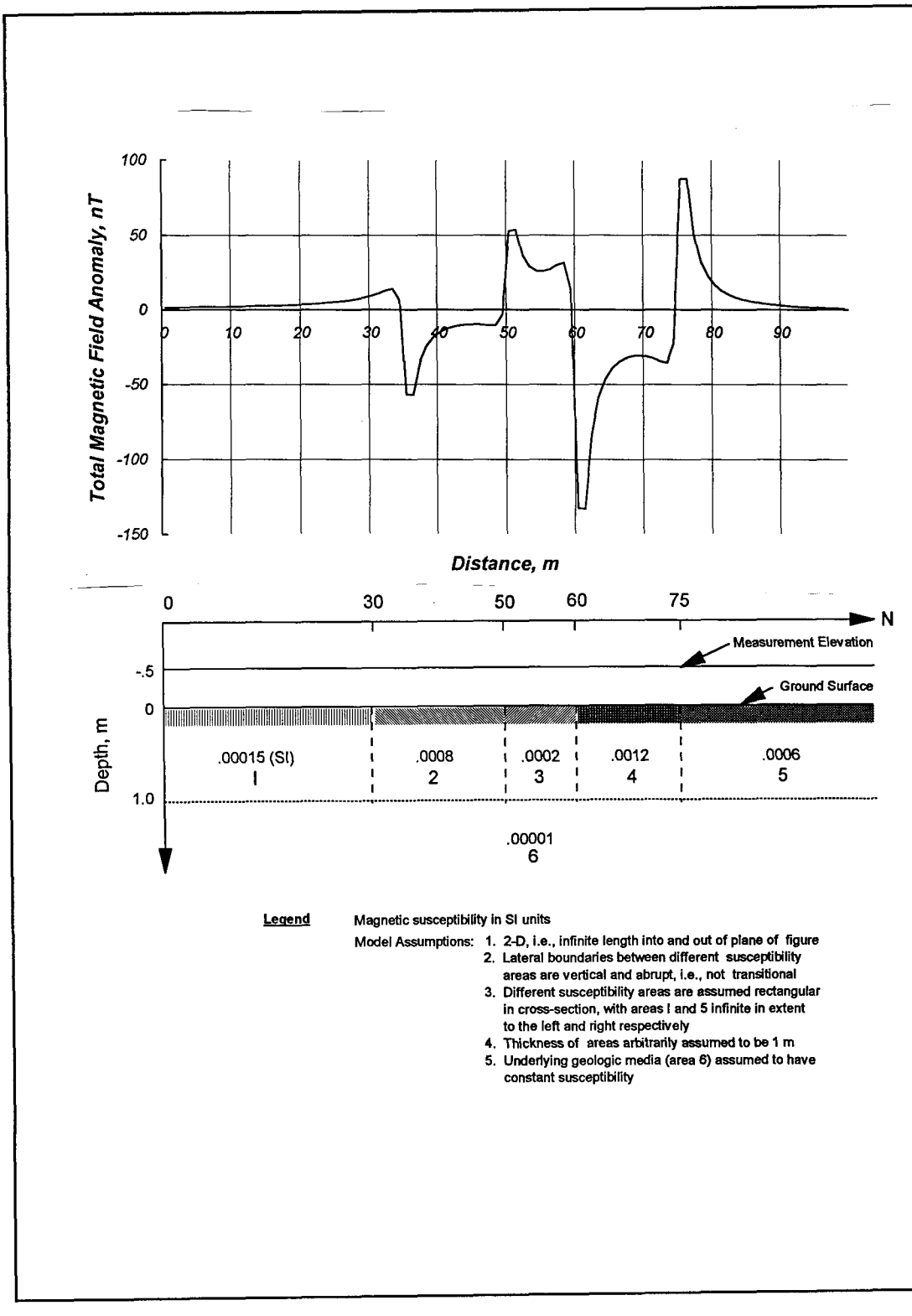

Figure 25. Total magnetic field anomaly calculations (2-D) for hypothetical model of susceptibility along line K based on Figure 21.

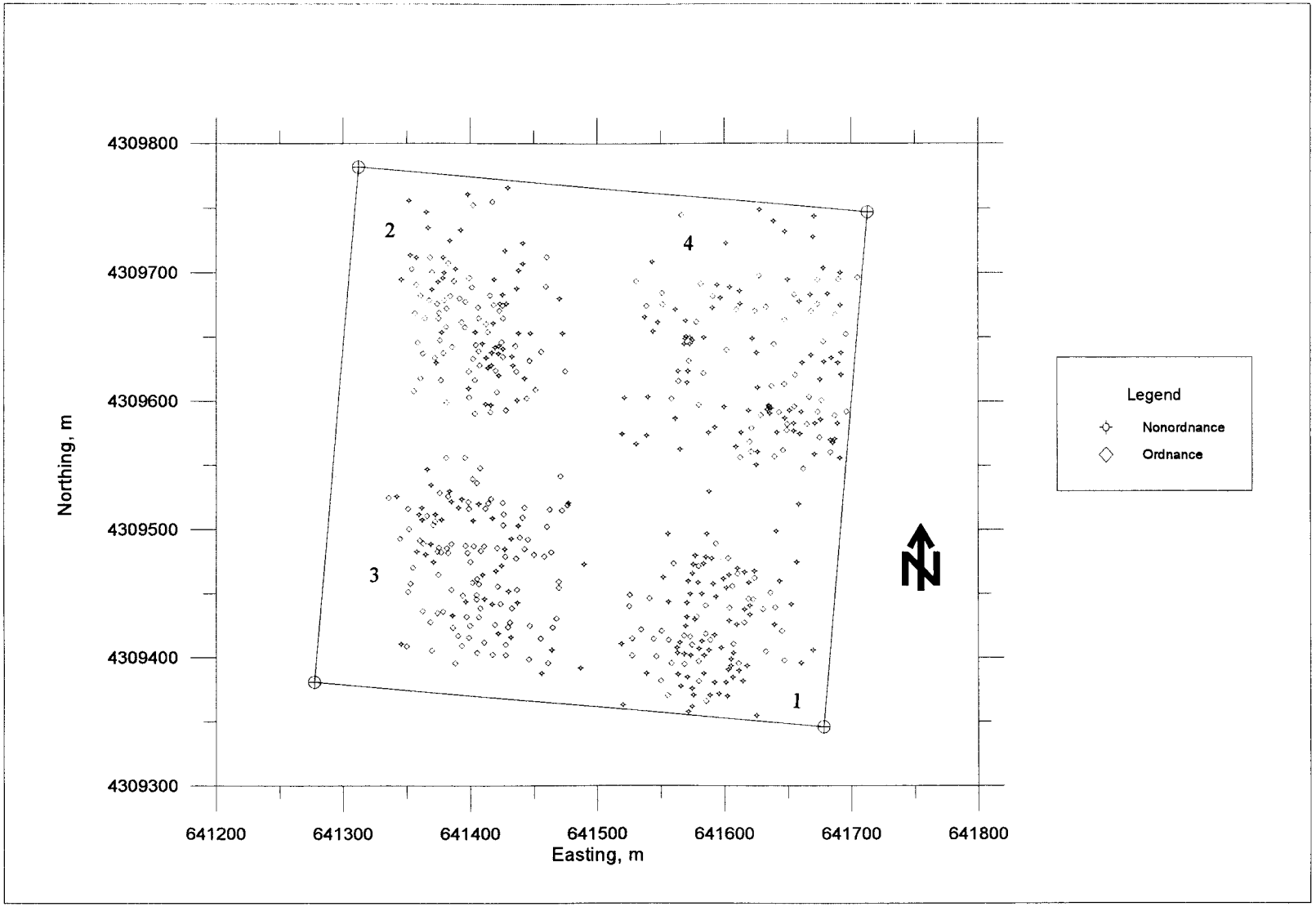

Figure 26. Distribution of baseline targets (ordnance and nonordnance) for JPG Phase III

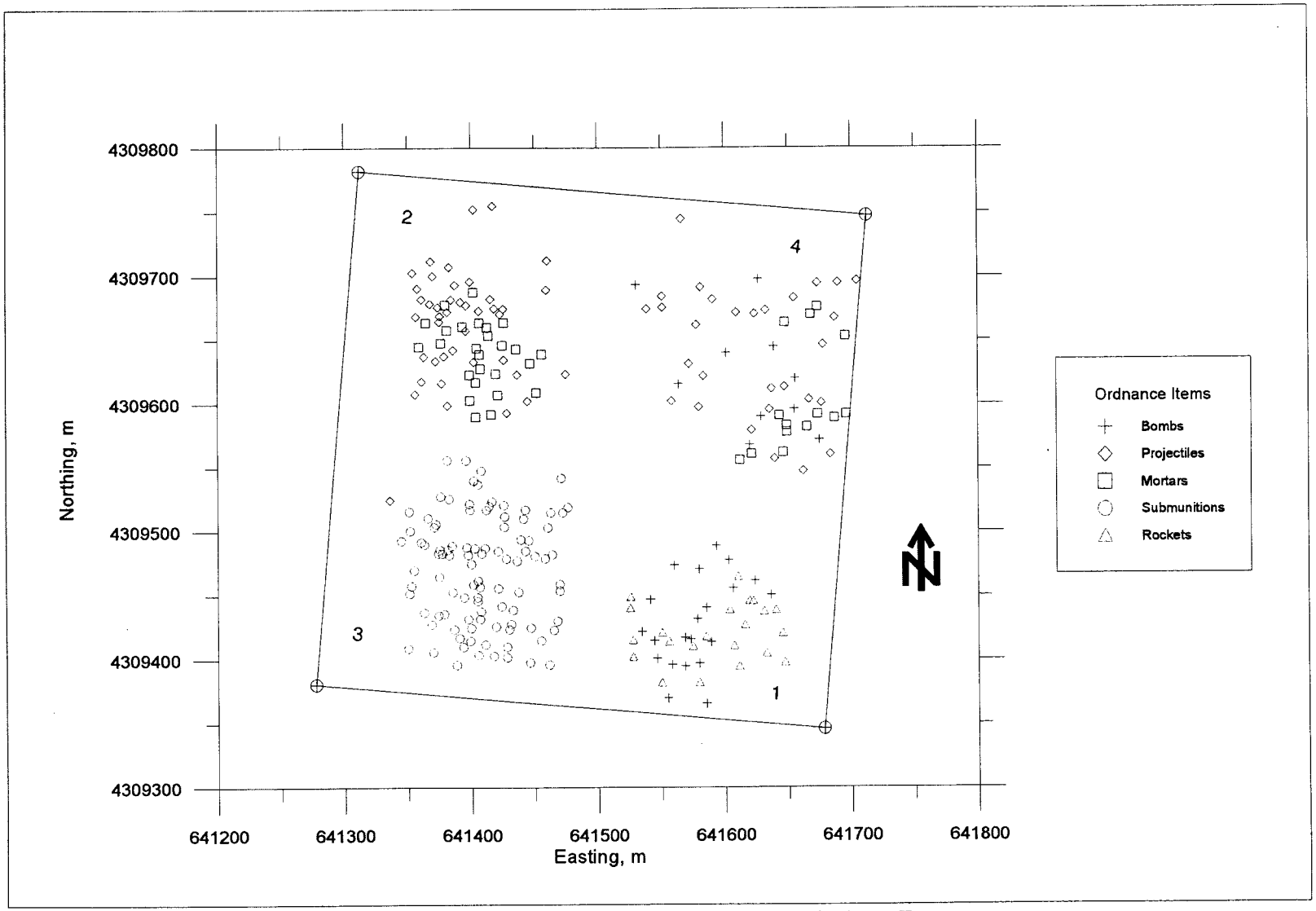

Figure 27. Distribution of baseline ordnance targets and location of the four scenario for JPG Phase III

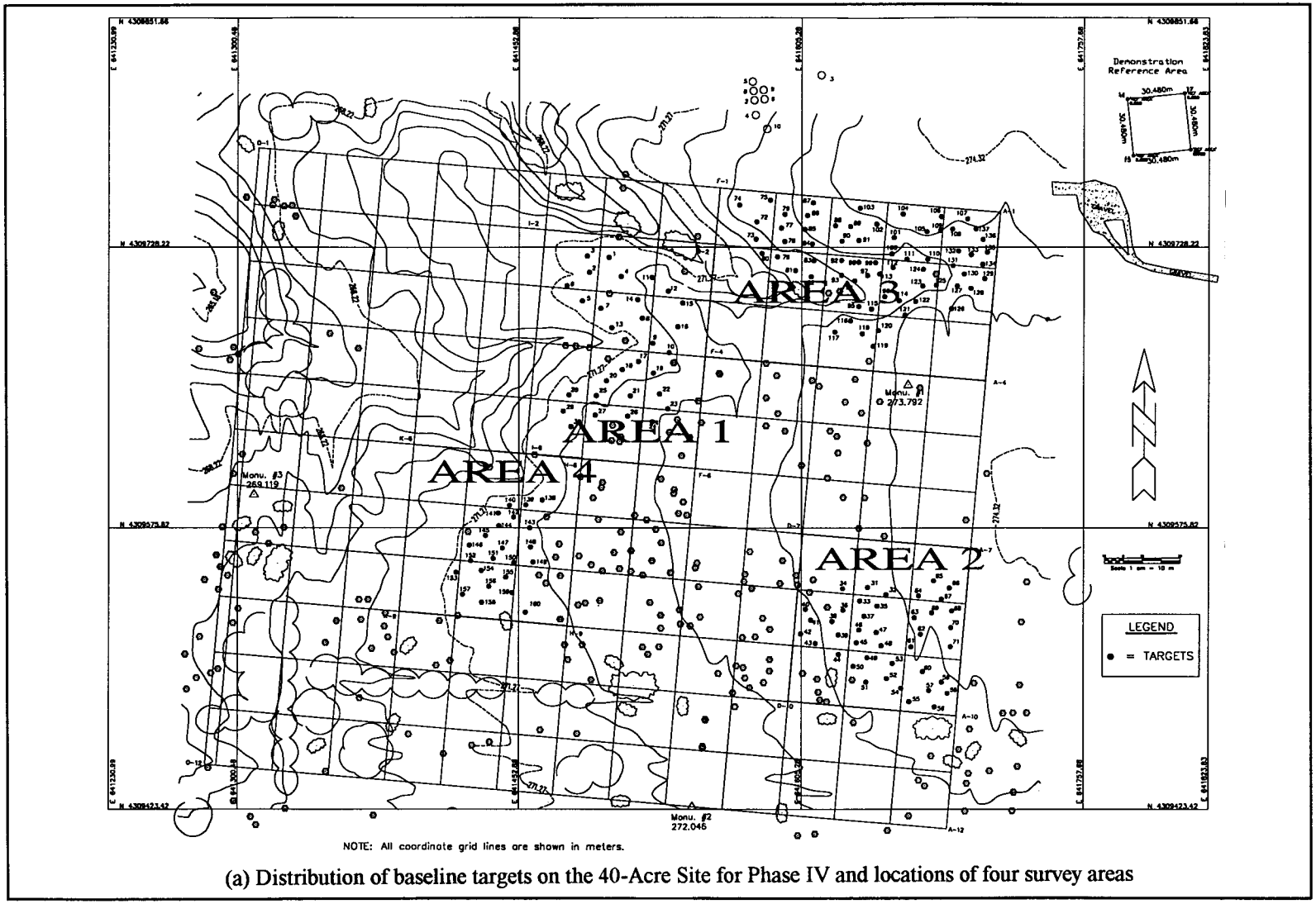

(a) Distribution of baseline targets on the 40-Acre Site for Phase IV and locations of four survey areas

Figure 28. JPG Phase IV: (a) baseline target locations and location of four survey areas; (b) baseline ordnance burial depths (Continued)

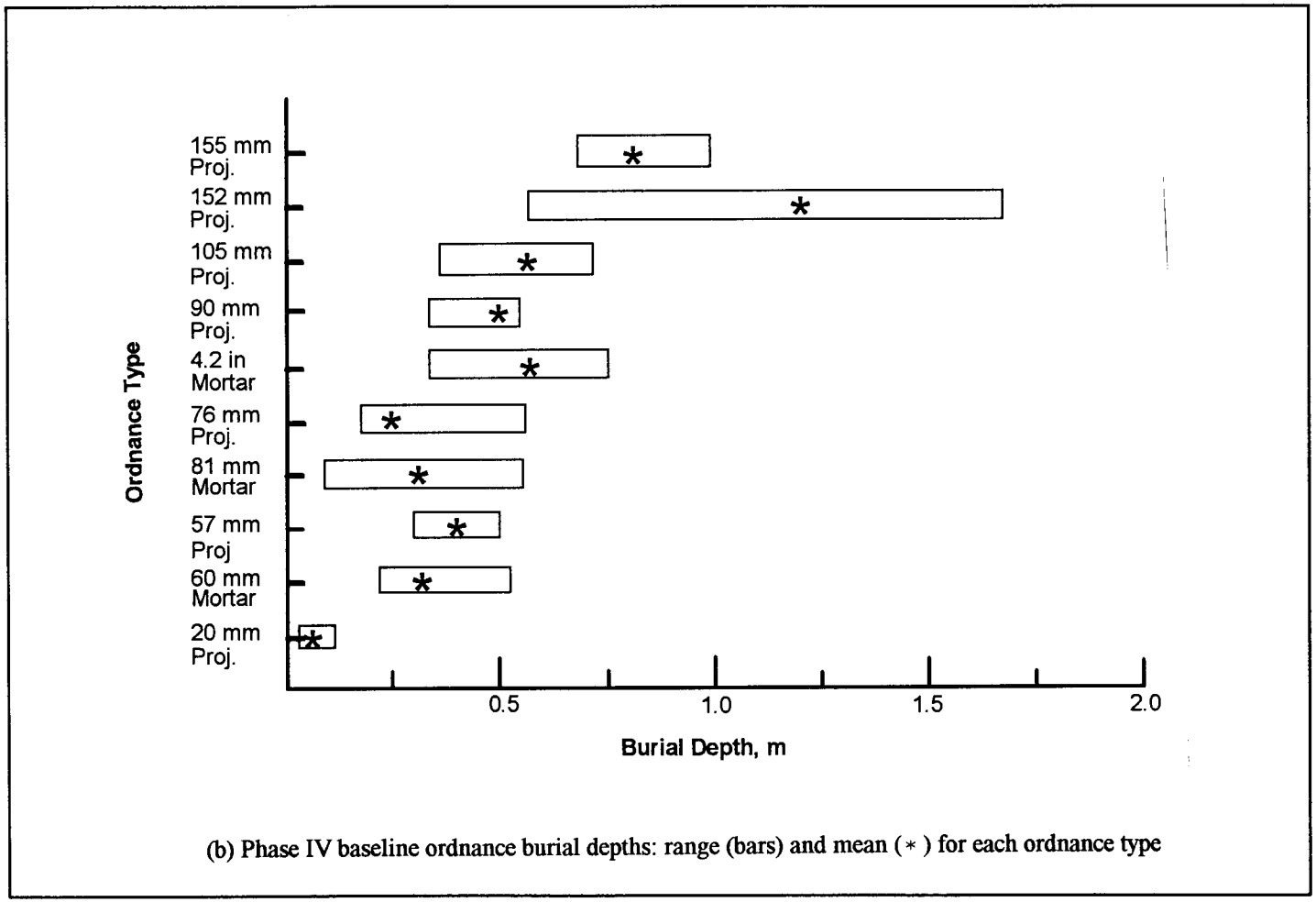

(b) Phase IV baseline ordnance burial depths: range (bars) and mean (*) for each ordnance type

Figure 28. JPG Phase IV: (a) baseline target locations and location of four survey areas; (b) baseline ordnance burial depths (Concluded)

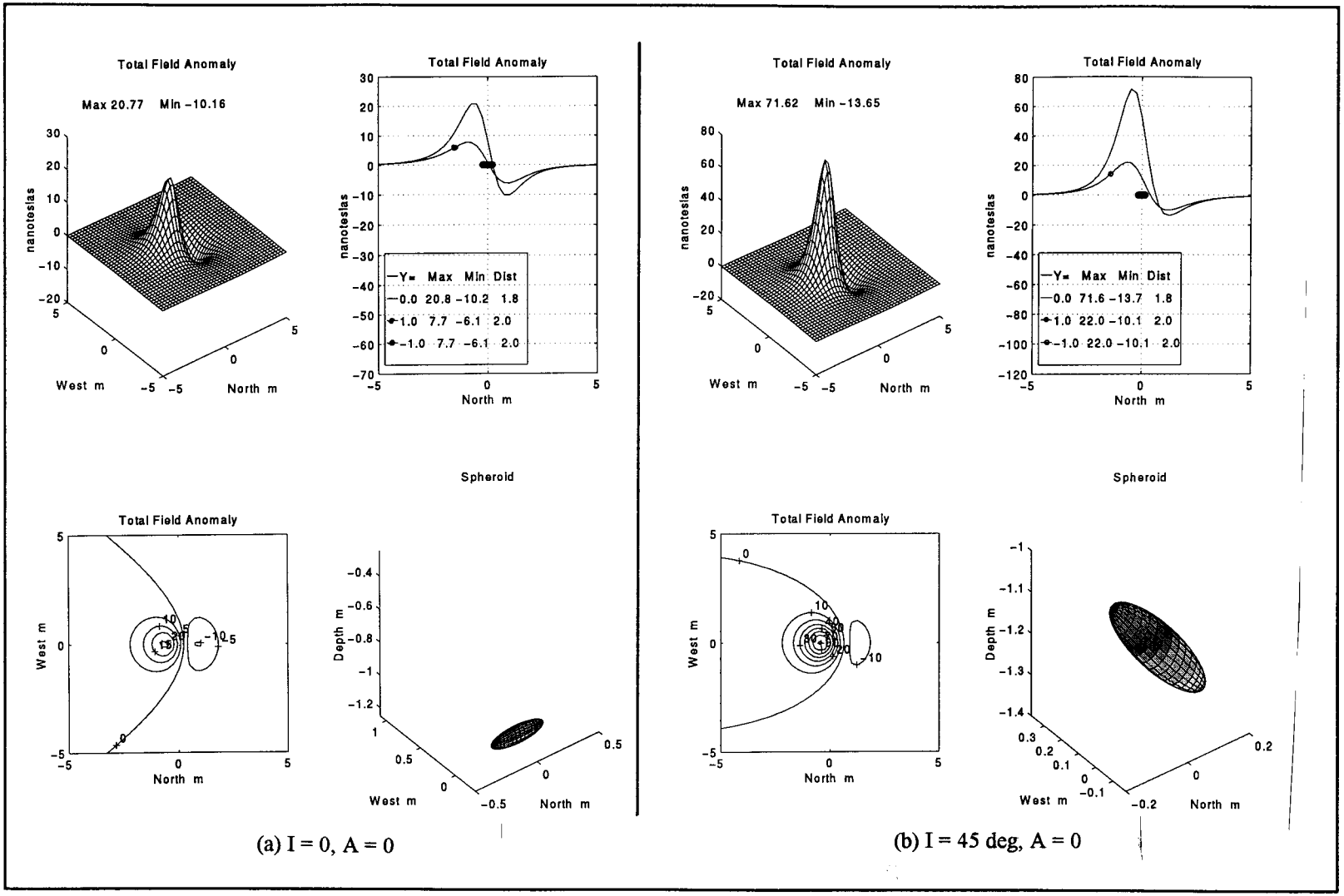

Figure 29. Total magnetic field model calculations for 105 mm artillery projectile, depth = 1.18 , for three orientations, with I the angle of long axis below horizontal and A the azimuth of the long axis counterclockwise from north: (a) I = 0, A = 0; (b) I = 45 deg, A = 0; (c) I = 45 deg, A = 45 deg; (d) I = 45 deg, A = 90 deg. (Continued)

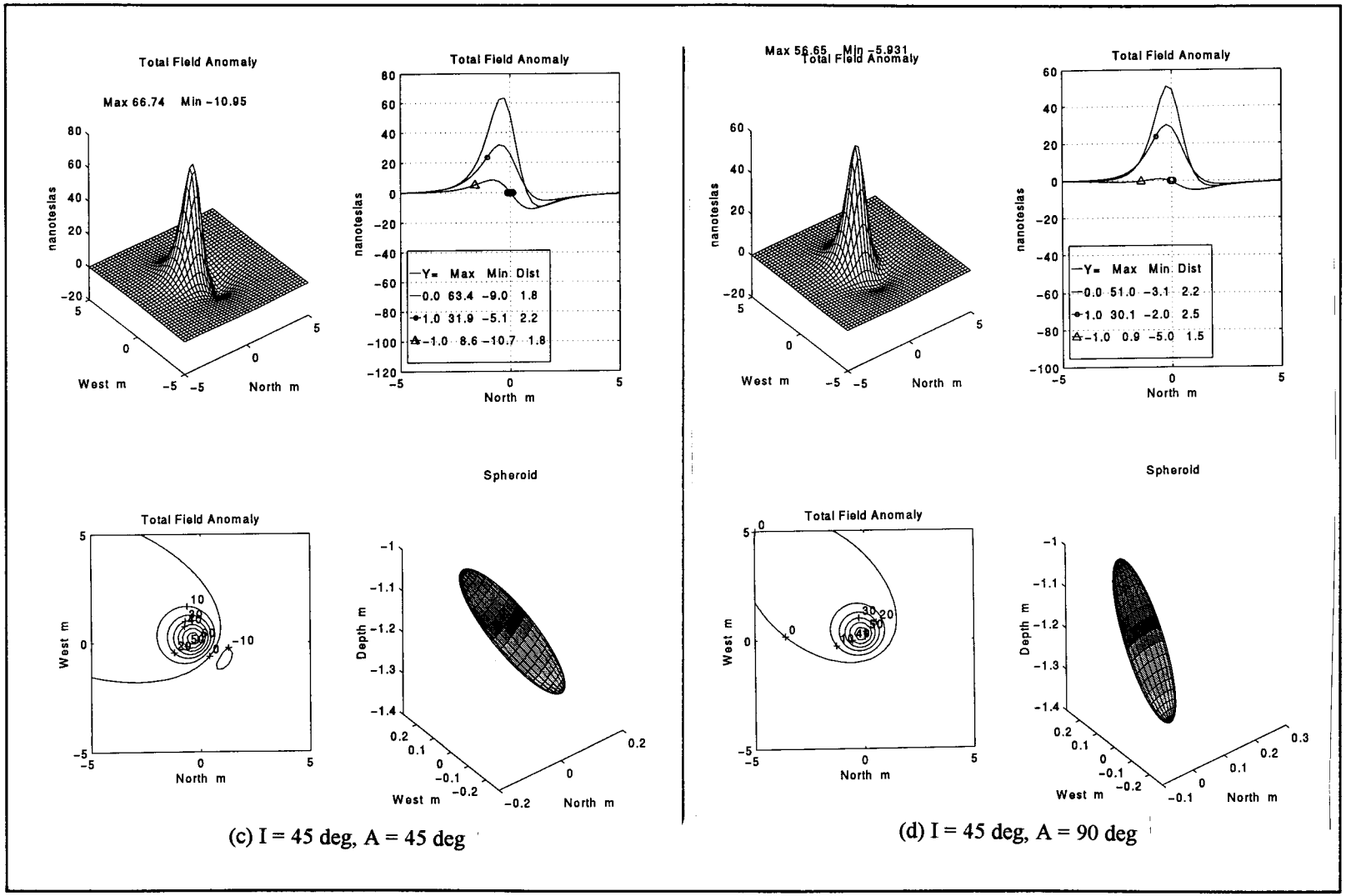

Figure 29. Total magnetic field model calculations for 105 mm artillery projectile, depth = 1.18 , for three orientations, with I the angle of long axis below horizontal and A the azimuth of the long axis counterclockwise from north: (a) I = 0, A = 0; (b) I = 45 deg, A = 0; (c) I = 45 deg, A = 45 deg; (d) I = 45 deg, A = 90 deg. (Concluded)

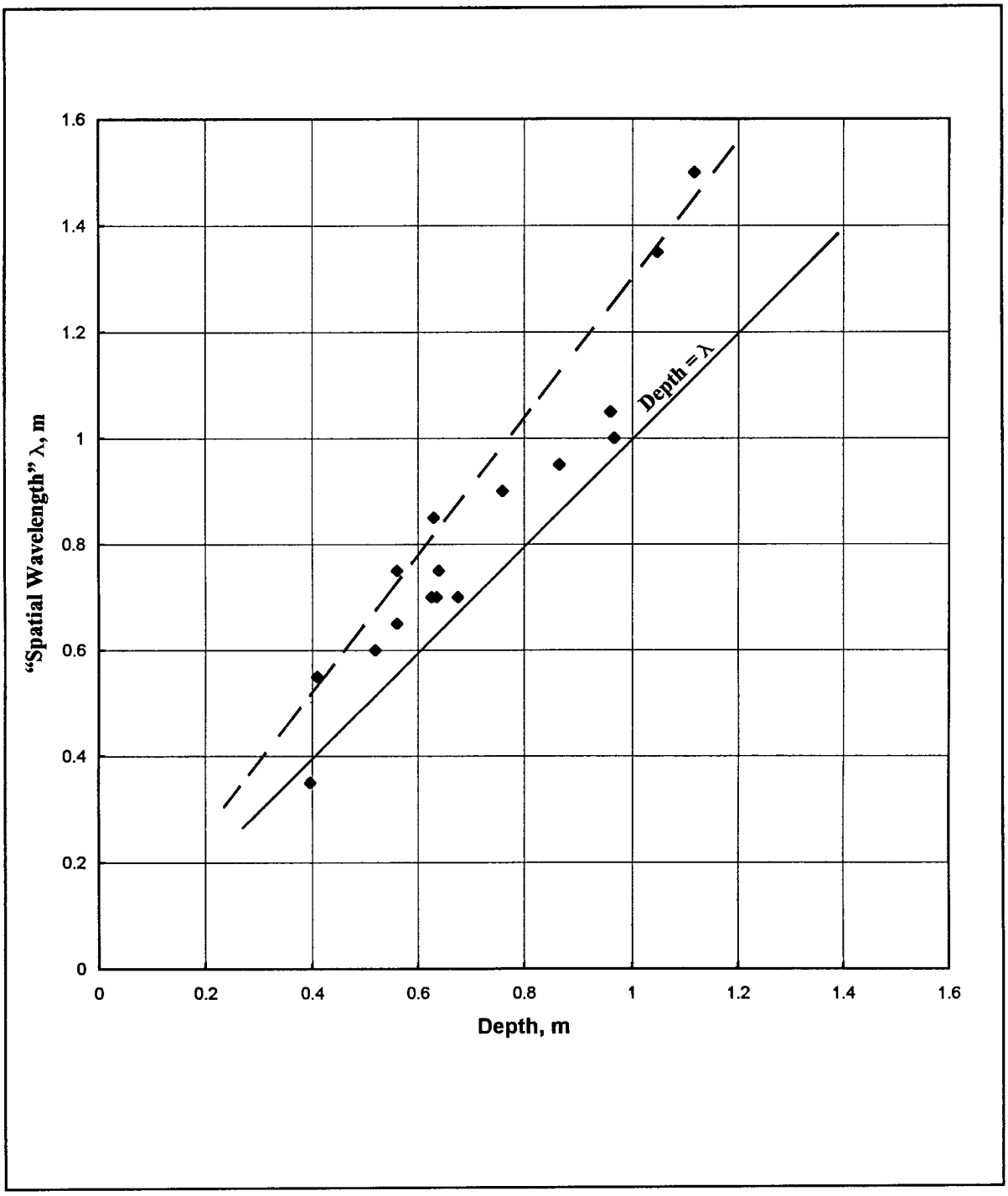

Figure 30. Results of total magnetic field signature modeling -- 60-mm mortars: spatial wavelength measure (λ) versus depth (= burial depth + measurement plane elevation) for all orientations

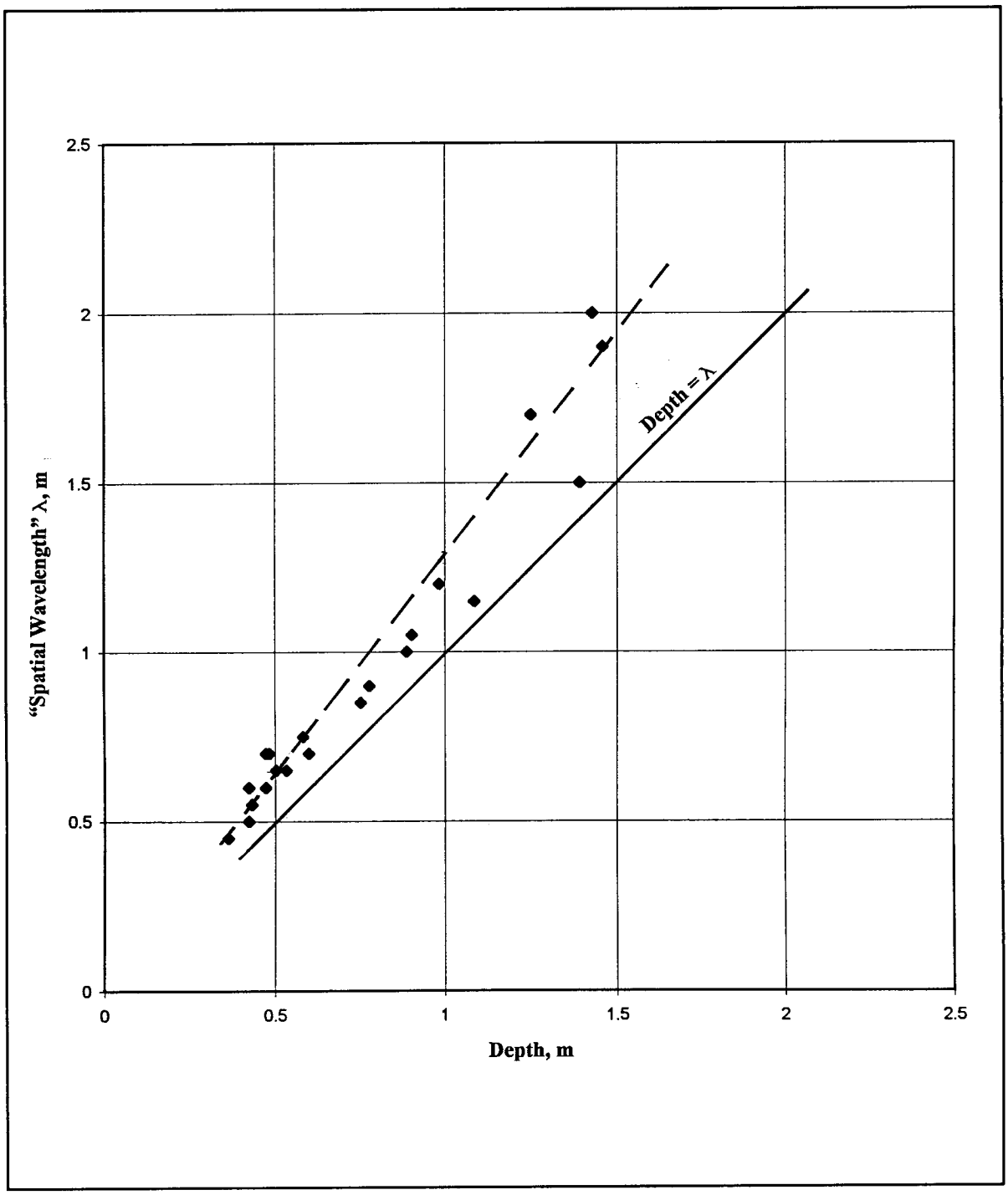

Figure 31. Results of total magnetic field signature modeling -- 105-mm projectiles: spatial wavelength measure (λ) versus depth (= burial depth + measurement plane elevation) for all orientations

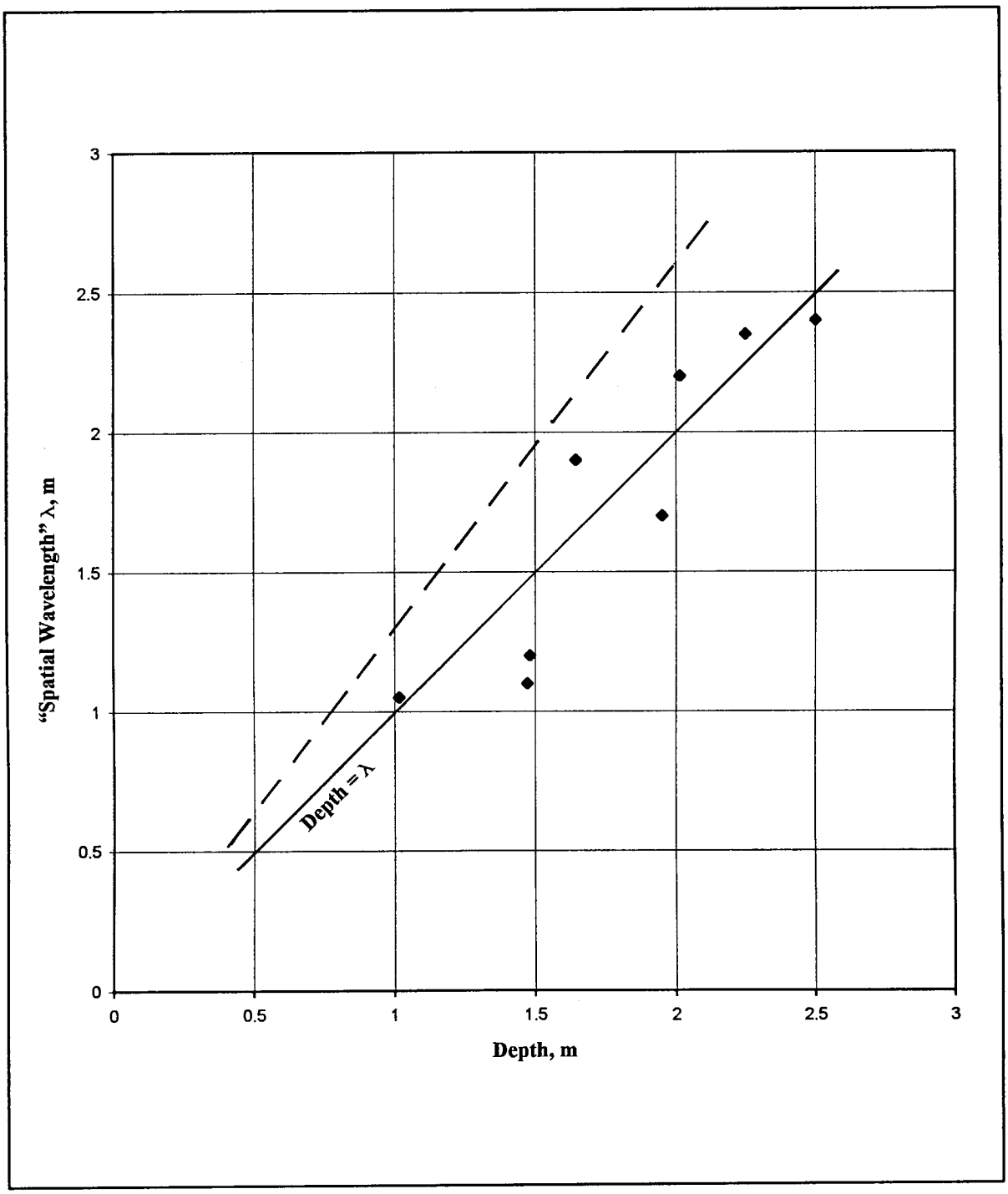

Figure 32. Results of total magnetic field signature modeling -- 250-lb bombs: spatial wavelength measure (λ) versus depth (= burial depth + measurement plane elevation) for all orientations

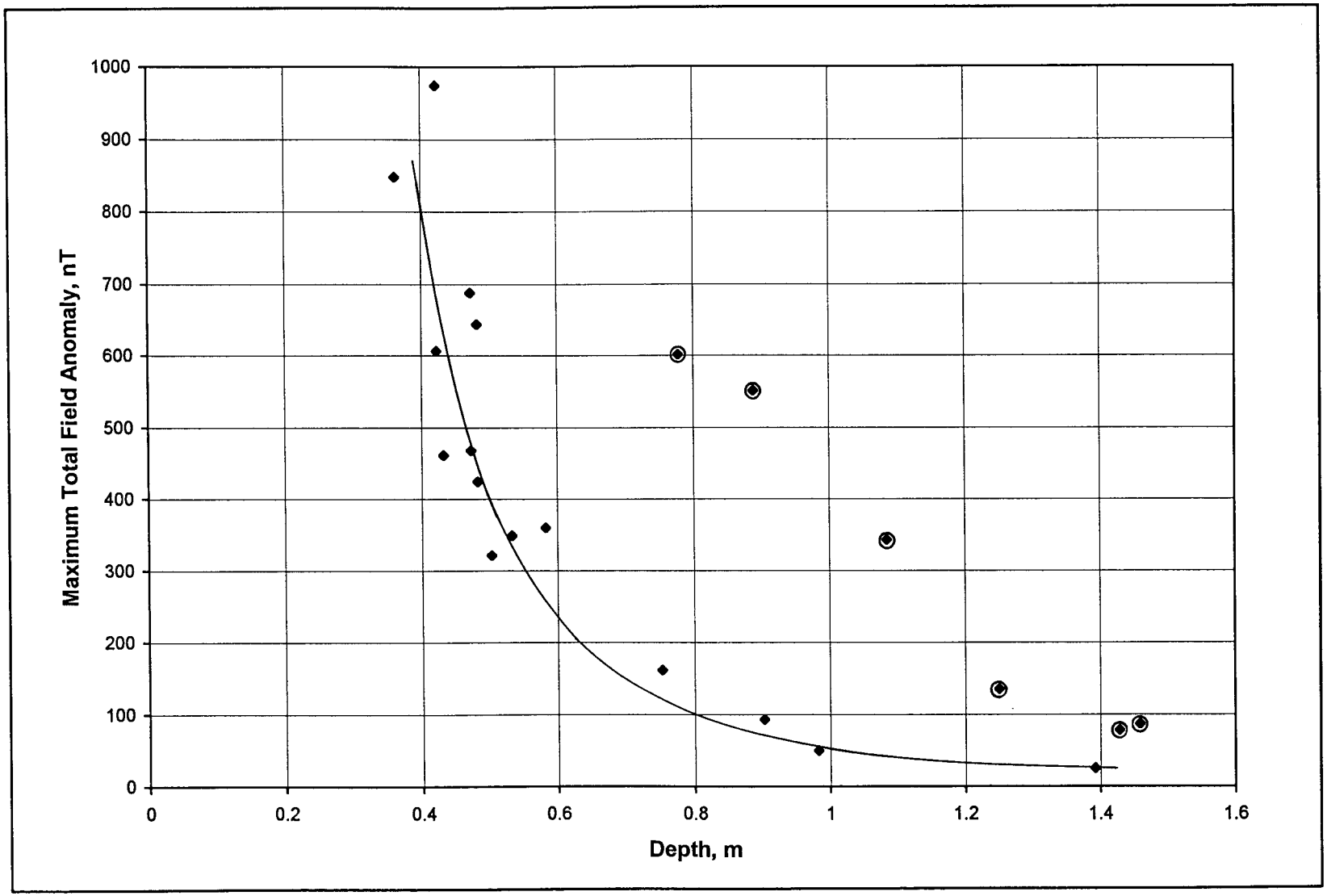

Figure 33. Maximum positive total magnetic field anomaly magnitude for all 105-mm projectiles in Phase III baseline versus depth (= burial depth + measurement height) for all orientations; circled points are for 45 deg inclination

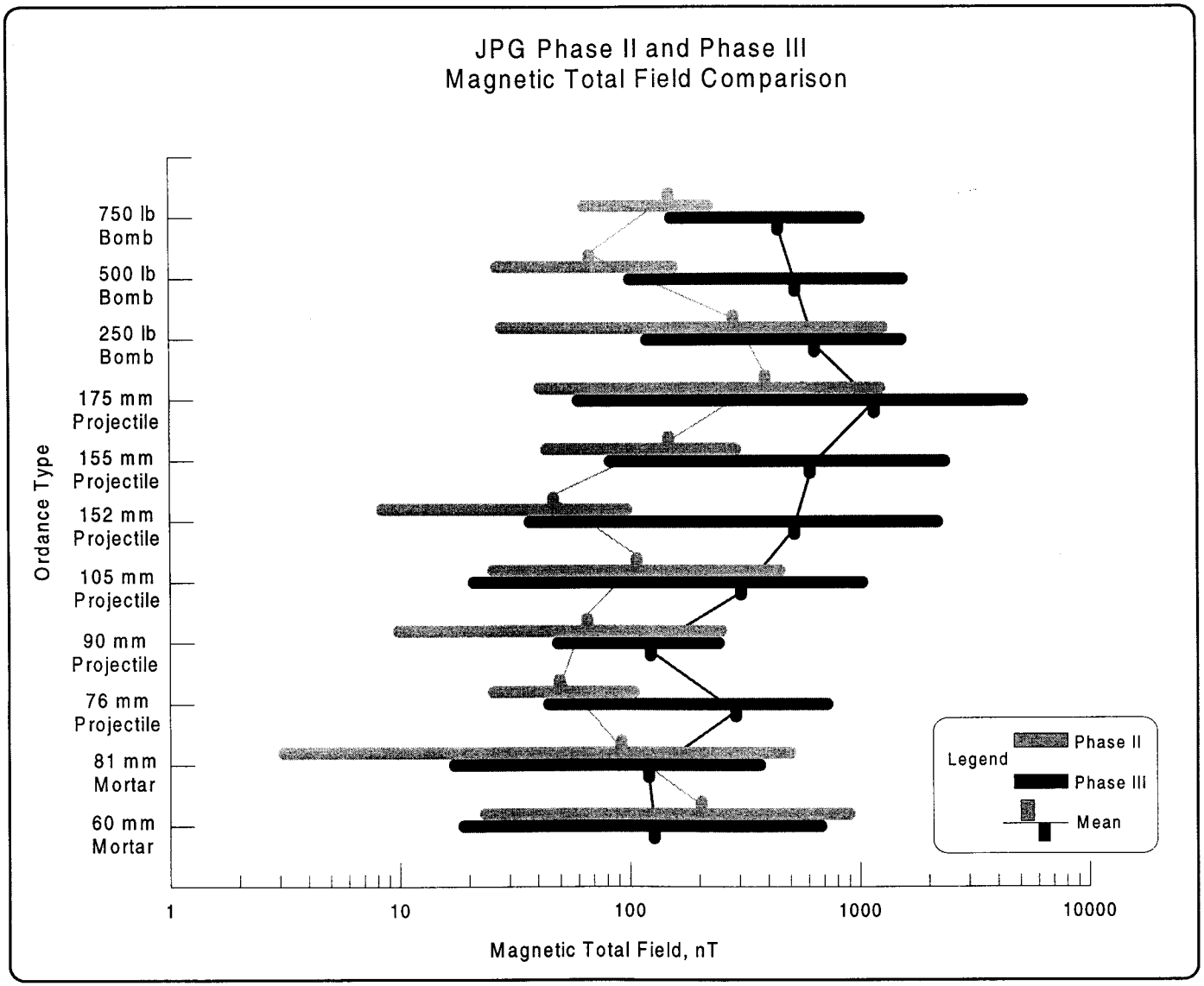

Figure 34. Calculated maximum positive total magnetic field anomaly for all Phase II and III baseline ordnance targets for all depths and orientations

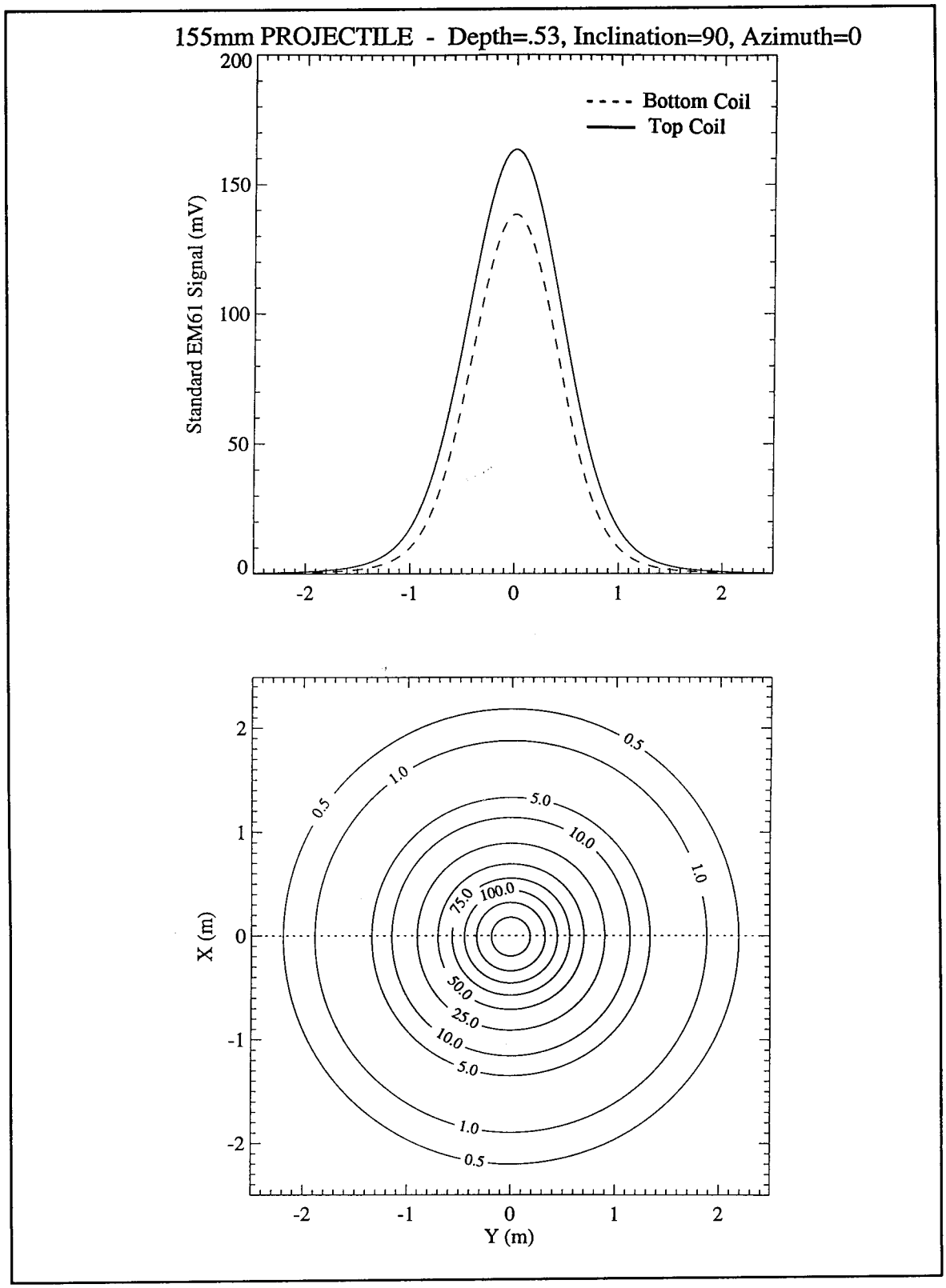

Figure 35. TDEM response calculation for a 155-mm projectile from the Phase III baseline; depth = 0.53 m, inclination = 90 deg, azimuth = 0 deg

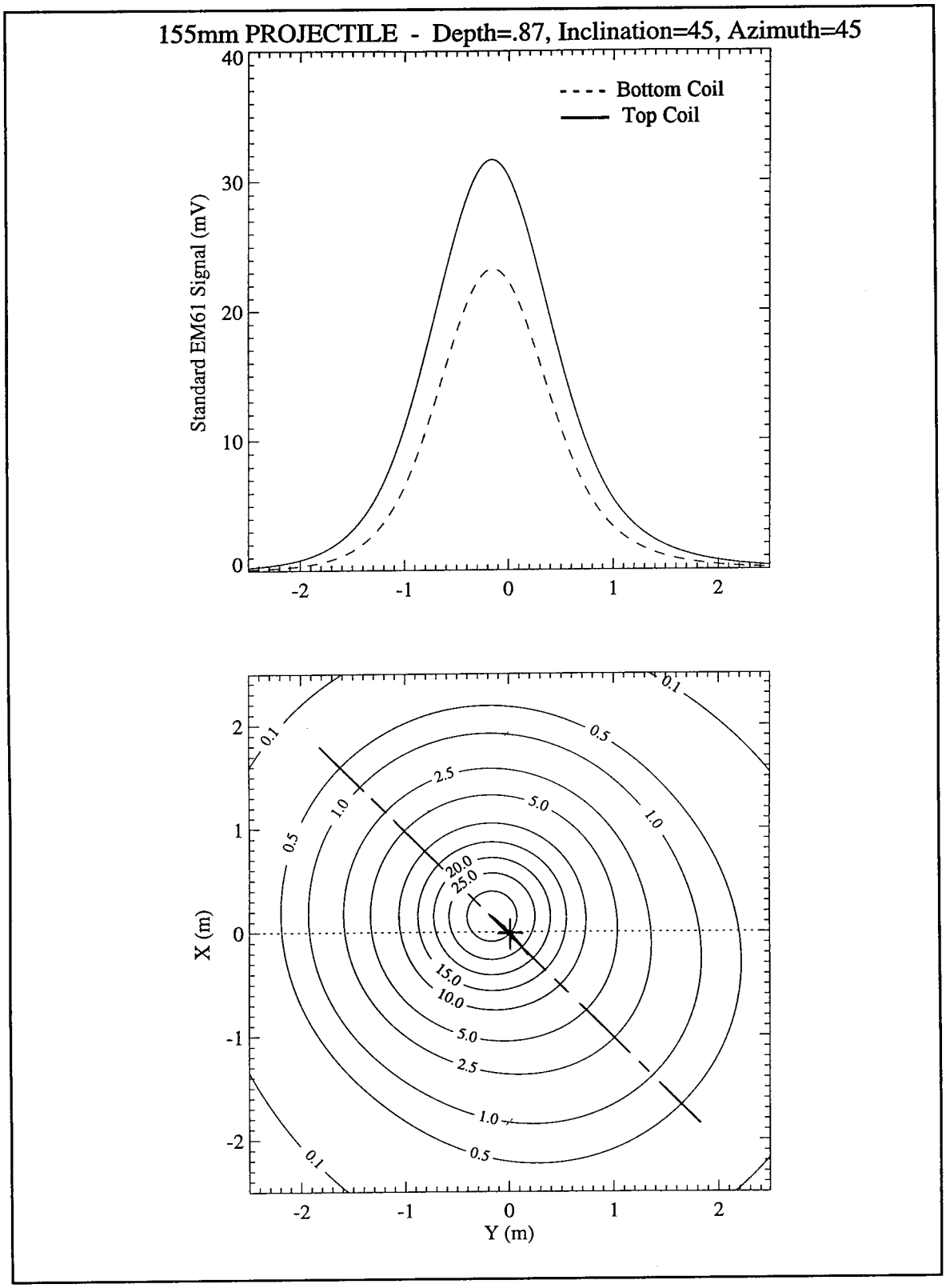

Figure 36. TDEM response calculation for a 155-mm projectile from the Phase III baseline; depth = 0.87 m, inclination = 45 deg, azimuth = 45 deg; '+' marks the geometric center

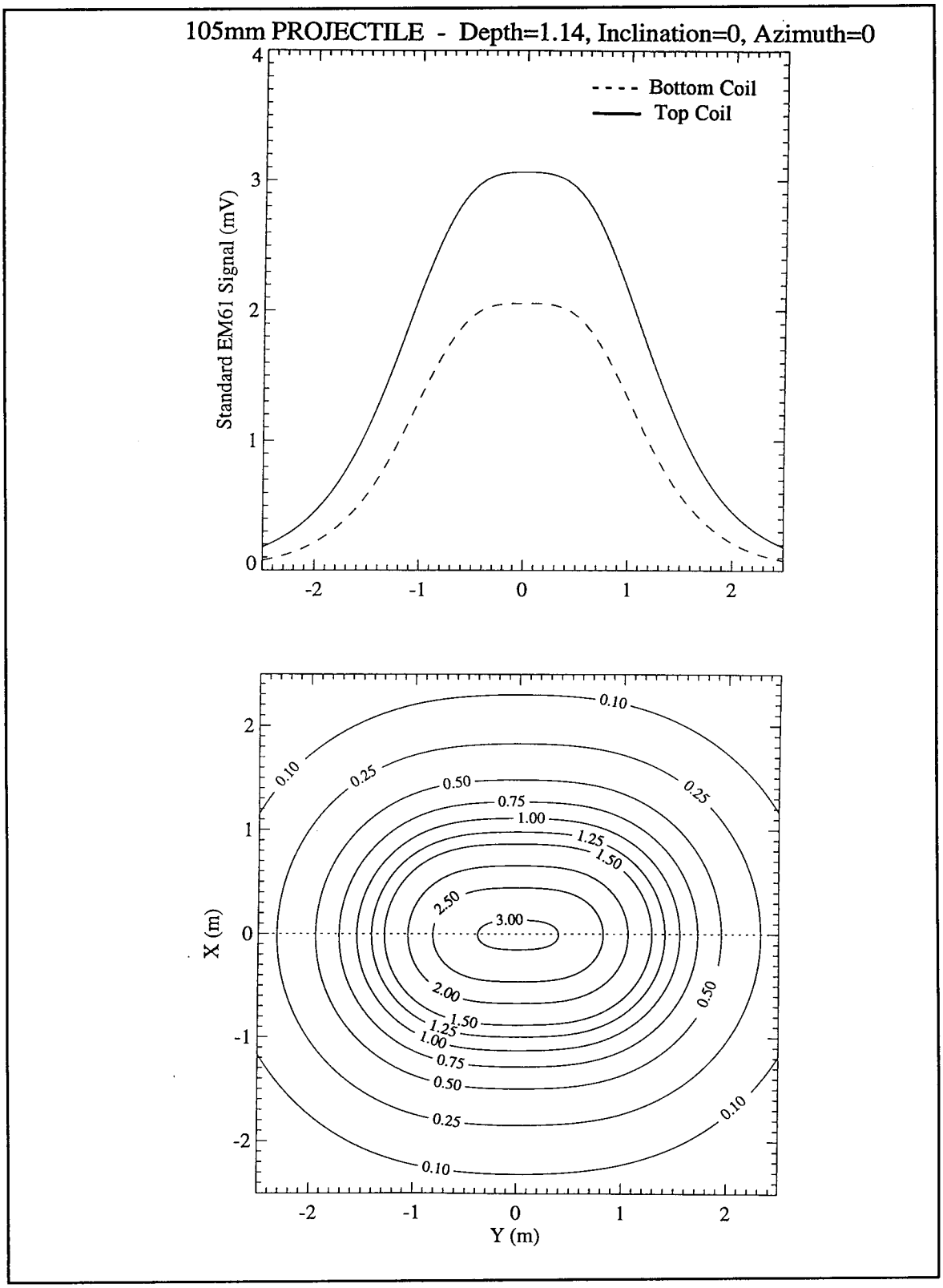

Figure 37. TDEM response calculation for a 105-mm projectile from the Phase III baseline; depth = 1.14 m, inclination = 0 deg, azimuth = 0 deg

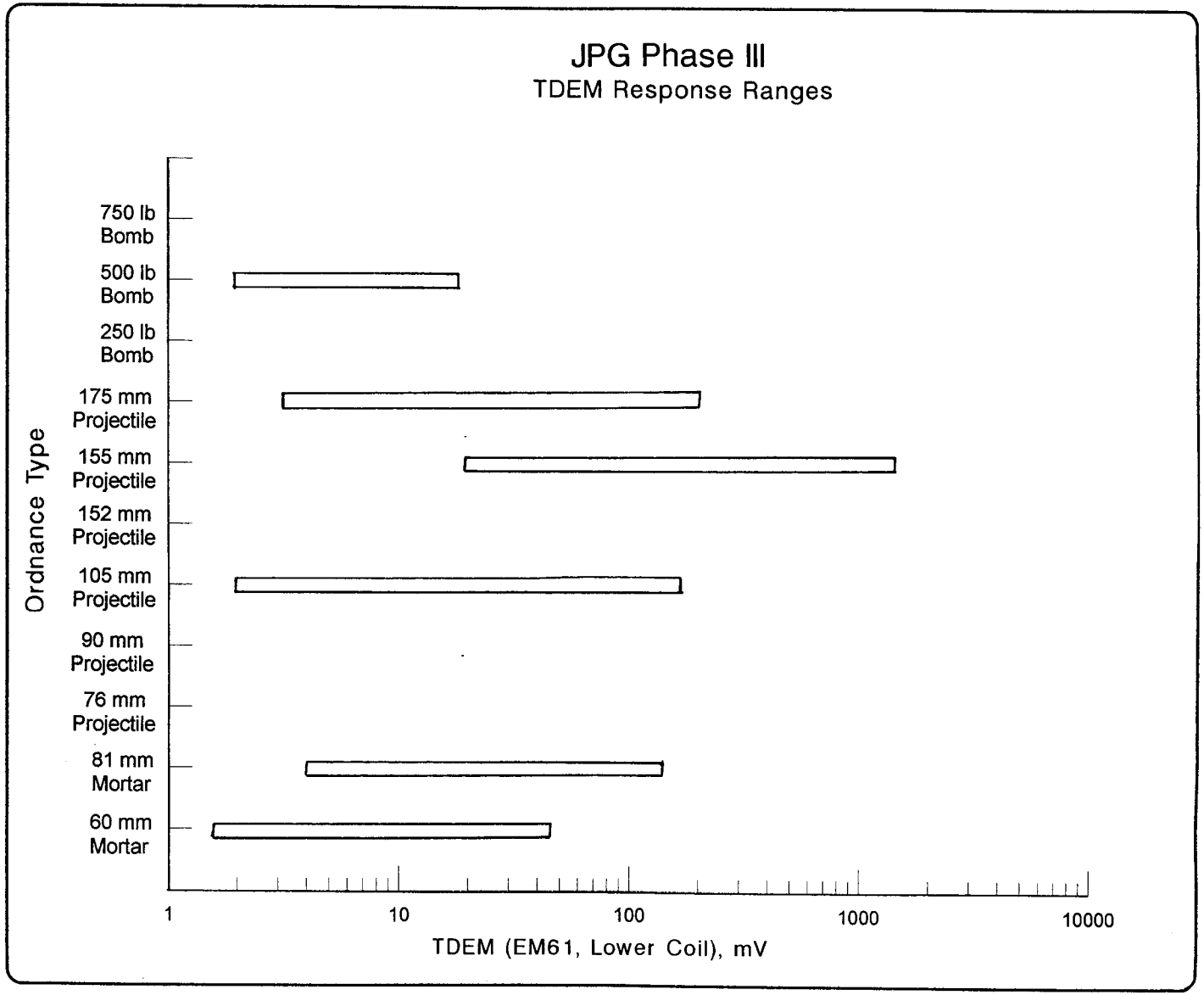

Figure 38. Maximum TDEM response ranges for selected Phase III ordnance items

REPORT DOCUMENTATION PAGE

Form Approved
OMB No. 0704-0188

1. AGENCY USE ONLY *(Leave blank)*	2. REPORT DATE	3. REPORT TYPE AND DATES COVERED
	July 1999	Final report

4. TITLE AND SUBTITLE
Phenomenological Investigations of the Jefferson Proving Ground UXO Technology Demonstrations

5. FUNDING NUMBERS
MIPR 3736
Work Unit AF25, 6.2

6. AUTHOR(S)
Dwain K. Butler, José L. Llopis, Janet E. Simms

7. PERFORMING ORGANIZATION NAME(S) AND ADDRESS(ES)
U.S. Army Engineer Waterways Experiment Station
3909 Halls Ferry Road, Vicksburg, MS 39180-6199

8. PERFORMING ORGANIZATION REPORT NUMBER
Technical Report GL-99-7

9. SPONSORING/MONITORING AGENCY NAME(S) AND ADDRESS(ES)
U.S. Army Environmental Center
Aberdeen Proving Ground, Maryland 21020-5401
U.S. Army Corps of Engineers
Washington, DC 20314-1000

10. SPONSORING/MONITORING AGENCY REPORT NUMBER

11. SUPPLEMENTARY NOTES
Available from National Technical Information Service, 5285 Port Royal Road, Springfield, VA 22161.

12a. DISTRIBUTION/AVAILABILITY STATEMENT
Approved for public release; distribution is unlimited.

12b. DISTRIBUTION CODE

13. ABSTRACT ***(Maximum 200 words)***

Environmental conditions and geophysical properties and their spatial and temporal variability for the JPG UXO test sites are examined. The four JPG phases are discussed, and geophysical anomaly signatures are calculated for Phases II and III baseline ordnance items. Rainfall and its resulting effect on soil water content are the dominant environmental parameters. The near-surface soil electrical conductivity varies significantly between wet site conditions and dry site conditions. Implications of wet-versus-dry site conditions for detection of buried ordnance are significant for ground penetrating radar (GPR) and somewhat less significant for the electromagnetic (EM) induction methods. The presence of a clay layer as shallow as 0.3 m and 1.5 to 5 m thick can cause significant difficulties for GPR detection of ordnance items buried within the layer for any site condition (wet or dry). Above the clay layer, the material is predominantly very fine-grained quartz, with only small amounts of clay minerals, which refutes prior claims that high-clay content soils limited the depth of investigation of GPR at the JPG sites. Significant spatial variation in near-surface magnetic susceptibility are discussed, with magnetic susceptibility of materials in the upper 0.5 m of the site varying by an order of magnitude over horizontal distances of 2 to 3 m. The susceptibility variations produce "geologic" magnetic anomalies that significantly interfere with detection of the magnetic anomalies of buried ordnance. Magnetic background areas of the 40-acre site vary from "quiet" (< 5 nT) to noisy

(Continued)

14. SUBJECT TERMS
Environmental and geologic backgrounds
Geophysical parameters
Geophysical phenomenology
Geophysics
Soil properties
Unexploded ordnance (UXO)

15. NUMBER OF PAGES
96

16. PRICE CODE

17. SECURITY CLASSIFICATION OF REPORT	18. SECURITY CLASSIFICATION OF THIS PAGE	19. SECURITY CLASSIFICATION OF ABSTRACT	20. LIMITATION OF ABSTRACT
UNCLASSIFIED	UNCLASSIFIED		

13. (Concluded).

(~ 20 nT). Predicted total magnetic field anomalies for the Phases II and III baseline ordnance items indicate the minimum peak positive anomaly magnitude for Phase III is 18 nT, while some Phase II baseline ordnance targets have anomaly values < 10 nT. For magnetically quiet areas of the site, only some of the Phase II baseline ordnance targets are problematically detectable. For magnetically noisy areas of the site, however, a small number of Phase III ordnance targets and a significant number of Phase II targets become problematically detectable. Similarly, EM61 time domain electromagnetic (TDEM) maps indicate considerable areas exist where background noise levels are < 2 mV, although some areas have noise levels ~5 - 10 mV. While only a small number of Phase III ordnance targets are problematically detectable with a TDEM system, a significantly larger number of Phase II targets could be problematically detectable, depending on the burial location at the site. The results indicate the need to evaluate the results of UXO detection surveys based on site-specific criteria. Selection of appropriate geophysical survey methods should be guided by a priori assessment of environmental parameter variations, topography, accessibility, geology and soil type variations, and geophysical parameter variations. Geophysical signature modeling for expected ordnance types and depths should be conducted, with site-specific signal-to-noise considerations.

Destroy this report when no longer needed. Do not return it to the originator.